

การพัฒนาโพลีเซลล์สำหรับการประยุกต์ใช้ทางโวลแทมเมตรี



นายภัตสรณ์พล งามอุโฆษ

สถาบันวิทยบริการ

จุฬาลงกรณ์มหาวิทยาลัย

วิทยานิพนธ์นี้เป็นส่วนหนึ่งของการศึกษาตามหลักสูตรปริญญาวิทยาศาสตรดุษฎีบัณฑิต

สาขาวิชาเคมี ภาควิชาเคมี

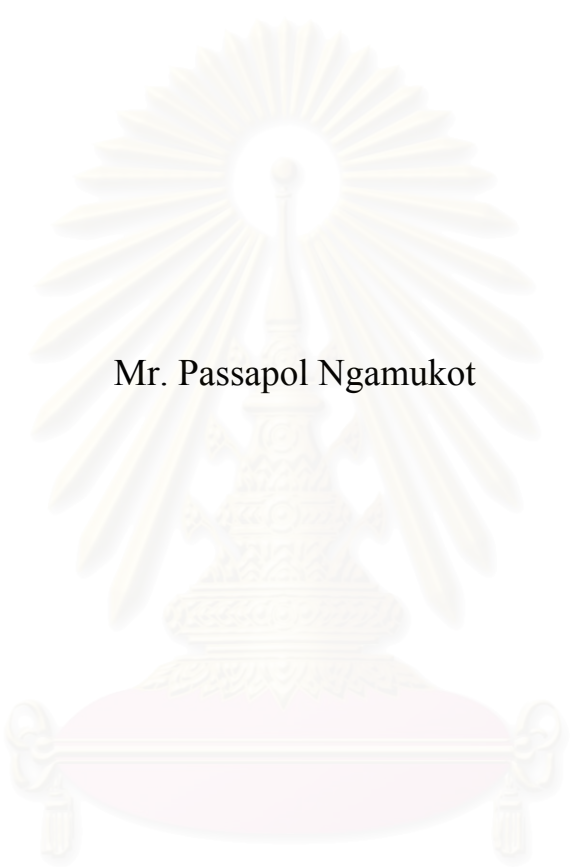
คณะวิทยาศาสตร์ จุฬาลงกรณ์มหาวิทยาลัย

ปีการศึกษา 2548

ISBN 974-17-3952-4

ลิขสิทธิ์ของจุฬาลงกรณ์มหาวิทยาลัย

# DEVELOPMENT OF FLOW CELL FOR VOLTAMMETRIC APPLICATIONS



Mr. Passapol Ngamukot

สถาบันวิทยบริการ  
A Dissertation Submitted in Partial Fulfillment of the Requirements  
for the Degree of Doctor of Philosophy Program in Chemistry

Faculty of Science  
Chulalongkorn University

Academic Year 2005

ISBN 974-17-3952-4

Thesis Title                      Development of flow cell for voltammetric applications  
By                                      Mr. Passapol Ngamukot  
Field of Study                      Chemistry  
Thesis Advisor                      Associate Professor Orawon Chailapakul, Ph.D.  
Thesis Co-advisor                      Assistant Professor Narong Praphairaksit, Ph.D.

---

Accepted by the Faculty of Science, Chulalongkorn University in Partial  
Fulfillment of the Requirements for the Doctor's Degree

*T. Vitidsant*  
..... Deputy Dean for Administrative Affairs,  
Acting Dean, The Faculty of Science  
(Associate Professor Tharapong Vitidsant, Ph.D.)

THESIS COMMITTEE

*Sophon Roengsumran*  
..... Chairman  
(Professor Sophon Roengsumran, Ph.D.)

*Orawon Chailapakul*  
..... Thesis Advisor  
(Associate Professor Orawon Chailapakul, Ph.D.)

*Narong Praphairaksit*  
..... Thesis Co-advisor  
(Assistant Professor Narong Praphairaksit, Ph.D.)

*T. Tuntulani*  
..... Member  
(Associate Professor Thawatchai Tuntulani, Ph.D.)

*Puttaruksa V.*  
..... Member  
(Puttaruksa Varanusupakul, Ph.D.)

*Winai Ouangpipat*  
..... Member  
(Winai Ouangpipat, Ph.D.)

ภัสสรพล งามอุโฆษ: การพัฒนาโพลีเมอร์เซลล์สำหรับการประยุกต์ใช้ทางโวลแทมเมทรี  
(DEVELOPMENT OF FLOW CELL FOR VOLTAMMETRIC APPLICATIONS) อาจารย์ที่ปรึกษา:  
รศ. ดร. อรวรรณ ชัยลภากุล; อาจารย์ที่ปรึกษาร่วม: ผศ. ดร. ณรงค์ ประไพรักษ์สิทธิ์; 92 หน้า. ISBN  
974-17-3952-4

งานวิจัยนี้ได้ทำการออกแบบ และสร้าง โพลีเมอร์เซลล์จากวัสดุราคาประหยัดที่สามารถหาซื้อได้  
จากร้านขายวัสดุอุปกรณ์ทั่วไป Hydrodynamic Behavior ของโพลีเมอร์เซลล์ที่สร้างขึ้นสามารถตรวจสอบ  
ได้โดยอาศัยสมการทางคณิตศาสตร์ เมื่อนำโพลีเมอร์เซลล์มาประกอบกับขั้วไฟฟ้าโบรอน โดปโดมอนด์  
สามารถประยุกต์ใช้เป็นอุปกรณ์ตรวจวัดในระบบโพลีอินเจกชันได้ ระบบนี้ถูกใช้วิเคราะห์ปริมาณ  
สารมาลาไคต์กรีน และลูโคมาลาไคต์กรีน ผลกระทบจาก pH และ อัตราเร็วของการให้ศักย์ไฟฟ้าใน  
ระบบแบบพัลส์สามารถทำได้โดยใช้เทคนิคโวลแทมเมทรี นอกจากนี้ยังได้สาธิตการใช้อุปกรณ์  
ตรวจวัดดังกล่าวกับระบบ HPLC และสามารถตรวจวัดสัญญาณของสารทั้งสองชนิดได้อย่างชัดเจน  
อีกด้วย ผลที่ได้จากการวิจัยแสดงให้เห็นถึงศักยภาพที่จะพัฒนาอุปกรณ์นี้เพื่อใช้เป็นอุปกรณ์ตรวจวัด  
สำหรับระบบ HPLC ในอนาคต ด้วยการออกแบบที่เหมาะสม โพลีเมอร์เซลล์อีกแบบหนึ่งสามารถประยุกต์  
ใช้เป็นอุปกรณ์ต่อเชื่อมในเครื่องมือที่เรียกว่า Electrochemical-Surface Plasmon Resonance (EC-SPR)  
เครื่องมือนี้สามารถใช้ตรวจสอบฟิล์มบางของสารเคคเคนไทออลบนขั้วไฟฟ้าทอง ที่เตรียมขึ้นโดยวิธี  
Self-Assemble Monolayer ได้ โดยสัญญาณเชิงไฟฟ้าและสัญญาณเชิงแสงของสารนี้สามารถถูกตรวจวัด  
ได้พร้อมๆ กัน ผลการวิจัยแสดงให้เห็นถึงประสิทธิภาพและศักยภาพในการที่จะพัฒนาเครื่องมือนี้ เพื่อ  
ใช้เป็นอุปกรณ์รับรู้เชิงชีวภาพ (biosensor) ต่อไปในอนาคต

## สถาบันวิทยบริการ จุฬาลงกรณ์มหาวิทยาลัย

ภาควิชา .....เคมี..... ลายมือชื่อนิสิต..... ภัสสร งามอุโฆษ  
สาขาวิชา.....เคมี..... ลายมือชื่ออาจารย์ที่ปรึกษา..... อรวรรณ ชัยลภากุล  
ปีการศึกษา.....2548..... ลายมือชื่ออาจารย์ที่ปรึกษาร่วม..... ณรงค์ ประไพรักษ์สิทธิ์

## 4473825023: MAJOR CHEMISTRY

KEY WORDS COST-EFFECTIVE FLOW CELL, HYDRODYNAMICS, ELECTROCHEMISTRY, AMPEROMETRIC DETECTOR, FLOW INJECTION ANALYSIS

PASSAPOL NGAMUKOT: DEVELOPMENT OF FLOW CELL FOR VOLTAMMETRIC APPLICATIONS. THESIS ADVISOR: ASSOC. PROF. ORAWON CHAILAPAKUL, Ph. D. THESIS CO-ADVISOR: ASST. PROF. NARONG PRAPHAIRAKSIT, Ph. D. 92 pp ISBN 974-17-3952-4

In this research, cost-effective flow cells were designed and fabricated using low-cost materials supplied from local hardware stores. Hydrodynamic behavior of these homemade flow cells was characterized using mathematical equation. The fabricated flow cell equipped with boron-doped diamond thin-film (BDD) electrode was used as an amperometric detector in a flow injection analysis system. Malachite green (MG) and leucomalachite green (LMG) were investigated using this system. Cyclic voltammetry as a function of the pH of supporting electrolyte solution and the scan rate in batch experiment was also studied. Determination of MG and LMG using BDD electrode as an amperometric detector in HPLC system was also demonstrated. The signals of both MG and LMG were clearly observed. These results indicate that BDD electrode has a potential to be a detector for HPLC system. With proper design, another fabricated flow cell was used as an interface in an electrochemical – surface plasmon resonance (EC-SPR) instrument. This instrument was used to investigate a self-assembled monolayer of decanethiol on gold surface. Both electrochemical and optical signals were recorded simultaneously. The results demonstrate that the electrochemical control coupled with sensitive optical measurements provides a basis for further development of this device into a powerful biosensor.

Department.....Chemistry.....Student's signature.....*Passapol Ngamukot*  
 Field of study.....Chemistry..... Advisor's signature.....*Orawon Chailapakul*  
 Academic year ..... 2005..... Co-advisor's signature .....*Narong Praphairaksit*

## ACKNOWLEDGEMENTS

The financial support from the University Development Committee (UDC) is gratefully acknowledged.

For all the strength, wisdom, and creativity, I am entirely indebted to my thesis advisor, Associate Professor Dr. Orawon Chailapakul, who always keeps her eyes set on my success and believes in me. I learned so much from her and accumulated hands-on experiences and skills critical to my future. Her untiring way of encouragement and support is so impressive that I will be forever thankful.

Deepest gratitude to my thesis co-advisor, Assistant Professor Dr. Narong Praphairaksit, for his suggestions, and encouragement throughout my research course. Invaluable guidance, comments, and suggestions from my oversea supervisor, Professor Phil Bartlett, Professor James Wilkinson and my co-worker, Dr. Anna Sheridan, are sincerely appreciated. I am also grateful for their warm hospitality during my stay in UK. I would like to thank Professor Dr. Sophon Roengsumran, Associate Professor Dr. Thawatchai Tuntulani, Dr. Puttaruksa Varanusupakul and Dr. Winai Ouangpipat for their substantial advice as thesis committee.

To my friends and colleagues, both at the Electrochemical Research Group (Thailand) and at the School of Chemistry, University of Southampton (UK). I wish to express my appreciation for sharing good times all the way through.

Finally, I am affectionately grateful to my father and mother for their wholehearted support, understanding, and unconditional love.

## CONTENTS

	<b>page</b>
ABSTRACT (IN THAI).....	iv
ABSTRACT (IN ENGLISH).....	v
ACKNOWLEDGEMENT.....	vi
CONTENTS.....	vii
LIST OF TABLES.....	x
LIST OF FIGURES.....	xi
LIST OF ABBREVIATIONS AND SYMBOLS.....	xvi
<b>CHAPTER I INTRODUCTION.....</b>	<b>1</b>
1.1 Cost-Effective Instrumentation.....	1
1.2 Objective of the Research.....	3
<b>CHAPTER II THEORY.....</b>	<b>4</b>
2.1 Electrochemical Method.....	4
2.1.1 Measurement of Potential.....	4
2.1.2 Measurement of Current.....	4
2.1.3 Potentiometry.....	5
2.1.4 Voltammetry.....	5
2.1.5 Cyclic Voltammetry.....	6
2.1.6 Amperometry.....	7
2.1.7 Hydrodynamics System.....	8
2.2 Flow Injection Analysis (FIA).....	8
2.3 Flow Cell Configurations.....	11
2.3.1 Channel Electrodes (Thin-layer).....	10
2.3.2 Wall-Jet Electrodes.....	12
2.4 Surface Plasmon Resonance.....	11
2.4.1 Evanescent Wave.....	13
2.4.2 Surface Plasmons.....	13
2.4.3 Waveguide-Based Configuration.....	15
2.5 Self-Assembled Monolayer (SAM): Reviews.....	17
2.6 EC-SPR Instrument: Reviews.....	19

	<b>page</b>
2.7 Malachite Green and Leucomalachite Green: Reviews.....	21
<b>CHAPTER III ELECTROCHEMICAL DETECTION</b>	
<b>OF MG AND LMG.....</b>	<b>23</b>
3.1 Designs and Fabrication of the Flow Cells.....	23
3.1.1 Position of the Electrodes.....	23
3.1.2 Materials.....	24
3.1.3 Internal Chamber.....	25
3.1.4 Tubing and Fitting.....	25
3.2 Wall-jet Electrodes Configuration.....	25
3.3 Channel Electrodes Configuration .....	28
3.4 Hybrid Electrodes Configuration.....	31
3.5 Characterizations of the Flow Cells.....	32
3.6 Electrochemistry of MG and LMG in batch experiment.....	37
3.6.1 Instrument, Reagents and Chemicals.....	37
3.6.2 Cyclic Voltammetric Investigation.....	38
3.6.3 Effect of pH.....	40
3.6.4 Scan Rate Dependence Study.....	41
3.7 Flow Injection Analysis with Amperometric Detection.....	44
5.2.1 Instrument, Reagents and Chemicals.....	44
5.2.2 Amperometric Detection of MG and LMG in FIA System....	45
3.8 Amperometric Detection of MG and LMG in HPLC System.....	57
3.8.1 Instrument, Reagents and Chemicals.....	57
3.8.2 HPLC Coupled with Boron-Doped Diamond Thin-Film Electrode.....	57
3.9 Conclusion.....	61
<b>CHAPTER IV EC-SPR SENSING OF AN DECANE-THIOL.....</b>	<b>62</b>
4.1 Oxide Formation on Gold Surface.....	62
4.2 Preparation of Thiol-SAM.....	64



	<b>page</b>
4.3 Contact Angle Measurement.....	65
4.4 Oxidative Desorption of Thiol-SAM on Gold Electrode.....	66
4.5 Fabrication of Waveguide.....	68
4.6 EC-SPR System.....	70
4.7 EC-SPR Sensing of Decanethiol.....	72
4.8 Conclusion.....	76
<b>CHAPTER V CONCLUSION.....</b>	<b>77</b>
5.1 Conclusion.....	77
5.2 Suggestions for Future Works.....	78
REFERENCES.....	79
APPENDIX .....	85
BIOGRAPHY .....	92



สถาบันวิทยบริการ  
จุฬาลงกรณ์มหาวิทยาลัย

**LIST OF TABLES**

<b>table</b>		<b>page</b>
<b>3.1</b>	A summary details of each configuration.....	36
<b>3.2</b>	Comparison of FIA data obtained from both flow cells.....	56



สถาบันวิทยบริการ  
จุฬาลงกรณ์มหาวิทยาลัย

## LIST OF FIGURES

<b>figure</b>	<b>page</b>
2.1	Potential-time waveforms are used in various electroanalytical techniques. Waveforms based on (a) square, (b) linear, and (c) triangular potential-time patterns are used in square wave, linear sweep, and cyclic voltammetry, respectively. .... 5
2.2	The current-potential (i-E) plot is called a cyclic voltammogram..... 6
2.3	Amperometry (E-t) waveform..... 7
2.4	Schematic diagram of a generic description of FIA..... 9
2.5	Single-line FIA manifold..... 10
2.6	Schematic Diagram of Channel Electrode. The arrows indicate the flow direction..... 11
2.7	Schematic Diagram of wall-jetl Electrode. The arrows indicate the flow direction..... 12
2.8	Schematic Diagram of evanescent wave. The energy field extends beyond the point of internal reflection..... 13
2.9	Schematic diagram of the Kretschmann configuration: $n_1$ , $n_2$ and $n_3$ are the reflective indices of glass prism, metal layer and sample layer, respectively..... 14
2.10	The shift resulting from the effect of the layer on the signal. The reflected light is monitored and the resonance condition is indicated by decreasing intensity of the reflected light as a function of incident angle..... 15
2.11	Schematic diagram of the waveguide-based configuration: $n_1$ , $n_2$ , $n_3$ and $n_4$ are the reflective indices of glass substrate, optical channel, metal layer and sample layer, respectively..... 16
2.12	Schematic Diagram of Self-Assembled Monolayer on Gold Surface..... 17
2.13	Chemical structures of (a) MG and (b) LMG..... 22

<b>figure</b>	<b>page</b>
3.1	The wall-jet flow cell (full assembled)..... 26
3.2	The wall-jet flow cell (explode parts)..... 26
3.3	The flow cell body. The nozzle was assign to be placed at the center..... 27
3.4	The working electrode (3mm gold disc) on the opposite side..... 27
3.5	(A) Shape of a gasket used in the wall-jet electrode. (B) The gasket was placed on top of an electrode holder with the gold electrode in the middle. An opening area in the middle of the gasket must be smaller than the electrode body. The arrows in the center represent the directions of the sample stream after impacting the electrode surface..... 28
3.6	The channel electrode has one inlet (brown tube) and one outlet (stainless tube)..... 29
3.7	The channel electrode (back view)..... 29
3.8	The channel electrode. The electrode holder (left) and the cell body (right)..... 30
3.9	(A) Shape of a gasket used in channel electrode. (B) The gasket was placed on top of an electrode holder with the gold electrode in the middle. An arrow in the center represents direction of the sample stream..... 30
3.10	A comparison between wall-jet, channel and hybrid electrode. The arrows in the diagram represent the directions of the sample stream..... 31
3.11	A schematic diagram of a flow system..... 32
3.12	Voltammetric oxidation of 1 mM $K_4Fe(CN)_6$ in 0.1 M KCl at gold electrode in quiescent and flow system. Both recoded at 15 mV/s (vs. Ag/AgCl). For clarity, only forward scan is shown. 33
3.13	A plot of $\log V_f$ against $\log I$ with gradient of 0.7253 (wall-jet electrode)..... 33
3.14	A plot of $\log V_f$ against $\log I$ with gradient of 0.31005 (channel electrode)..... 34
3.15	A plot of $\log V_f$ against $\log I$ with gradient of 0.32379 (hybrid electrode)..... 34
3.16	Cyclic voltammogram of 1 mM malachite green in buffer (pH 2) at BDD electrode (solid line) and glassy carbon electrode (dash line). The scan rate was 50mV/s..... 38

<b>figure</b>	<b>page</b>
3.17 Cyclic voltammogram of 1 mM malachite and leucomalachite green in buffer (pH 2) at BDD electrode. The scan rate was 50 mV/s.....	39
3.18 A pH dependent study of malachite green. The highest oxidation peak was observed at pH 2.....	41
3.19 A scan rate dependence study of 1 mM malachite at BDD electrode in 0.1 M phosphate buffer pH 2.....	42
3.20 A scan rate dependence study of 1 mM leucomalachite at BDD electrode in 0.1 M phosphate buffer pH 2.....	43
3.21 A schematic diagram of flow injection analysis system with amperometric detector.....	44
3.22 The flow cell used in this experiment: BAS flow cell (left) and homemade channel electrode (right).....	45
3.23 Hydrodynamic voltammetric I-E curve obtained at the BDD electrode for 20 $\mu$ L injection of 0.05 mM of malachite green in 0.1 M phosphate buffer pH 2 (above). Hydrodynamic voltammetric S/B ratios versus potential curve (bottom). The signals were obtained from the commercial flow cell.....	46
3.24 Hydrodynamic voltammetric I-E curve obtained at the BDD electrode for 20 $\mu$ L injection of 0.05 mM of leucomalachite green in 0.1 M phosphate buffer pH 2 (above). Hydrodynamic voltammetric S/B ratios versus potential curve (bottom). The signals were obtained from the commercial flow cell.....	47
3.25 Hydrodynamic voltammetric I-E curve obtained at the BDD electrode for 20 $\mu$ L injection of 0.05 mM of malachite green and leucomalachite green in 0.1 M phosphate buffer pH 2 . The signals were obtained from the homemade flow cell.....	48
3.26 Signals of malachite green (above) and leucomalachite green (bottom) at the various concentrations. The data were obtained from commercial flow cell.....	49
3.27 A relationship between the current response and the concentrations of malachite green using a commercial flow cell. A linear range is shown in the inset.....	50

<b>figure</b>	<b>page</b>
3.28 A relationship between the current response and the concentrations of leucomalachite green using a commercial flow cell. A linear range is shown in the inset.....	51
3.29 A relationship between the current response and the concentrations of malachite green using a homemade flow cell. A linear range is shown in the inset.....	52
3.30 A relationship between the current response and the concentrations of leucomalachite green using a homemade flow cell. A linear range is shown in the inset.....	53
3.31 Flow injection signals of 0.2 mM malachite green in 0.1 M phosphate buffer pH 2 at flow rate 1 ml / min. The signals were obtained from the homemade flow cell (at 1.1 V vs. Ag/AgCl).....	54
3.32 The limit of detection of malachite green (50 nM at S/N > 3) in 0.1 M phosphate buffer pH 2 at flow rate 1 ml / min. The signals were obtained from the commercial flow cell (at 8.5 V vs. Ag/AgCl).....	55
3.33 A schematic diagram of HPLC system with amperometric detector.....	58
3.34 A Teflon version of channel electrode.....	58
3.35 Signals of MG (5.38 $\mu$ M) and LMG (15.13 $\mu$ M) standard solution obtained from HPLC system (C18 column) using BDD electrode as an amperometric detector. The calibration curve of both compounds also shown in the inset (Linear Range <sub>MG</sub> 50 nM – 10 $\mu$ M, Linear Range <sub>LMG</sub> 0.15 $\mu$ M – 30 $\mu$ M; R <sup>2</sup> <sub>MG</sub> 0.998, R <sup>2</sup> <sub>LMG</sub> 0.999).....	59
3.36 A chromatogram of spiked sample using preparation procedure from the literatures to eliminate the matrices. The signals of both malachite green and leucomalachite green can be clearly observed.....	60

<b>figure</b>	<b>page</b>	
4.1	Schematics diagram on the mechanism of oxide formation on gold metal. Region I represents the state of gold surface when no potential is applied. Region II shows the adsorption of the OH <sup>-</sup> layer onto the gold surface. Region III represents the replacement turnover of oxygen layer underneath gold layer and another OH <sup>-</sup> layer on top. (white circle = gold atom, gray circle = OH <sup>-</sup> ion and black circle = oxygen atom).....	63
4.2	Cyclic voltammogram of bare gold electrode in 1 mM sulfuric acid. Scan rate = 20 mV/s (vs. SMSE).....	64
4.3	The contact angle measurements of the water droplet on gold surface. A) bare gold, B) decanethiol-modified electrode.....	65
4.4	A set of sequential cyclic voltammograms for a decanethiol-modified gold electrode recorded at a scan rate of 20 mV/s in 10 mM H <sub>2</sub> SO <sub>4</sub> . Inset: Charge calculated from area under the reduction peak for sequential cycles.....	67
4.5	Cyclic voltammograms of decanethiol-modified electrode (solid line) and bare gold electrode (dashed line) recorded at a scan rate of 20 mV/s in 10 mM H <sub>2</sub> SO <sub>4</sub> .....	68
4.6	Schematic diagram of the integrated waveguide sensor chip used in EC-SPR instrument.....	70
4.7	Schematic diagram of EC-SPR instrument.....	71
4.8	Simultaneous signals of cyclic voltammetry (solid line) and SPR transmission (dashed line) recorded from a bare evaporated gold electrode (1 mm long) in 10 mM H <sub>2</sub> SO <sub>4</sub> at 20 mV/s.....	72
4.9	The set of sequential cyclic voltammograms (solid lines) and simultaneous measurement of the SPR transmission (dashed lines) showing the oxidative desorption of decanethiol from the evaporated gold electrodes recorded at 20 mV/s in 10 mM H <sub>2</sub> SO <sub>4</sub> . The signals were obtained from a 2 mm (A) and a 1 mm long electrode (B).....	74
4.10	The SPR transmission at 0.0 V plotted against the fractional coverage of the thiol calculated from the charge for the oxide stripping.....	76

## LIST OF ABBREVIATIONS AND SYMBOLS

EC-SPR	Electrochemical – Surface Plasmon Resonance
HPLC	High Performance Liquid Chromatography
FIA	Flow Injection Analysis
GC	Glassy Carbon Electrode
BDD	Boron-Doped Diamond Thin-Film Electrode
SPE	Solid-phase extraction
Au	Gold
mg	milligram
mL	milliliter
kg	kilogram
$\mu\text{m}$	micrometer
$\mu\text{L}$	microliter
i.d.	Internal diameter
o.d.	Outer diameter
$R^2$	Correlation coefficient
LOD	Limit of Detection
TLC	Thin-Layer Chromatography
CE	Capillary Electrophoresis
FIA	Flow injection analysis
MG	Malachite Green
LMG	Leucomalachite Green
BAS	Bioanalytical System, Inc.
WE	Working Electrode
RE	Reference Electrode
CE	Counter Electrode
Ag/AgCl	Silver / Silver Chloride Reference Electrode
SMSE	Saturated Mercury / Mercurous Sulfate Reference Electrode
$i$	current (A)
$i_{pa}$	anodic peak current (A)
$i_{pc}$	cathodic peak current (A)



$E_{pa}$	anodic peak potential (V)
$E_{pc}$	cathodic peak potential (V)
$E_{det}$	Detection potential (V)
$E_{oxd}$	Oxidation potential (V)
$E_{red}$	Reduction potential (V)
TM	Transverse Magnetic
TE	Transverse Electric



สถาบันวิทยบริการ  
จุฬาลงกรณ์มหาวิทยาลัย

# CHAPTER I

## INTRODUCTION

### 1.1 Cost-Effective Instrumentation

Cost-effectiveness should always be taken into consideration when performing an analysis. Apart from analytical characteristics such as accuracy, precision, selectivity and sensitivity, the cost of an instrument including the cost of system maintenance should also be taken into account when only a limited budget is available. Since the cost of some commercial instruments are very expensive. The use of the homemade version of these instruments would be an ideal alternative choice, especially for those with economical problems.

Electrochemical approach is also considered a relatively low-cost instrumentation. Electrochemistry is an ideal analytical tool for the determination of analyte both qualitatively and quantitatively. It can be used to study some electrochemical properties of an analyte such as conductivity and the rate of the electrochemical reactions. The word 'Electroanalysis' means the use of electrochemistry in an analytical context. Basically, the two electroanalytical observables are the potential (also called the voltage) and the current (or its integral with respect to time, defined as charge).

Another interesting technique is flow injection analysis (FIA), which is first introduced by Ruzicka and Hansen in 1975. This technique offered the cost-effectiveness along with high efficiency for various routine analysis and automation system. FIA is based on the injection of a sample solution into a stream of suitable liquid. The injected sample forms a zone, then moves toward a detector that is continuously recording. The signal response could be an absorbance, electrode potential, electrical current or other physical parameters as it continuously changes due to the passage of the sample through the flow cell.

In a typical research group, which has many researchers and students working in the same laboratory. The use of individual flow cell would be the best way to prevent a cross – contamination problem. Unfortunately, the commercial flow cell available in the market is very expensive despite the design is quite simple. Many research groups are unable to afford such cost. Making of some cost – effective flow cell would be a logical choice for this situation.

Flow cell can be used for many purposes. One of the most popular objectives is to use the flow cell as a detector especially in flow-based electrochemical technique. This detector comprises a flow cell and a couple of electrodes. An analyte flows into this part then the electrochemical reaction takes place. The flow cell equipped with some excellent performance electrode, *e.g.* boron-doped diamond thin-film (BDD) electrode, can be used as an amperometric detector for a determination of some toxic residues in food additive or pharmaceutical industry.

Malachite green (MG) is one of the most extremely effective against protozoal and fungal infections in the aquaculture industry. It's also used as a food coloring agent, food additive, a medical disinfectant as well as a dye in silk, wool, leather, cotton and paper. It has been reported to cause carcinogenesis and respiratory toxicity. Many countries concern about the residues of malachite green and its reduced form, which is leucomalachite green (LMG). The use of malachite green has been banned in many countries and not approved by US Food and Drug Administration. Therefore, many methods including electrochemistry techniques have been developed for the detection of MG and LMG at low levels. However, an electroanalysis of these compounds at boron-doped diamond thin-film electrode has never been reported before. The used of flow cell equipped with BDD electrode as an amperometric detector for determination of MG and LMG is first reported in this research.

In some particular cases, the flow cell can be used as an interface for some hyphenated techniques, such as those seen in an electrochemical – surface plasmon resonance (EC-SPR) instrument. A stand-alone SPR instrument is a powerful surface-sensitive instrument capable to investigate a very thin film that deposit on metal surface. An analyte could be an oxide film, spin-coated organic polymer or a very thin film, which is produced by self-assembled monolayer (SAM) technique.

A combination of SPR with electrochemical technique offers more information of analyte. Both electrochemical and optical signals can be simultaneously observed in real time. Many EC-SPR instruments have been developed but mostly based on Kretschmann configuration. The investigation of decanethiol-SAM on gold surface using waveguide-based EC-SPR instrument is reported in this research.

## 1.2 Objective of the Research

Due to an expensive cost of the commercial flow cells available in the market. This research aims to design and construct the cost – effective flow cells for the hydrodynamic system. Moreover, the fabricated flow cell can be applied with some other techniques. This dissertation described two main applications:

- (i) Development of an amperometric detector for the determination of malachite and leucomalachite green in FIA system using boron-doped diamond thin-film electrode.
- (ii) Electrochemical – Surface Plasmon Resonance sensing of thiol containing compounds on gold electrode.

สถาบันวิทยบริการ  
จุฬาลงกรณ์มหาวิทยาลัย

## CHAPTER II

### THEORY

#### 2.1 Electrochemical Method<sup>1,2</sup>

##### *2.1.1 Measurement of potential*

Electrochemist usually measures potentials with a voltmeter, or any device capable of replicating the behavior of an accurate voltmeter. Normally, the potential is measured under equilibrium conditions (the measurement is performed at zero current). The high-impedance voltmeter is used in order to minimize the error caused by the resistance of the solution (which is called the IR drop).

##### *2.1.2 Measurement of current*

The current can be measured by using an ammeter, or any device capable of acting as an ammeter. In oxidation reaction, electrons are given away by the electroactive species:



The electron as a product of this equation will be collected by an electrode. The other type of redox reaction that can occur is the reverse of oxidation, in which electroactive specie receives an electron in a reduction reaction.

Redox changes will always accompany current passage because each electron is used to perform an electrochemical reaction. The number of electron passed is a direct proportion to the amount of analyte. A large number of electrons consumed or given imply that a large amount of an analyte has been electrochemically modified during the current passage. In summary, the passage of current indicates the changes in composition inside an electrochemical cell. Based on the explanation above, the potential measured at zero current imply that no compositional changes inside the electrochemical cell.

In the electrochemist point of view, a measurement that accompanies compositional changes is dynamic, while a measurement that is performed without compositional changes occurring is static or at equilibrium.

### 2.1.3 Potentiometry

Techniques that measure the potentials of electrochemical cells are called potentiometry. These measurements are performed with a little or no current. Potentiometric methods require a working electrode, a reference electrode and a device for measuring the potentials. Potentiometry is the most widely used in analytical technique because of its simplicity, versatility and low cost. It is used to detect analyte in titration, biological fluids, etc. However, the potentiometric methods play a minor role in electrochemical detection for HPLC system.

### 2.1.4 Voltammetry

Voltammetry is one of the electroanalytical techniques that measures the current as a function of potential. Voltammetry is typically comprised of three electrodes: working electrode (WE), reference electrode (RE) and counter electrode (CE). The potential is applied to the working electrode as a function of time, and then the signal in the form of current as a function of potential obtained is called voltammogram. The most common waveforms used in voltammetry are shown in Figure 2.1.

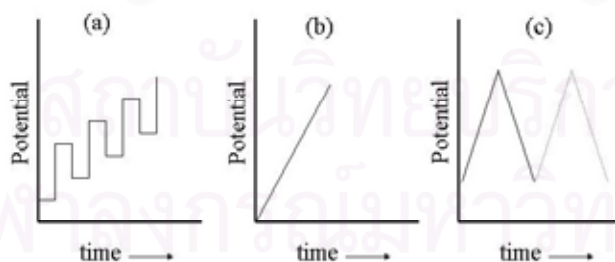


**Figure 2.1** Potential-time waveforms are used in various electroanalytical techniques. Waveforms based on (a) square, (b) linear, and (c) triangular potential-time patterns are used in square wave, linear sweep, and cyclic voltammetry, respectively.

### 2.1.5 Cyclic voltammetry

Cyclic voltammetry (CV) is a powerful electroanalytical technique for the study of electroactive species. The current at the working electrode is monitored, while the potential is applied in a triangular waveform to the electrode. The resulting voltammogram can be analyzed for fundamental information regarding the redox reaction. The potential at the working electrode is controlled relatively to that of a reference electrode. The controlling potential applied across the working electrode and the counter electrode is the excitation signal. Then the potential is scanned in reverse, causing a negative scan back to the original potential to complete the cycle. Single or multiple cycles can be used on the same surface. A cyclic voltammogram is the plot of the response current at the working electrode vs. applied excitation potential. When the potential is applied, electroactive species will approach the electrode surface. This movement, known as mass transport, occurs via three separate mechanisms, namely migration, convection and diffusion. Basically, if a solution is quiescent and contains supporting electrolyte, then electroactive species will approach the electrode surface by diffusion mode only

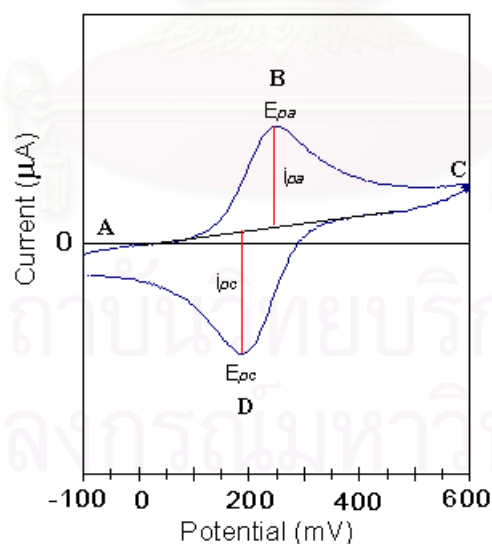


**Figure 2.2** The current-potential (i-E) plot is called a cyclic voltammogram.

The current-potential (i-E) plot is called a cyclic voltammogram (Fig. 2.2). The significant parameters in cyclic voltammogram are the cathodic peak potential ( $E_{pc}$ ), the anodic peak potential ( $E_{pa}$ ), the cathodic peak current ( $i_{pc}$ ), and anodic peak current ( $i_{pa}$ ).

### 2.1.6 Amperometry

Amperometry is an electrochemical technique in which a constant potential is applied at the working electrode. A simple potential-time waveform for amperometry is shown in Figure 2.3. At the potential applied, the analytes underwent an oxidation or reduction at the electrode. The current responses are directly proportion to the concentration of the analyte. The major drawback of amperometry is the lack of reproducibility because of some adsorption of detection products and/or impurities on the electrode surface. To obtain reproducible results, during analysis the electrode surface must often be cleaned by polishing or performing electrochemical process.

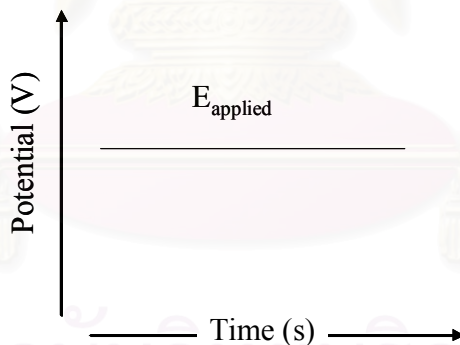


**Figure 2.3** Amperometry (E-t) waveform



### 2.1.7 Hydrodynamic System

Hydrodynamic voltammetry differs from a normal voltammetry in term of mass transport mode. A principal mode of mass transport in the typical voltammetry is diffusion. Mass transport by migration is minimized by adding an inert ionic salt to the sample solution and convection is totally eliminated by keeping the solution still (quiescent). In hydrodynamic system, the principal mode of mass transport is convection. Mass transport by migration can be eliminated by the same way as in the typical voltammetry. Mass transport by diffusion can never be totally eliminated if there are differences in concentration throughout the solution (e.g. as cause by current flow), but convection is such an effective form of mass transport when compared with either migration or diffusion. In hydrodynamic system, convection can arise from the movement of the electrode or flowing the solution past the electrode surface. Convection is only effective in order to bring electroactive species to the electrode surface faster where the concentration gradient already occurred. In electrochemistry, the concentration gradients always occur in the boundary layer close to the electrode surface. When convection is present in the system, current densities will be 3-100 times greater than the steady state diffusion limit

## 2.2 Flow Injection Analysis

The concept of flow injection analysis (FIA) was introduced by Ruzicka and Hansen in 1975<sup>3</sup>. This technique is based on the injection of a liquid sample into a moving stream of a suitable carrier solution. The zone of injected sample is formed in a narrow tube and then transported toward a detector. In order to propel the carrier solution through a narrow tube, a pump is used as a propelling device. The analyte of interest is then detected and the detector response such as absorbance, electrode potential or current is recorded as it continuously changes due to the movement of the analyte sample through the flow cell.

The schematic diagram in Fig. 2.4 groups the FIA process into three stages to help visualize how the FIA performs a method or analysis.

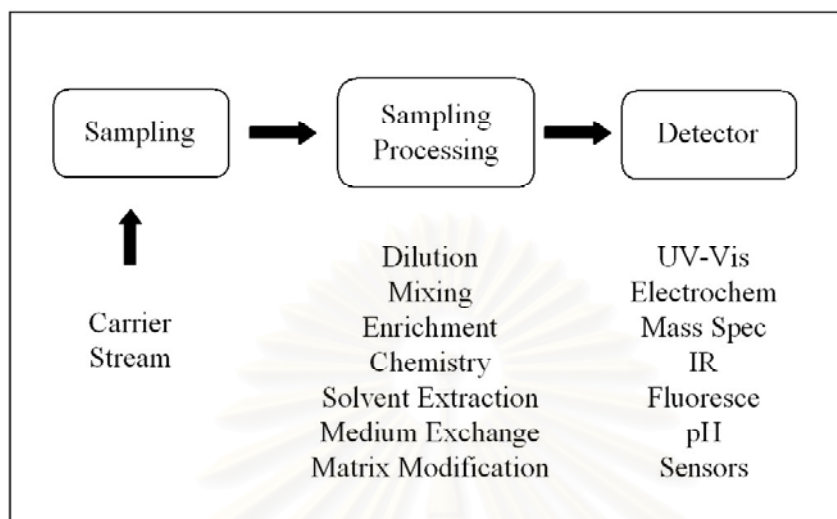


**Figure 2.4** Schematic diagram of a generic description of FIA

The first step is sampling where the sample is injected into the flowing carrier stream. This step is generally performed with a sample injection valve. The second stage is called sample processing. The purpose of this step is to transform the analyte into a species that can be measured by the detector and manipulate its concentration into a range that is compatible with the detector, using one or more of the indicated processes. The third stage is detection where the analyte, or its derivative, generates a signal, which is used for quantitative analysis. As indicated, a large variety of detectors can be used in FIA system.

The FIA manifold can be designed in order to obtain the best analytical results. The simplest FIA manifold is the single-line FIA manifold. In this case, the sample solution is rigorously and precisely transported to the flow cell in undiluted form. The example of the single-line FIA manifold is shown in Fig 2.5.

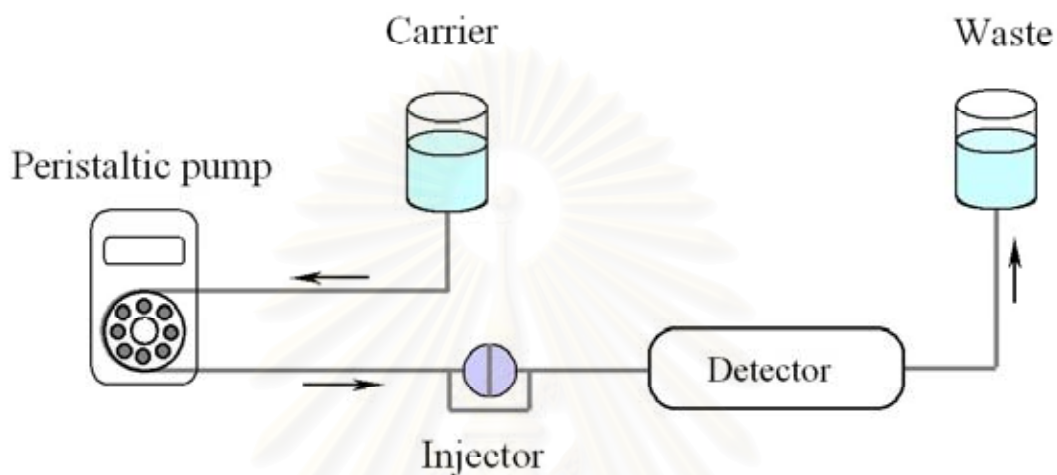


**Figure 2.5** Single-line FIA manifold

The power of FIA as an analytical tool lies in its ability to combine these analytical functions in a wide variety of different ways to create a broad range of different methodologies, and perform these methodologies rapidly and automatically within a few minutes and with low amount of sample.

The thin-layer cell design is commonly used as an amperometric detector for liquid chromatography. An electrochemically active substance passes over an electrode held at a potential sufficiently great (positive or negative) for an electron transfer (either oxidation or reduction) to occur. An amperometric current is produced that is proportional to concentration of analyte entering the thin-layer cell.

## 2.3 Flow Cell Configurations<sup>4</sup>

### 2.3.1 Channel Electrodes (Thin-layer)

Channel electrodes configuration relies on the thin-layer of the solution that flows parallel over the planar electrode surface (Fig. 2.6). In theory, the electrode material is embedded in the insulator. It is solid and absolutely immobile. Since the electrode surface is flush with the surrounding insulator, the incidence of turbulent flow is inhibited. In addition, the electrode is polished to prevent turbulence.

The relationship between limiting current, flow rate and cell geometry is given by this equation:

$$I_{lim} = 0.925nFD^{2/3} [V_f/h^2d]^{1/3} wX^{2/3} C_{analyte} \quad (2.2)$$

Where

$I_{lim}$  = limiting current,  $n$  = number of electron,

$F$  = Faraday constant,  $D$  = diffusion coefficient,

$V_f$  = volume flow rate,  $h$  = internal height of the channel,

$X$  = length of the electrode,  $d$  = internal width of the channel,

$w$  = width of the electrode,  $C_{analyte}$  = concentration of analyte

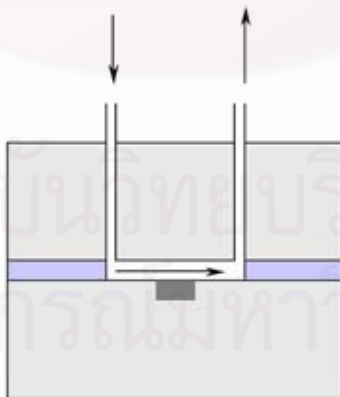


**Figure 2.6** Schematic Diagram of Channel Electrode. The arrows indicate the flow direction.

### 2.3.2 Wall-jet Electrodes

In the wall-jet configuration (Fig. 2.7), the solution stream from the nozzle flows perpendicularly onto the electrode surface (“the wall”) then spreads out radially over the surface. Basically, the working electrode used in this configuration is circular (disc electrode) and flat. The current response is measured while the fine jet or spray of analyte solution is squirted under relatively high pressure towards the center of the working electrode. In order to prevent splash back, the nozzle diameter should be narrow (not larger than 10% of the working electrode). The distance between the nozzle and the electrode surface is critical, i.e. it must not be either too short or too long.

The limiting current at the wall jet electrode is given by the following equation:

$$I_{lim} = 1.59knFD^{2/3}u^{-5/12} a^{-1/2} r^{3/4} V_f^{3/4} C_{analyte} \quad (2.3)$$

where

$I_{lim}$  = limiting current,  $n$  = number of electron,

$F$  = Faraday constant,  $D$  = diffusion coefficient,

$V_f$  = volume flow rate,  $k$  = a combination of constant,

$u$  = kinematic viscosity of solution,  $a$  = diameter of the jet,

$r$  = radius of the electrode,  $C_{analyte}$  = concentration of analyte

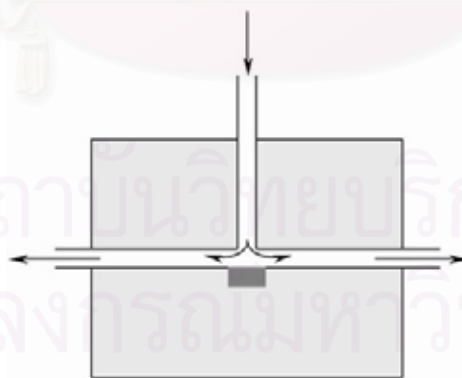


**Figure 2.7** Schematic Diagram of wall-jet Electrode. The arrows indicate the flow direction.

## 2.4 Surface Plasmon Resonance<sup>5,6</sup>

### 2.4.1 Evanescent Wave

When total internal reflection occurs at the interface, there is interference between the incident and reflected rays of light. This results in a standing wave as shown in Fig. 2.8. There would be one of these standing waves at each point of internal reflection. These standing waves are associated with a very important quality that is basis for many sensing applications. Vector analysis of the waves at the points of reflection show that an intensity component extends beyond the edge boundary. This extension of light intensity is referred to as the evanescent wave.

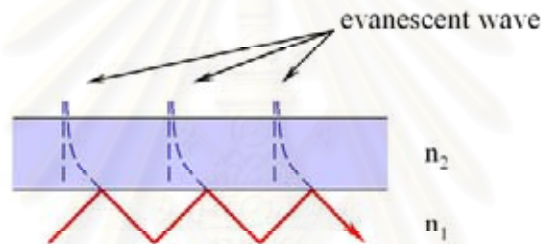


**Figure 2.8** Schematic Diagram of evanescent wave. The energy field extends beyond the point of internal reflection

### 2.4.2 Surface Plasmons

Metals have often been described as seas of electrons. That concept is useful when describing surface plasmons. One can envision a surface wave created by an oscillating electrical charge on the surface of the metal. This oscillating charge density is called plasmon. The surface plasmons can be excited by light or by electron beams. The most useful are plasmons excited by evanescent waves.

The usual Kretschmann configuration is shown in Fig. 2.9. Light undergoes total internal reflection so that the evanescent wave interacts with thin metal film on the surface of the prism. Silver and gold have the highest optical constant for this purpose. The incidence angle of coherent, TM polarized light is varied. At some particular angle

the electric vector of the incident light induces a resonance with the surface plasmons. This is known as surface plasmon resonance.

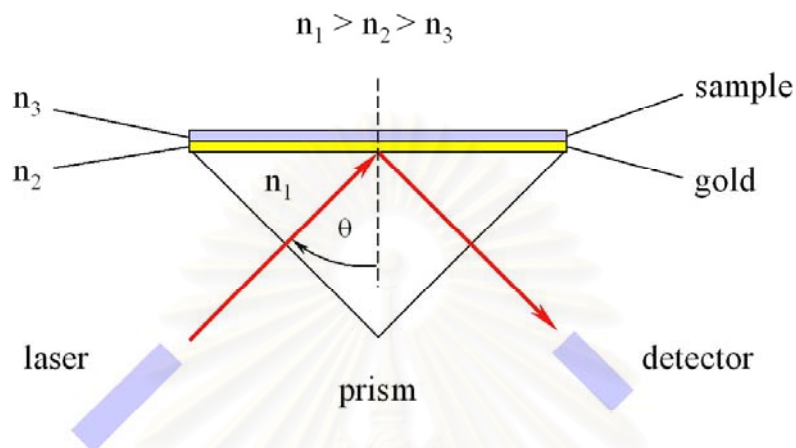


**Figure 2.9** Schematic diagram of the Kretschmann configuration:  $n_1$ ,  $n_2$  and  $n_3$  are the refractive indices of glass prism, metal layer and sample layer, respectively

If a thin film of differing dielectric is immobilized on the opposite metal surface, the evanescent wave of the surface plasmon couple to that layer. Chemical changes in that film then modulate the reflected light from the prism. The reflected light is monitored and the resonance condition is indicated by decreasing intensity of the reflected light as a function of incident angle (Fig. 2.10). The angle at which the minimum occurs is referred to as SPR angle. For example, a resonance valley would occur at one angle of incident for the bare gold surface, whereas the SPR angle would shift when an organic film adsorbed on the gold.

จุฬาลงกรณ์มหาวิทยาลัย

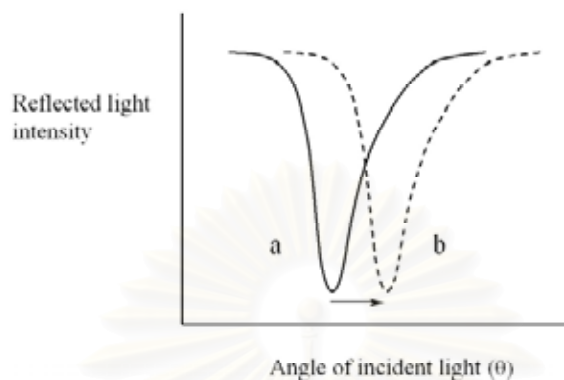


**Figure 2.10** The shift resulting from the effect of the layer on the signal. The reflected light is monitored and the resonance condition is indicated by decreasing intensity of the reflected light as a function of incident angle.

#### 2.4.3 Waveguide-Based Configuration

There are many designs of instrument in the general area of SPR, but the principle of total internal reflection still applies for many of these configurations since the involvement of the evanescent wave. One of those configurations based on an optical waveguide (as shown in Fig. 2.11). The measurement is operated at a fixed angle. The chemical changed on the top of the gold surface will cause the change in the reflected intensity. This waveguide-based configuration can be applied with other techniques especially the electrochemistry as described in this research. The evaporated gold film on the waveguide itself can be used as working electrode.



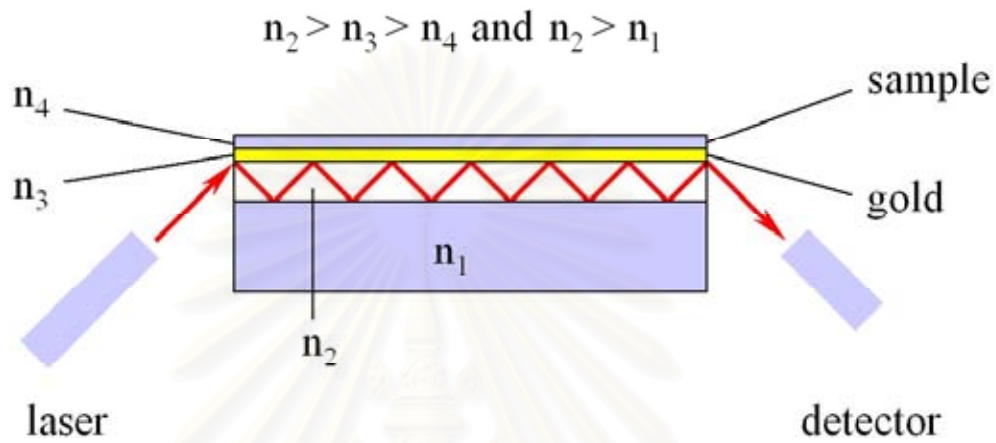


**Figure 2.11** Schematic diagram of the waveguide-based configuration:  $n_1$ ,  $n_2$ ,  $n_3$  and  $n_4$  are the refractive indices of glass substrate, optical channel, metal layer and sample layer, respectively.

สถาบันวิทยบริการ  
จุฬาลงกรณ์มหาวิทยาลัย

## 2.5 Self-Assembled Monolayer (SAM): Reviews

Self-assembled monolayer (SAM) technique provides a powerful tool to generate monomolecular films of organics or biological molecules on a variety of substrates. The formation of such monolayer systems is extremely versatile and can provide a method for the development of bio-surfaces, which are able to mimic naturally occurring molecular recognition processes. SAMs also provide a reliable control of the packing density at a substrate surface.

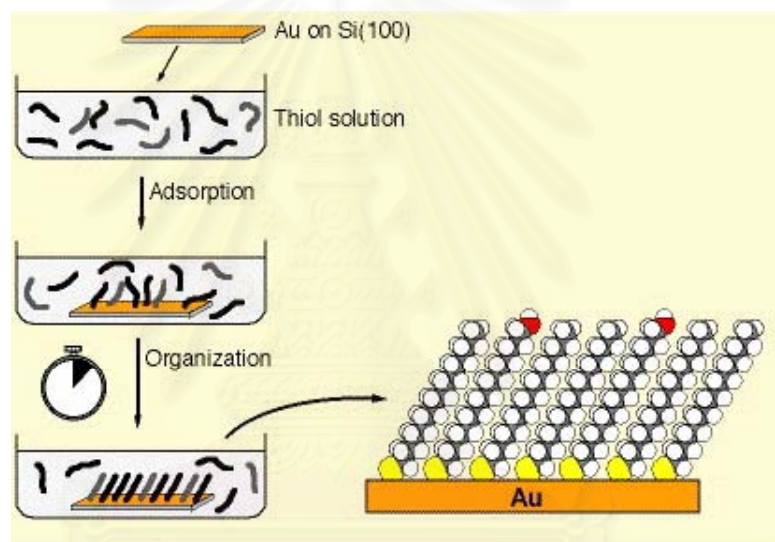


**Figure 2.12** Schematic Diagram of Self-Assembled Monolayer on Gold Surface.

SAMs can be prepared using different types of molecules and different substrates. Most of the works in analytical applications have concentrated on SAMs of functionalized alkanethiols on gold surfaces (Fig. 2.12). The principle is simple. A molecule, which is essentially a normal alkane chain, typically with 10-20 methylene units, is given a head group with a strong preferential adsorption to the substrate used. Thiol (S-H) head groups and gold substrates have been shown to work excellently. The thiol molecules adsorbed from diluted solution onto the gold, create a dense monolayer with the tail group pointing outwards from the surface. By using thiol molecules with

different tail groups, the resulting chemical surface properties can be varied within wide range.

The adsorption and organization of molecular SAMs on substrate surfaces has been the subject of extensive research. This technique plays an important role in many fields of chemistry, especially in analytical applications<sup>7</sup>. SAMs technology also provides a powerful tool to generate monomolecular films of biological molecules on a variety of substrates<sup>8, 9</sup>. The formation of such monolayer systems is extremely versatile and can provide a method for the development of biosurfaces or biosensor, which are able to mimic naturally occurring molecular recognition processes. Redox enzymes assembled in a monolayer on a solid surface by a potential-assisted self-assembly method as well as a thiol-gold self-assembly method have been reported. These enzymes communicate electronically with the solid substrate through a molecular interface conducting polymer and a covalently bound mediator<sup>10</sup>. Covalently immobilized of phospholipids and enzymes, such as cytochrome c, cytochrome c oxidase and horseradish peroxidase (HRP), to SAMs of 3-mercaptopropionic acid on gold electrode has also been reported<sup>11</sup>. The covalent immobilization of enzymes with alkanethiols has the very attractive feature of providing generic immobilization technologies<sup>12</sup>. A variety of surface based detection principles have been employed for biochips<sup>13</sup>.

Molecular interactions occurring at biomolecular monolayer surfaces can be studied using a wide range of analytical techniques such as: surface plasmon resonance (SPR)<sup>14-18</sup>, atomic force microscopy<sup>19</sup>, quartz crystals microbalance (QCM)<sup>20</sup>, temperature programmed desorption (TPD)<sup>21</sup>, electrochemical techniques, e.g. cyclic voltammetry (CV) and amperometry<sup>22, 23</sup>. Electrochemical characteristic of SAMs on gold have been widely studied during the past 15 years. Most of the works has been focused on alkanethiol SAMs. Monolayer transient total capacitance as well as differential capacitance changed during the CV scans in the presence of redox probes were studied simultaneously. The transient capacitive currents of dynamic processes of redox reaction were related to the electrochemical behavior of a monolayer<sup>24</sup>. Critical thermal variation of displacement of hexadecanethiols has also been investigated by a measurement of a capacitance changed under cyclic scanning variations of temperature<sup>25</sup>.

The structure and growth of two classes of self-assembled monolayers (SAMs)

on gold derived from the adsorption of the functionalized thiol hexyl azobenzenethiol (12-(4-(4-hexylphenylazo) phenoxy) dodecane-1-thiol) and the partially fluorinated alkanethiols  $\text{CF}_3(\text{CF}_2)_9(\text{CH}_2)_{11}\text{SH}$  and  $\text{CF}_3(\text{CF}_2)_7(\text{CH}_2)_6\text{SH}$  were examined. The structural properties of the SAMs were strongly influenced by the interactions between the functional groups comprising the tails of the molecules<sup>26</sup>. Competing interaction of different thiol species on gold surfaces show very interesting properties. The possibilities of creating mixed thiol films, consisting of aliphatic hexadecanethiol and the aromatic 2-mercapto-benzothiazol (MBT) have been investigated. The interaction of both species after successive adsorption on gold was investigated using XPS<sup>27</sup>.

Structural disorder of octadecyl mercaptan SAM has been investigated by cyclic voltammetry and electrochemical impedance spectroscopy (EIS). CV experiments show that well-assembled thiol monolayers on gold are essentially free of pinhole defects<sup>28</sup>. Monolayers and bilayers self-assembled on metal electrodes have also been reported. Three types of aliphatic thiols, *n*-dodecanethiol, *n*-hexadecanethiol and *n*-octadecanethiol, were tested as the sub-layer for the adjacent phospholipids layer<sup>29</sup>. Electron transfer kinetics across a self assembled dodecanethiol monolayer between  $[\text{Fe}(\text{CN})_6]^{3-/4-}$  and a gold electrode has been investigated using electrochemical impedance spectroscopy (EIS) at various negative dc potentials relative to the formal potential of the  $[\text{Fe}(\text{CN})_6]^{3-/4-}$  couple<sup>30</sup>.

Many electrochemical studies of aromatic containing monolayer or other molecules such as 4-mercaptobiphenyl<sup>31</sup>, aminothiophenol<sup>32</sup>, 6-mercaptapurine<sup>33</sup>, *N*-benzyl-1,4-dihydronicotinamide<sup>34</sup>, alkylthiolates<sup>35</sup>, carotenoid<sup>36</sup> and porphyrin<sup>37</sup> have also been reported. A self-assembled monolayer (SAM) on gold prepared from a binary mixture of a thiol analogue of thiocholesterol and a functionalized 11-mercaptoundecanoic acid has been investigated by voltammetry<sup>38</sup>.

## 2.6 EC-SPR Instrument: Reviews

The growing need for fast and sensitive sensors for the detection of biological molecules has led to a great deal of research in this field, resulting in a wide range of sensor designs. A common technique to be employed is surface plasmon resonance (SPR)

where a change in refractive index due to coupling of light to a surface plasmon mode formed at the metal/dielectric interface is measured<sup>39</sup>. The technique is extremely sensitive to changes in refractive index close to the sensor surface and has been exploited both commercially and in research for biosensor applications<sup>40, 41</sup>. In addition, electrochemistry is commonly employed as a transduction mechanism in biosensors<sup>42</sup>. Devices combining both SPR and electrochemistry were first demonstrated in the late 1970s<sup>43, 44</sup>. This has predominantly been achieved using the prism or Kretschmann configuration where a gold film acts as both the sensing region for SPR measurements as well as the electrode for electrochemical investigations<sup>43-47</sup>. For example Chao *et al.* used SPR and ellipsometry to study the electrochemistry of gold in sulfuric acid<sup>44</sup>. At that time Kötzt *et al.*<sup>43</sup> used the Kretschmann configuration to investigate the effects of the electrode potential in the double layer region on the surface plasmon resonance frequency for gold and silver electrodes in perchlorate solution. More recently Iwasaki *et al.* have used the Kretschmann configuration to study (111) oriented gold films and electrode reactions at gold surfaces<sup>45, 46</sup>. The Kretschmann configuration is limited to the study of thin evaporated metal films and to overcome this Tadjeddine *et al.* have used the Otto configuration which allows single crystal metal surfaces to be used, although this technique introduced other experimental difficulties<sup>48, 49</sup>. Both these systems are bulky and not well suited to multi-sensor operation. A number of studies have recently demonstrated the power of combining electrochemistry with planar waveguide structures – mostly using planar waveguides coated with a conducting tin oxide film<sup>50, 51</sup>. In contrast very few papers have described the use of integrated optical channel waveguide structures<sup>17, 18, 52</sup> where standard photolithography and ion-exchange are used to define the waveguides, despite the advantages of allowing more complex designs containing, for instance, reference channels, as well as allowing many devices on a single chip for multi-sensor operation. An additional advantage is the reduced size of the sensor and required sample volume. Abanulo *et al.* have recently demonstrated a combined waveguide SPR electrochemical device to study the electrochemical oxidation of a gold electrode surface<sup>18</sup>. Such a device has the potential to be used as a platform upon which to construct a variety of biological sensors. As a key first step in constructing such sensors it is necessary to derivatize the gold surface. This is commonly achieved by forming a self-

assembled monolayer of an alkanethiol, which can then be used to attach a variety of other molecules to the surface including enzymes and lipid monolayers. As a first step towards the fabrication of such sensors we have investigated monolayers of decanethiol self-assembled on the waveguide structure and their subsequent oxidative desorption<sup>53</sup>. Desorption of thiol has been studied extensively, with most work focusing on reductive desorption. Oxidative desorption has been studied in less detail and the exact mechanism for desorption process is not yet fully understood<sup>53-56</sup>.

## 2.7 Malachite Green and Leucomalachite Green: Reviews

Malachite green (MG), a triphenylmethane dye ( $C_{23}H_{26}N_2O$ ), is used as a fungicide, ectoparasiticide and antiseptic in the aquaculture industry. It is extremely effective against protozoal and fungal infections. Moreover, malachite green is also used as a food coloring agent, food additive, a medical disinfectant and anthelmintic as well as a dye in silk, wool, leather, cotton and paper. Now many countries concern about the residues of MG and its reduced form, leucomalachite green (LMG), because of toxicity of these dyes. It has been reported to cause carcinogenesis, mutagenesis, chromosomal fractures, tetragenicity and respiratory toxicity. The use of malachite green has been banned in various countries and not approved by US Food and Drug Administration<sup>57</sup>. Therefore, a number of methods have been developed for the detection of MG and LMG at low levels. The structures of MG and LMG are shown in Fig. 2.13.

Several methods have been described for the determination of MG and LMG in a variety of matrices, including liquid chromatography<sup>58-62</sup>, gas chromatography<sup>63</sup>, capillary electrophoresis<sup>64</sup>, visible spectrometry<sup>65</sup>, and spectrofluorometry<sup>66</sup>. HPLC is commonly used to detect MG and LMG with different detection techniques, such as visible<sup>67, 68</sup>, fluorescence<sup>69</sup>, mass spectrometry<sup>70-73</sup>, and electrochemical detection. Most of these methods use post-column oxidation of LMG to MG with lead (IV) oxide ( $PbO_2$ )<sup>74-77</sup>, or electrochemical cell are normally required<sup>78</sup>. These techniques need expensive apparatus and reagents as well as time-consuming. A sensitive, rapid and cheap method for analysis is still needed.

Electrochemical methods are widely used in many applications because they are simple, fast and economical. The electrochemical detection of MG has been reported using carbon fiber microelectrode<sup>79</sup> and Pt electrode as the working electrode. However, the sensitivity and reproducibility of these electrodes were poor because the electrode surface was contaminated by the fouling products and impurities. Boron-doped diamond thin film electrodes can be used to eliminate these problems. The unique properties of BDD electrodes are more attractive, including wide electrochemical potential window, very low background current and long-term stability of the responses<sup>80, 81</sup>. BDD electrodes have been successfully used for the detection of various analytes such as, captopril<sup>82</sup>, acetaminophen<sup>83</sup>, tiopronin<sup>84</sup>, lincomycin<sup>85</sup>, etc. There has been no report on using BDD electrodes for the detection of MG and LMG.

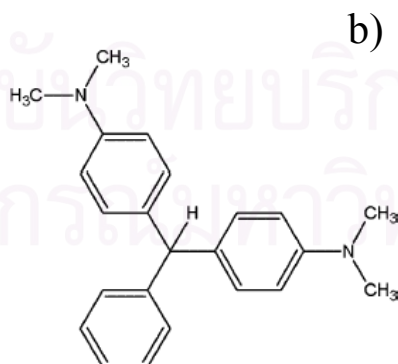
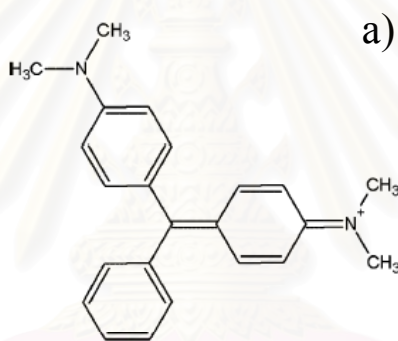


**Figure 2.13** Chemical structures of (a) MG and (b) LMG

## CHAPTER III

# ELECTROCHEMICAL DETECTION OF MG AND LMG

This chapter describes the design, fabrication and characterization of the flow cells. Three different configurations of the flow cell, wall-jet electrode, channel electrode and hybrid electrode, were designed and fabricated. Following the fabrication procedure, hydrodynamic experiments were carried out to examine the mass-transport behavior of each configuration. The experiment involved measuring the electrochemical response at a various flow rate. An electrochemical oxidation of malachite green and leucomalachite green at boron-doped diamond thin-film (BDD) electrode was studied by cyclic voltammetry. The fabricated flow cell equipped with BDD electrode was also used as amperometric detector in the flow injection analysis (FIA) and HPLC system.

### 3.1 Designs and Fabrications of the Flow Cells

The cell designs must fulfill the requirements of high signal-to-noise ratio, low dead volume, well-define hydrodynamics, small ohmic drop, and ease of fabrication and maintenance. In this research, all flow cell configurations were designed in almost the same geometry (e.g. electrodes position, dimension of the cell body) for ease of comparison. Except for some points, such as the inlet/outlet positions and a shape of gasket, which depend on a theory of each type. All electrodes and accessories can be interchanged between each configuration.

#### *3.1.1 Position of the Electrodes*

Because three-electrodes system is used in every configuration, it is important to properly assign the position for each electrode. As the current passed through the working electrode, then the current of the same magnitude (with an opposite sign) must pass through the counter electrode. Consequently, the counter electrode will be surrounded by the products of electrolysis. These products are not allowed to pass over the working



electrode since they might interfere with the current response. In order to ensure this criterion, the counter electrode was placed downstream.

Since the current is not allowed to flow through the reference electrode, it would not yield any products to contaminate the working electrode. By this reason, the reference electrode seems to be placed either upstream or downstream. But in fact, placing the reference electrode up stream can cause some problems. A breeding of an internal solution from the reference electrode itself can interfere with an analysis in some particular cases. In addition, if the connector between the reference electrode and the cell body has some void volumes, the analyte will be trapped inside and the tailing signal will be obtained. Moreover, if there is a leakage problem at this connector, some amount of analyte will dribble out of the chamber and cause a dilution effect. To prevent these kinds of problem, the reference was also placed downstream. All three electrodes were placed as close as possible in order to minimize the ohmic drop.

### *3.1.2 Materials*

Flow cell can be fabricated from several kinds of material. Glass would be a very first choice, especially for the electrochemical applications, due to its relatively high-chemical resistance. However, the fabrication of glass flow cell needs a proficient technician and a glassblower shop. Using of the polymer instead of glass would be an alternative choice. With a present technology, several kinds of polymer were produced for a various purpose. These polymers come along with the various chemical properties as well. Plexiglas, (Polymethylmethacrylate: PMMA), has a moderate chemical resistance but compatible with an aqueous system in the wide range of pH. This material is transparent, quite rigid and very easy to shape up by hand machining. Moreover, Plexiglas is not very expensive and can be purchased from a local hardware store.

In some applications such as non-aqueous electrochemistry or high performance liquid chromatography (HPLC), the flow cell body must be made from a higher chemical resistance material to avoid a swelling problem from organic solvent or mobile phase. Teflon (Polytetrafluoroethylene: PTFE) or Kel-F (Polychlorotrifluoroethylene: PCTFE) would be an ideal material in this regard.

### 3.1.3 Internal Chamber

Since a gold disc electrode ( $\varnothing$  3 mm with 10 mm Teflon body, Metrohm) was used to characterize the mass transport behavior, the chamber inside the flow cell was designed to be smaller than the size of the electrode body. This helps to minimize the possibilities of turbulence flows over the edge of the electrode. A silicone rubber and Teflon gasket used in this research were cut precisely. The opening area of the gasket must fit perfectly to the inlet and outlet. This helps to minimize the dead volume inside the chamber.

### 3.1.4 Tubing and Fitting

Each fabricated flow cell was equipped with Teflon tubing (1/16" OD, 0.75 mm ID). When the flow cell is used as a detector in FIA or HPLC system, a transfer line (PEEK microbore tubing, 1/16" OD, 0.05 mm ID, 8 cm in length) will be added in order to control the dispersion of sample prior to entering the flow cell. This part was added between the sample injection port and the cell body when used in FIA system. In case of HPLC, the transfer line was added between a separation column and the flow cell. All flow cell configurations were designed to adopt the same fitting size (1/4" – 28 UNF thread, flat bottom type, high pressure), which is one of standard LC adaptors.

## 3.2 Wall-jet Electrodes Configuration

The fabricated wall-jet electrodes configuration is shown in Fig.3.1-3.4. The flow cell was built by two Plexiglas blocks pressing a silicone rubber gasket (1mm in thickness) in the middle (see Fig.3.5 for details). The nozzle was placed at the center of the flow cell body perpendicularly to the working electrode (centrosymmetric design). The solution was sprayed directly onto the center of the electrode surface then spread out radially through the twin outlet cavities. The Ag/AgCl reference electrode and the counter electrode (made from stainless tube) were connected to one of these outlets. Both electrodes were placed as close as possible to each other in order to minimize the IR drop. Another outlet was directly connected to waste reservoir.

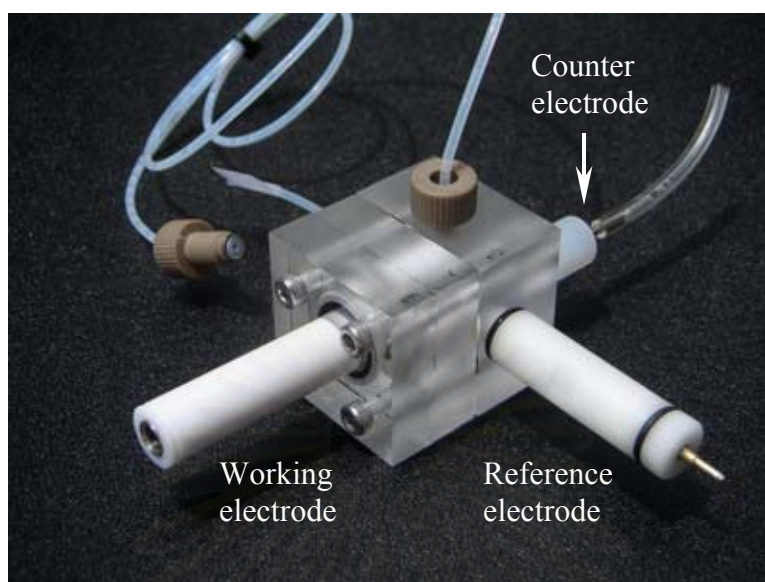


**Figure 3.1** The wall-jet flow cell (full assembled).

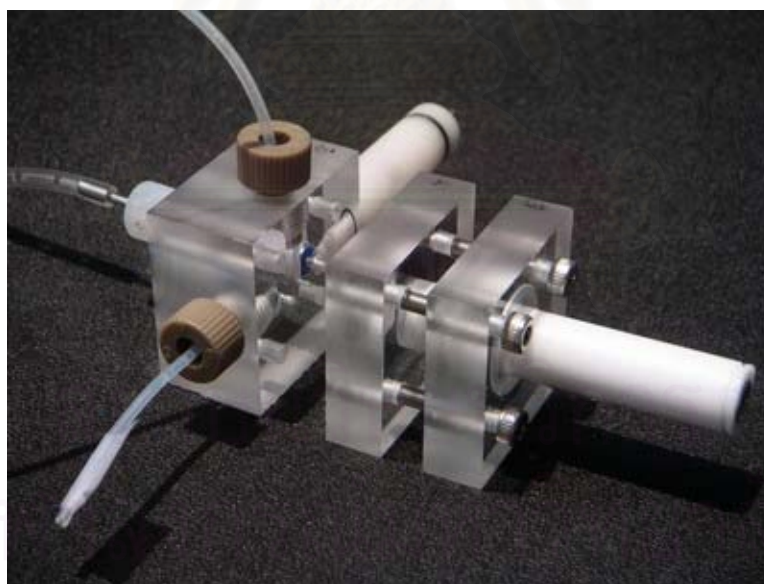


**Figure 3.2** The wall-jet flow cell (exploded parts).

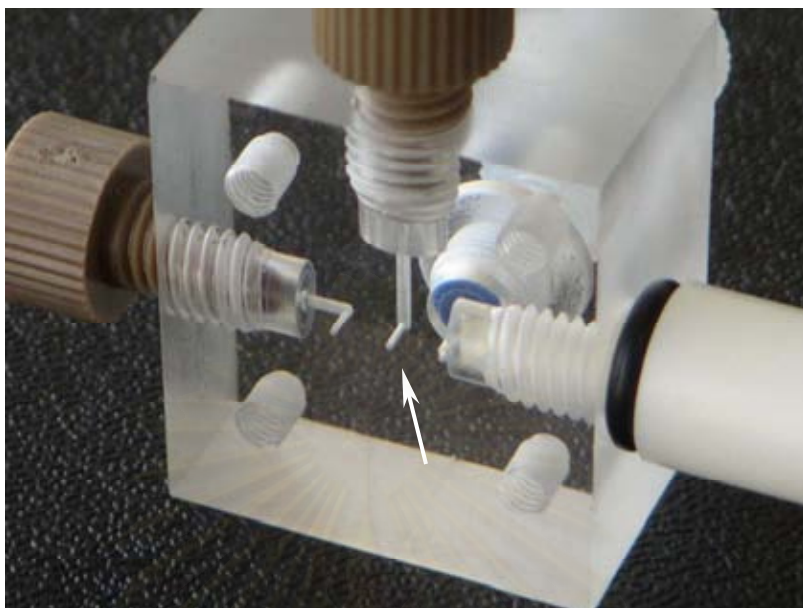


**Figure 3.3** The flow cell body. The nozzle was assign to be placed at the center.

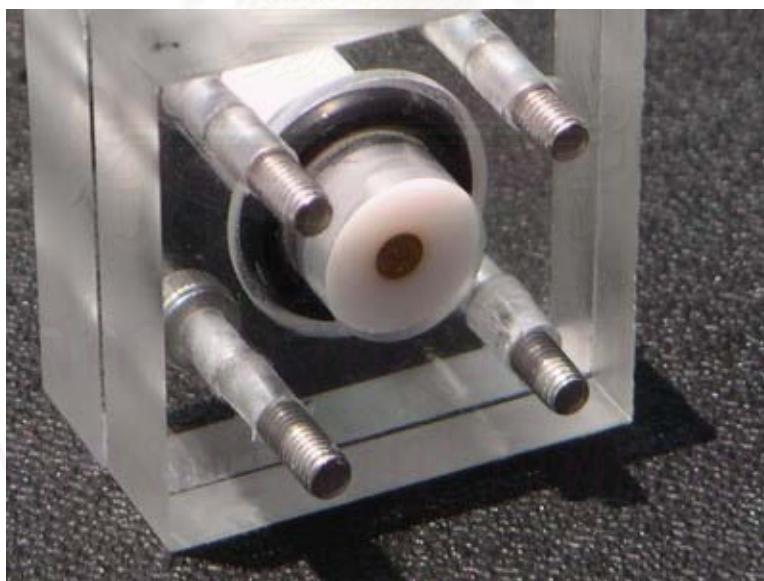


**Figure 3.4** The working electrode (3mm gold disc) on the opposite side.

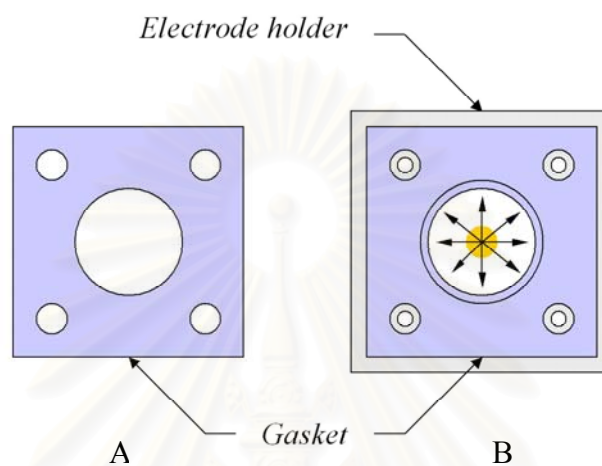


**Figure 3.5** (A) Shape of a gasket used in the wall-jet electrode. (B) The gasket was placed on top of an electrode holder with the gold electrode in the middle. An opening area in the middle of the gasket must be smaller than the electrode body. The arrows in the center represent the directions of the sample stream after impacting the electrode surface.

### 3.3 Channel Electrodes Configuration

The flow cell was constructed in the same manner as described in wall-jet configuration. This configuration has one inlet and one outlet as shown in Fig. 3.6 - Fig. 3.8. The Ag/AgCl reference electrode and the counter electrode were connected to the outlet. Solution from inlet flowed parallel to the surface of working electrode, then passed through the outlet (see Fig. 3.9 for details on the gasket).

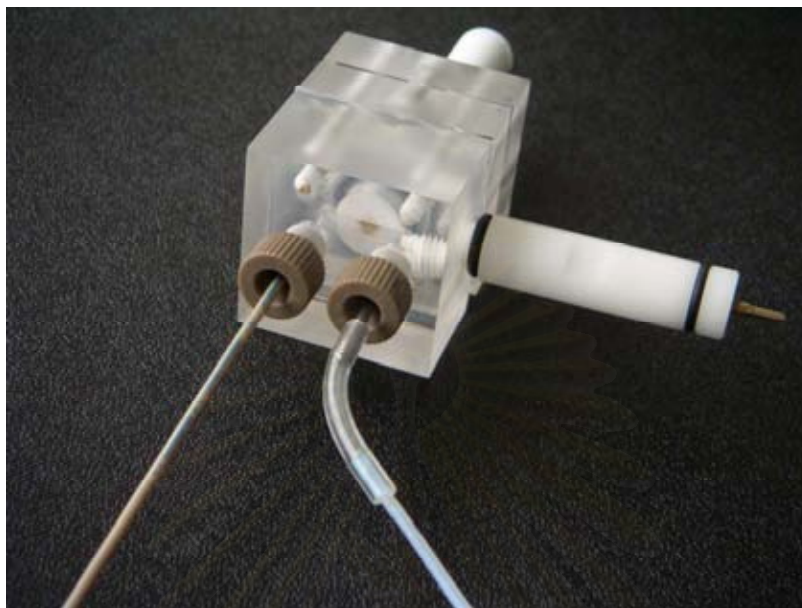


**Figure 3.6** The channel electrode has one inlet (brown tube) and one outlet (stainless tube).

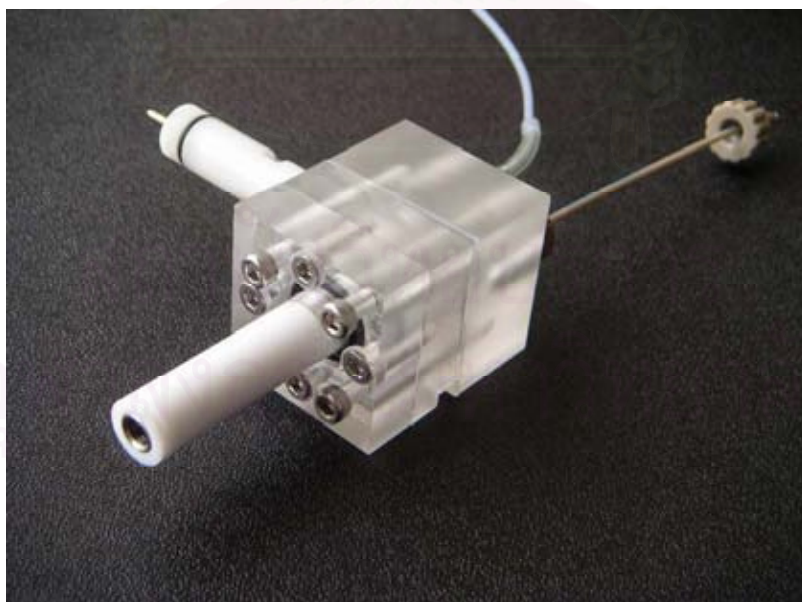


**Figure 3.7** The channel electrode (back view).

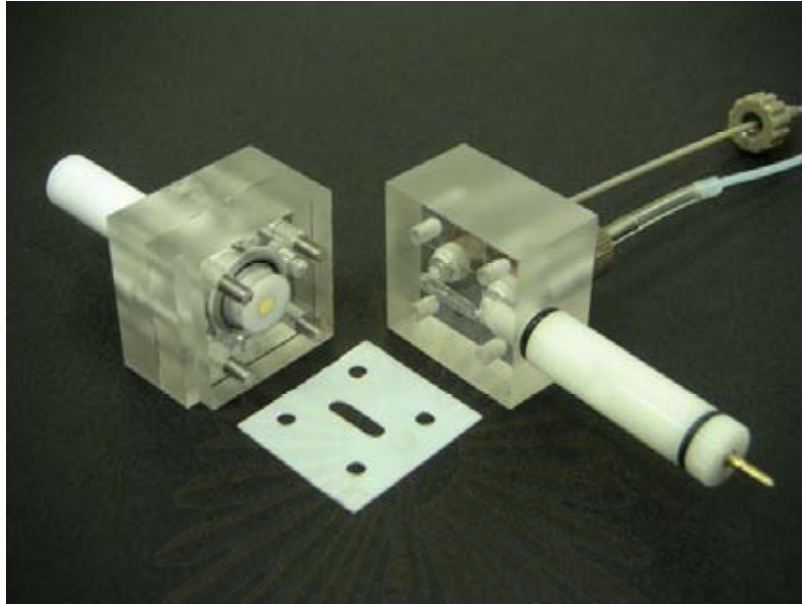


**Figure 3.8** The channel electrode. The electrode holder (left) and the cell body (right)

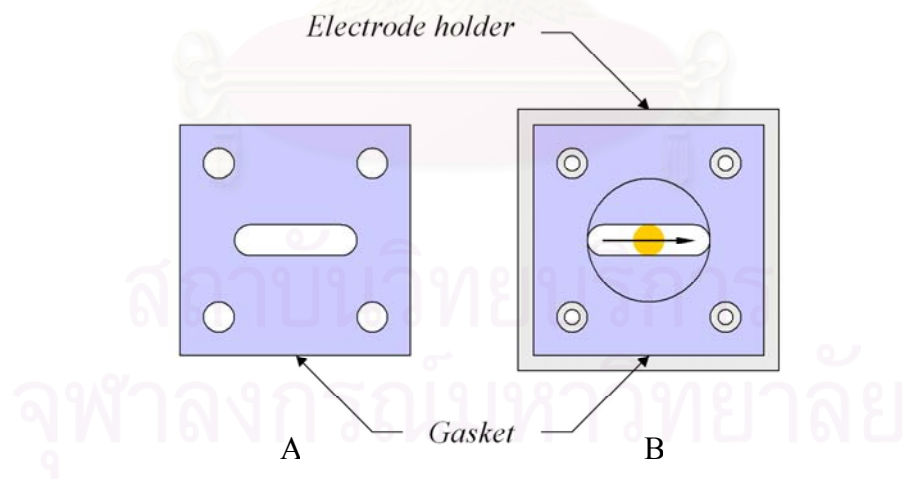


**Figure 3.9** (A) Shape of a gasket used in channel electrode. (B) The gasket was placed on top of an electrode holder with the gold electrode in the middle. An arrow in the center represents direction of the sample stream.

### 3.4 Hybrid Electrodes Configuration

Another approach combined the features of both channel electrode and the wall-jet configuration, known as Unijet<sup>®</sup> flow cell, which was first introduced and developed by Bioanalytical System, Inc. This type uses a centrosymmetric design within a thin layer. The flow radiates from the center of the electrode to its edges. The diffusion layer is constricted within a very thin, cylindrical volume. In this research, some modifications were added into the original configuration and the fabricated flow cell was simply called hybrid electrode. The flow cell body based on wall-jet configuration. The distance between the nozzle and the electrode surface was adjusted by changing the gasket thickness. The silicone gasket in wall-jet configuration (1 mm in thickness) was replaced with a thin Teflon gasket (0.2 mm in thickness). Unfortunately, there is no mathematical equation to explain the hydrodynamic behavior of this configuration. A comparison diagram of all configurations was depicted in Fig. 3.10.

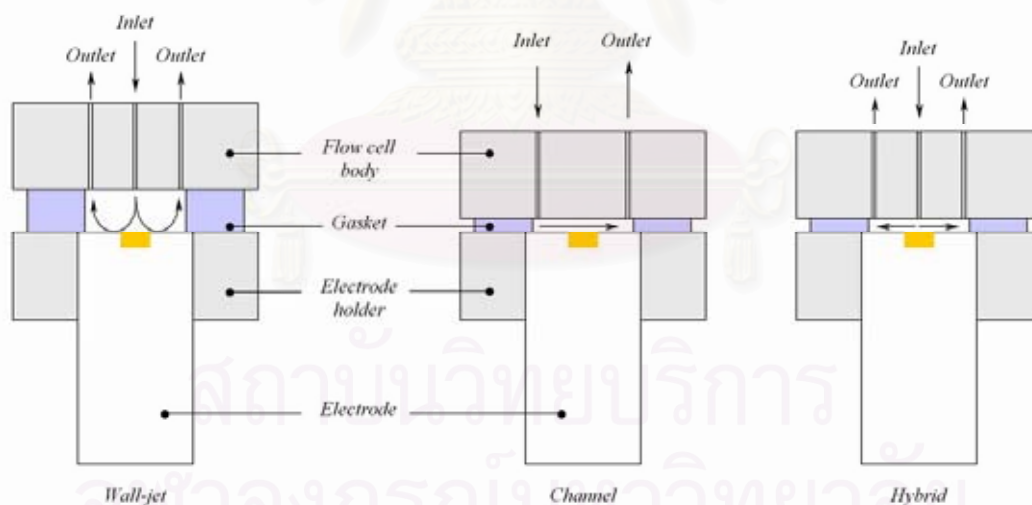


**Figure 3.10** A comparison between wall-jet, channel and hybrid electrode.

The arrows in the diagram represent the directions of the sample stream.



### 3.5 Characterization of the Flow Cells

The mass transport behavior of the flow cell was characterized using a well-known equation.

$$I_{lim} = kC_{analyte} V_f^y \quad (3.1)$$

where  $I_{lim}$  is limiting current (mA),  $V_f$  is the rate of solution flow (express as a volume per unit of time, normally in  $\text{cm}^3/\text{s}$ ) and  $y$  is an exponent, which depends on the cell design. The solution of 0.1 M  $\text{K}_4\text{Fe}(\text{CN})_6$  in 0.1 M KCl was pumped into the flow cell continuously without injection port and the limiting current was recorded at a different flow rate. Plots of  $\log I_{lim}$  as 'y' against  $\log V_f$  as 'x' should be linear with a gradient of 0.33 for channel electrode and 0.75 for wall-jet electrode, respectively. A schematic diagram of a flow system used in this experiment was shown in Fig. 3.11.

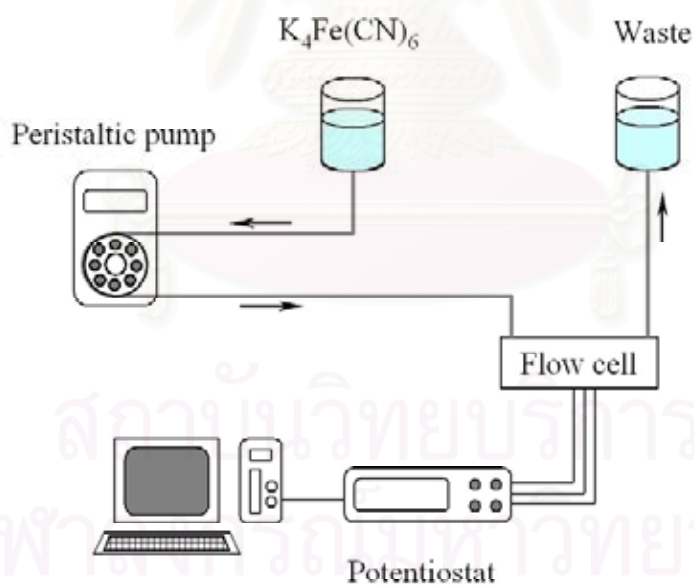


**Figure 3.11** A schematic diagram of a flow system.

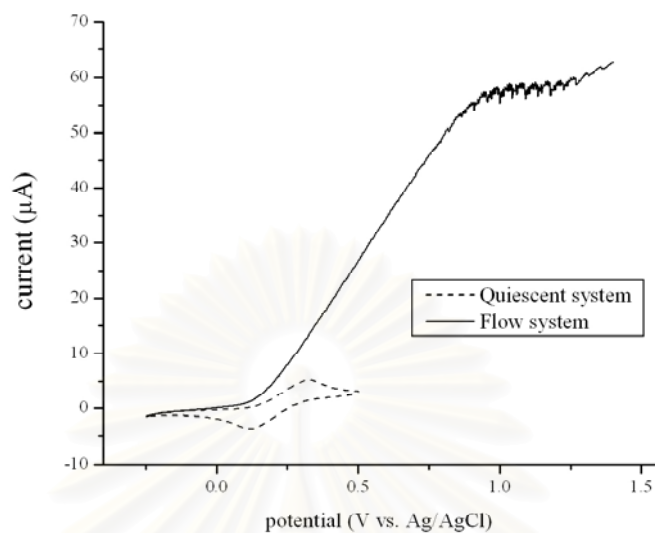


**Figure 3.12** Voltammetric oxidation of 1 mM  $K_4Fe(CN)_6$  in 0.1 M KCl at gold electrode in quiescent and flow system. Both recorded at 15 mV/s (vs. Ag/AgCl). For clarity, only forward scan is shown.

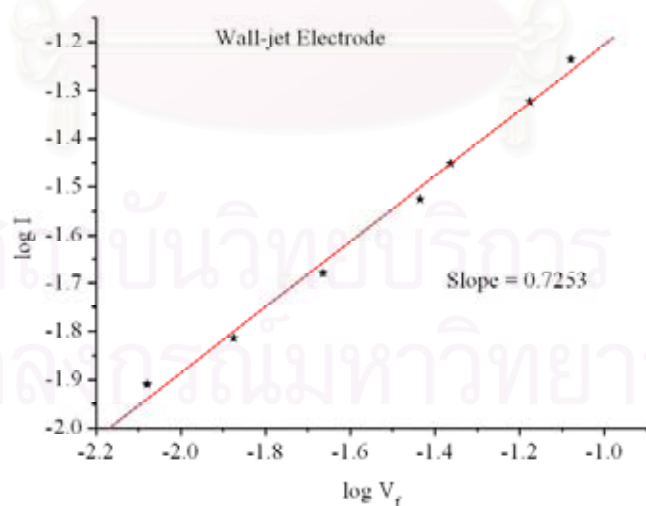


**Figure 3.13** A plot of  $\log V_f$  against  $\log I$  with gradient of 0.7253 (wall-jet electrode).

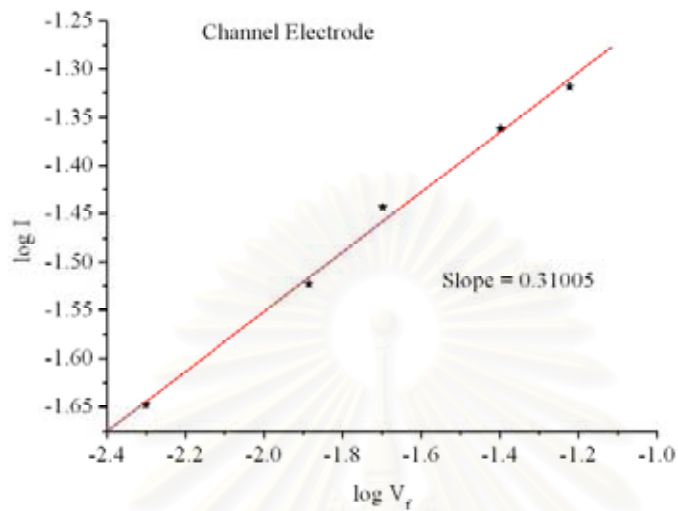


**Figure 3.14** A plot of  $\log I_f$  against  $\log I$  with gradient of 0.31005 (channel electrode).

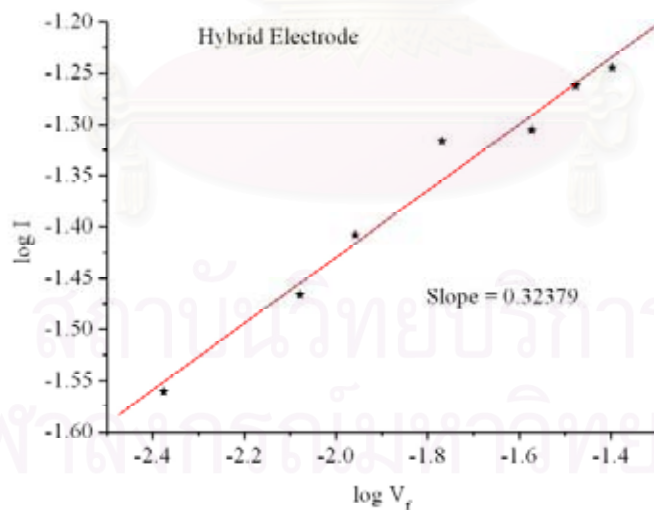


**Figure 3.15** A plot of  $\log I_f$  against  $\log I$  with gradient of 0.32379 (hybrid electrode)

In the hydrodynamic system, a higher signal can be obtained because analyte approach the electrode faster due to the convective force of the flowing stream. Fig. 3.12 shows the hydrodynamic voltammograms of 1 mM  $K_4Fe(CN)_6$  obtained from both systems. This result is consistent with a literature report<sup>86</sup>. From equation 1, the higher of an exponent value means the higher mass-transport rate of analyte over the electrode surface. The exponent values obtained from wall-jet and channel electrode (as shown in Fig. 3.13 and Fig. 3.14) are 0.73 and 0.31, respectively. These values are slightly different from the expected value (0.75 and 0.33) and these also indicate that both flow cells are working properly.

In hybrid electrode, no hydrodynamic equation was found from textbooks or literatures. But the exponent value can be roughly estimated by comparison with both wall-jet and channel electrode. Even the cell design of hybrid is based on wall-jet electrode, but the mass-transport over the electrode surface occurred within a thin layer (laminar flow). Hence, the exponent value should be very close to channel electrode, which is 0.33. The exponent value obtained from hybrid electrode is 0.32 (Fig. 3.15).

In term of a construction, making of wall-jet and hybrid flow cells are more difficult than making of channel electrode. Because both wall-jet and hybrid electrode use centrosymmetric design, it is quite difficult to make the nozzle aligned at the center of the electrode. Hence, the applications in this research are focused on channel electrode configuration. The details of each configuration were summarized in Table 3.1.

**Table 3.1** A summary details of each configuration.

	Configuration		
	Wall-jet electrode	Channel Electrode	Hybrid Electrode
Design	Centrosymmetric	Thin-layer (cross flow)	Centrosymmetric within a thin-layer
Electrode geometry	Disc	Non specific (could be disc or any flat electrode)	Disc
Gasket	Silicone Rubber, Circle Cut (1mm in thickness)	Teflon, Slot Cut (0.2mm in thickness)	Teflon, Circle Cut (0.2mm in thickness)
Hydrodynamic condition *	Turbulent (exponent = 0.73)	Laminar (exponent = 0.31)	Laminar (exponent = 0.32)
Ease of construction	Difficult to align the nozzle tip to a concentric position of the electrode	Easy	Same as wall-jet electrode

\*The exponent values were obtained from the plots using equation 1 (triplicate runs).

สถาบันวิทยบริการ  
จุฬาลงกรณ์มหาวิทยาลัย

### 3.6 Electrochemistry of MG and LMG in Batch Experiment

#### 3.6.1 Instrument, Reagents and Chemicals

All reagents were analytical grade and all solutions were prepared by using deionized water. Malachite green oxalate and leucomalachite green were obtained from Sigma Chemical (USA). Sodium dihydrogen orthophosphate (BDH), sodium hydroxide (Merck) and phosphoric acid 85% (Merck) were used to prepare the buffer solution. Phosphate buffer solution with pH ranges from 2.0 to 8.0, were prepared from 0.1 M sodium dihydrogen orthophosphate and adjusted to the desired pH using phosphoric acid and sodium hydroxide. The MG and LMG were prepared by dissolving an appreciate amount of MG and LMG in the buffer solution. The solutions were prepared daily.

The BDD electrodes were used as received without any further modifications. A glassy carbon (GC) electrode was purchased from Bioanalytical System, Inc. (area  $0.07 \text{ cm}^2$ ). GC electrodes was pretreated by sequential polishing with 1 and  $0.05 \mu\text{m}$  of alumina/water slurries on felt pads, followed by rinsing with ultrapure water prior to use.

Electrochemical experiments were conducted in a single compartment three - electrode glass cell. The BDD electrode was pressed against a smooth ground joint at the bottom of the cell, isolated by an O-ring (area  $0.07 \text{ cm}^2$ ). Electrical contact was made by placing the backside of the Si substrate onto a brass holder. The GC carbon was used as working electrode for the comparison. The Ag/AgCl with salt bridge and Pt wire were used as reference electrode and counter electrode, respectively. The voltammetric measurement was performed with the three-electrodes system using Autolab Potentiostat 100 (Eco-Chemie, The Netherlands). All experiments were performed at room temperature. In order to reduce the electronic noise, a copper faradaic – cage was used through out the whole research.

### 3.6.2 Cyclic Voltammetric Investigation

Fig. 3.16 shows typical cyclic voltammogram for 1 mM of malachite with the corresponding background current of 0.1 M phosphate buffer (pH 2) at 50 mV/s. BDD electrode exhibited well-defined and higher current response than GC electrode (both BDD and GC electrodes have the same electrode area). In addition, the background current of GC electrode was much higher. Malachite green gave a higher current response than leucomalachite green regardless of BDD or GC electrodes were used (as shown in Fig. 3.17).

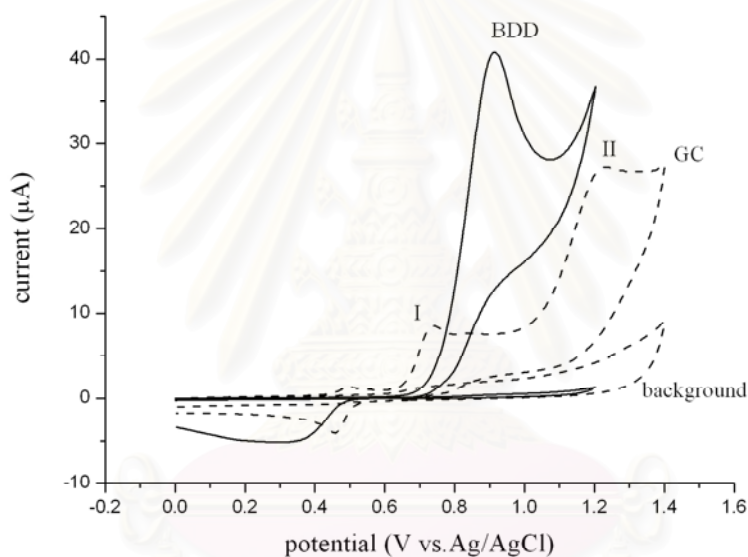


**Figure 3.16** Cyclic voltammogram of 1 mM malachite green in buffer (pH 2) at BDD electrode (solid line) and glassy carbon electrode (dash line). The scan rate was 50 mV/s.

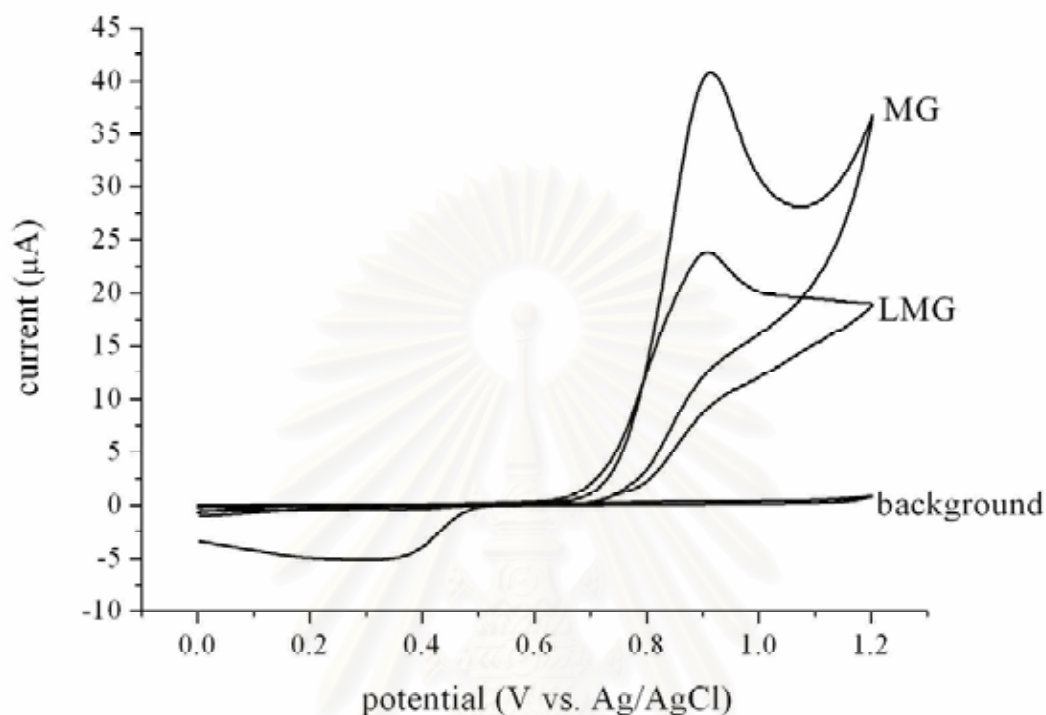


**Figure 3.17** Cyclic voltammogram of 1 mM malachite and leucomalachite green in buffer (pH 2) at BDD electrode. The scan rate was 50 mV/s.

From the literature, the electrochemical mechanisms of both compounds have not been investigated. However, it has been reported that MG can be oxidized by azide radical which is a well-known one-electron oxidant. This oxidation reaction generates MG radical easily due to the strong resonance electron-donating effect of the dimethylamino groups. Therefore, we believe that the electrooxidation process would occur via MG/LMG radical at N atom containing lone pair electron (the easiest losing electron position).

Two anodic peaks obtained for MG at GC electrode could be resulted from an electrochemical 'ECE' reaction (electron transfer followed by a chemical reaction, which in turn produces a new electroactive species). In case of BDD electrode, the second peak of MG should be observed if the potential was swept further to an anodic direction.



According to the property of BDD electrode, the potential should be stopped before exceeding 1.2 V to avoid the oxide formation on the surface. The slightly shifted of the oxidation peak on BDD electrode would be affected from the slower kinetic.

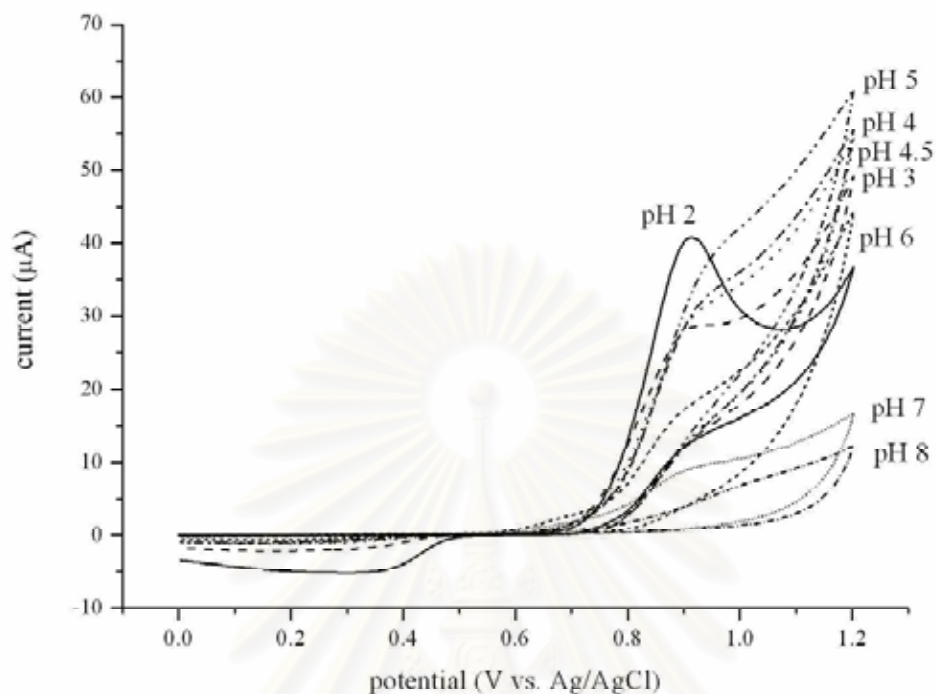
The reduction peak of MG was found at 0.35 V in the reversed scan and the potential difference between  $E_{ox}$  and  $E_{red}$  much larger than 59 mV/n (in this case  $n = 1$ ) indicated that this electrooxidation was a quasi-reversible process.

For LMG, no reduction peak was observed on the reversed scan, and only one anodic peak was obtained. This evidence made clear that the oxidation of LMG was irreversible and could be an electrochemical 'EC' reaction (electron transfer followed by a chemical reaction). The difference in electrochemical response between MG and LMG can be affected from the structures of both compounds. LMG is neutral, whereas MG is positive charge molecule.

### 3.6.3 Effect of pH

The effect of pH was investigated from pH 2 – pH 8 for malachite green (Fig. 3.18). It was found that the higher the buffer pH is, the less the oxidation peak will be. It was reported that malachite green has two forms depending on pH. The initial strong green color of MG is obtained at low pH (acidic), while in alkaline aqueous solution; it is converted to a colourless carbinol form. From this study, MG provided the highest oxidation peak at pH 2 at BDD electrode and the lowest response at the pH 8. It could be explained that the higher the pH, the less MG due to the conversion of MG form to carbinol form.

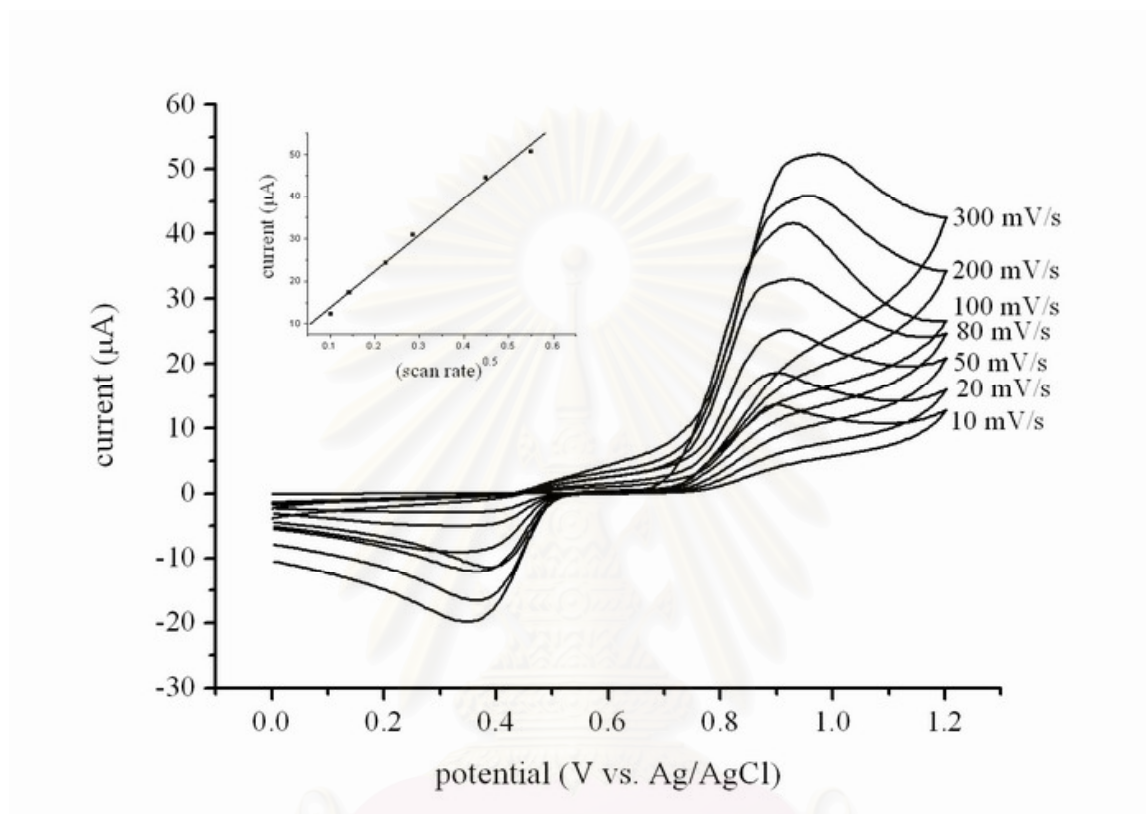
It also has been found that pH effect the solubility of both MG and LMG. Because MG has less polarity than water,  $H^+$  in acidic solution would protonate on N atom and increase the polarity of the molecule. Therefore, decreasing the buffer pH would help the compound to dissolve in water. LMG also has the solubility problem as it cannot be dissolved in buffer between pH 3 to pH 8. Only in the buffer pH 2, LMG dissolved and provided the oxidation peak. Therefore, buffer pH 2 was chosen to prepare both of MG and LMG in all experiments.



**Figure 3.18** A pH dependent study of malachite green. The highest oxidation peak was observed at pH 2

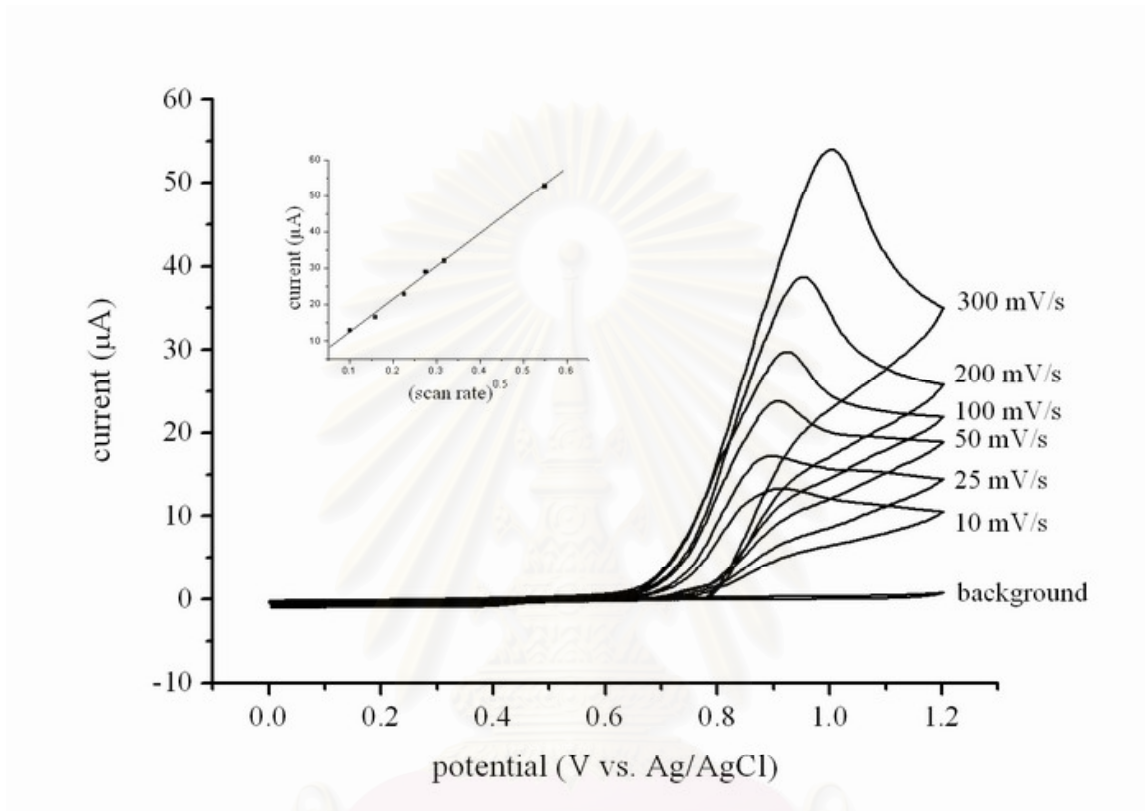
#### 3.6.4 Scan Rate Dependence Study

Fig. 3.19 and Fig. 3.20 show the cyclic voltammetric response of 1 mM malachite and leucomalachite green at BDD electrode in 0.1 M phosphate buffer pH 2 with variation of the scan rate from 0.01 to 0.3 V/s. A plot of oxidation current versus the square root of the scan rate,  $v^{1/2}$ , is highly linear ( $r > 0.99$ ) for both compounds as shown in the inset of the figures. The results indicate that the electrochemical reaction is a diffusion-controlled process.



**Figure 3.19** A scan rate dependence study of 1 mM malachite at BDD electrode in 0.1 M phosphate buffer pH 2

สถาบันวิทยบริการ  
จุฬาลงกรณ์มหาวิทยาลัย



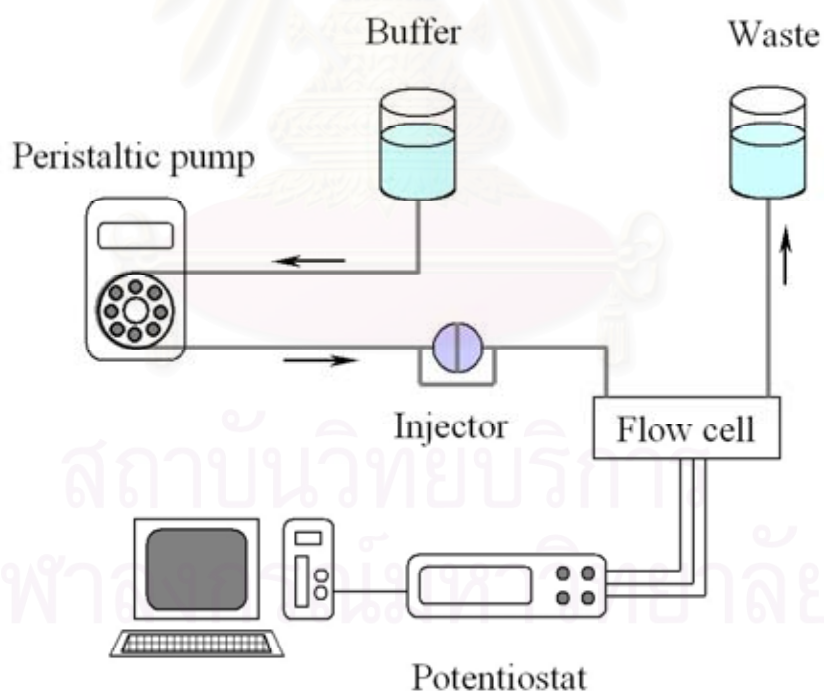
**Figure 3.20** A scan rate dependence study of 1 mM leucomalachite at BDD electrode in 0.1 M phosphate buffer pH 2

สถาบันวิทยบริการ  
จุฬาลงกรณ์มหาวิทยาลัย

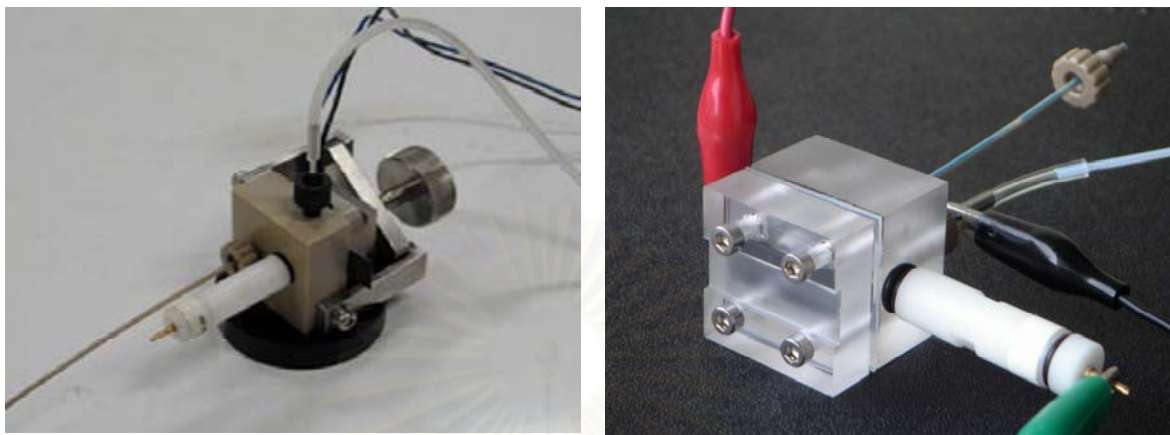
### 3.7 Flow Injection Analysis with Amperometric Detection

#### 3.7.1 Instrument, Reagents and Chemicals

The flow injection system consisted of a thin-layer flow cell (Bioanalytical System, Inc) and a homemade flow cell (channel electrode configuration), a 20  $\mu\text{L}$  stainless steel loop of injection port (Rheodyne 7725), a peristaltic pump, and electrochemical detection (Autolab potentiostat 100). The carrier solution, 0.1 M sodium dihydrogen orthophosphate, was regulated at a flow rate of 1 ml / min. The thin-layer flow cell consisted of silicone rubber gasket as a spacer, a BDD electrode as the working electrode, Ag/AgCl electrode as the reference electrode and a stainless steel tube as a counter electrode (also function as an outlet of the flow cell). A schematic diagram of flow injection analysis system and the flow cells used in this experiment were shown in Fig. 3.21 and Fig. 3.22, respectively.



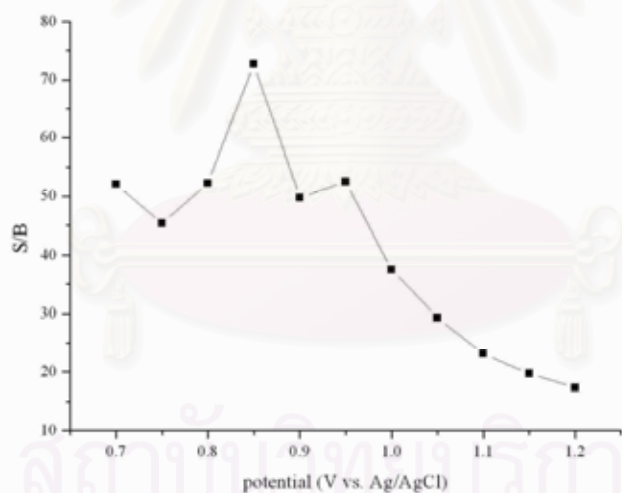
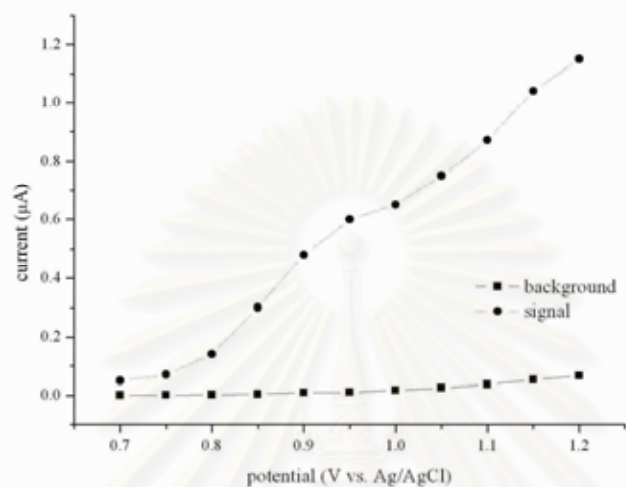
**Figure 3.21** A schematic diagram of flow injection analysis system with amperometric detector



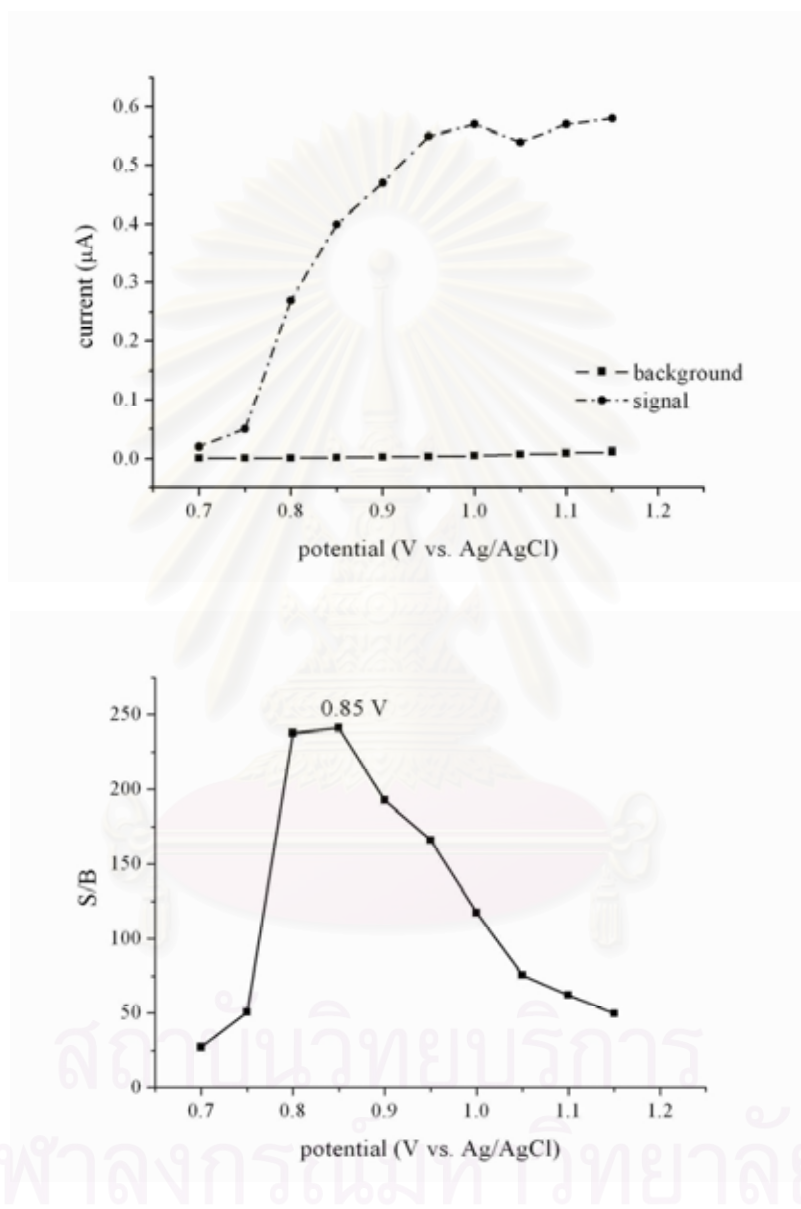
**Figure 3.22** The flow cell used in this experiment: BAS flow cell (left) and homemade channel electrode (right).

### *3.7.2 Amperometric Determination of MG and LMG in FIA System*

In order to obtain the optimal potential for amperometric detection in a flow injection analysis, the hydrodynamic behavior of malachite and leucomalachite green were studied. Fig. 3.23 and Fig. 3.24 shows a hydrodynamic voltammetric I-E curve obtained at the BDD electrode for 20  $\mu\text{L}$  injection of 0.05 mM of malachite and leucomalachite green in 0.1 M phosphate buffer (pH 2), respectively. Each point represents the average value of a triplicate injection. The background current at each potential is also shown for comparison. In case of the commercial flow cell, the S/B ratio at each point was calculated to obtain the optimum potential. The hydrodynamic voltammetric S/B ratios versus potential curve are shown in the bottom of each figure. The results show the maximum ratio at 8.5 V for both malachite and leucomalachite green.



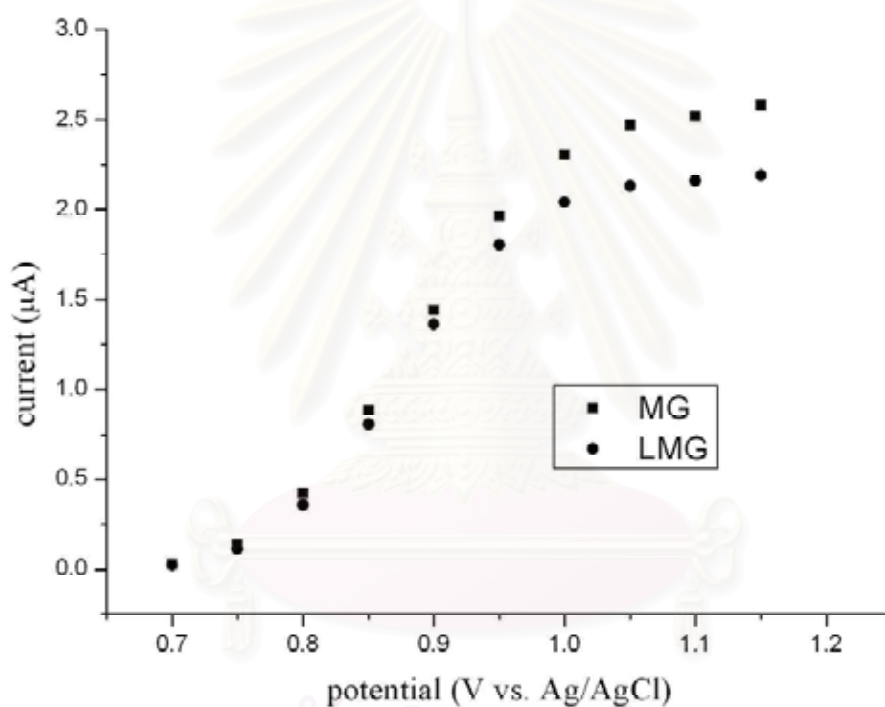
**Figure 3.23** Hydrodynamic voltammetric I-E curve obtained at the BDD electrode for 20  $\mu\text{L}$  injection of 0.05 mM of malachite green in 0.1 M phosphate buffer pH 2 (above). Hydrodynamic voltammetric S/B ratios versus potential curve (bottom). The signals were obtained from the commercial flow cell.



**Figure 3.24** Hydrodynamic voltammetric I-E curve obtained at the BDD electrode for 20  $\mu\text{L}$  injection of 0.05 mM of leucomalachite green in 0.1 M phosphate buffer pH 2 (above). Hydrodynamic voltammetric S/B ratios versus potential curve (bottom). The signals were obtained from the commercial flow cell.

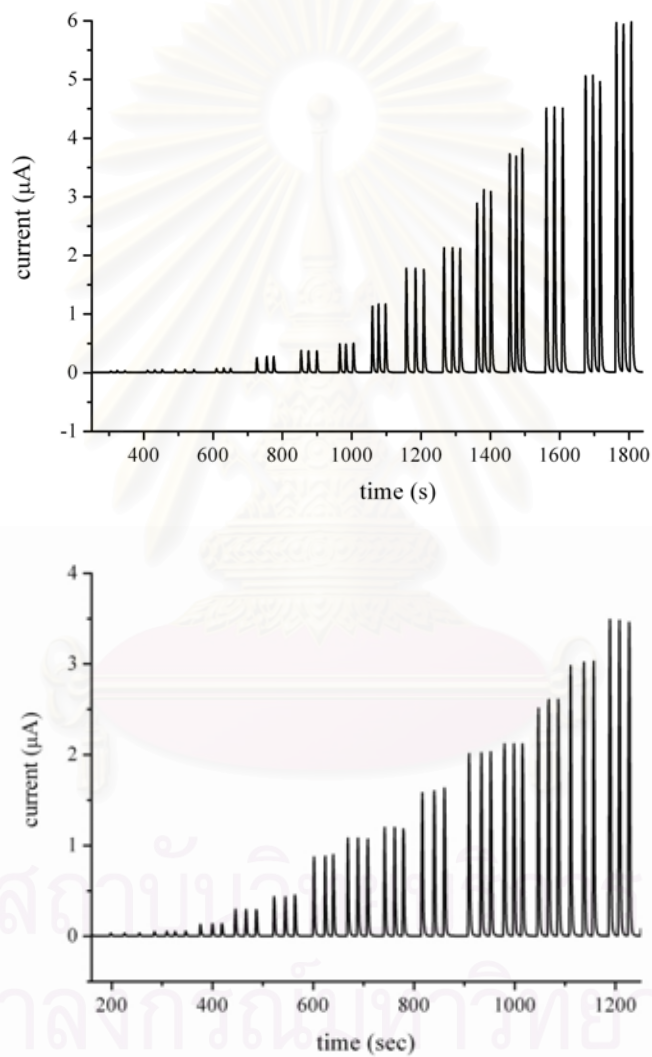


In case of the homemade flow cell, the hydrodynamic voltammogram of both malachite and leucomalachite green exhibited a sigmoidal curve (as shown in Fig. 3.25). Therefore, the optimal potential was simply chosen from the hydrodynamic voltammogram at the point that gave the steady-state current, which is 1.1 V for both compounds. The results are shown in Table 3.2. The difference in term of the hydrodynamic behavior and the optimal potential between both flow cells could be affected from the cell geometry (the position of WE, RE and CE).

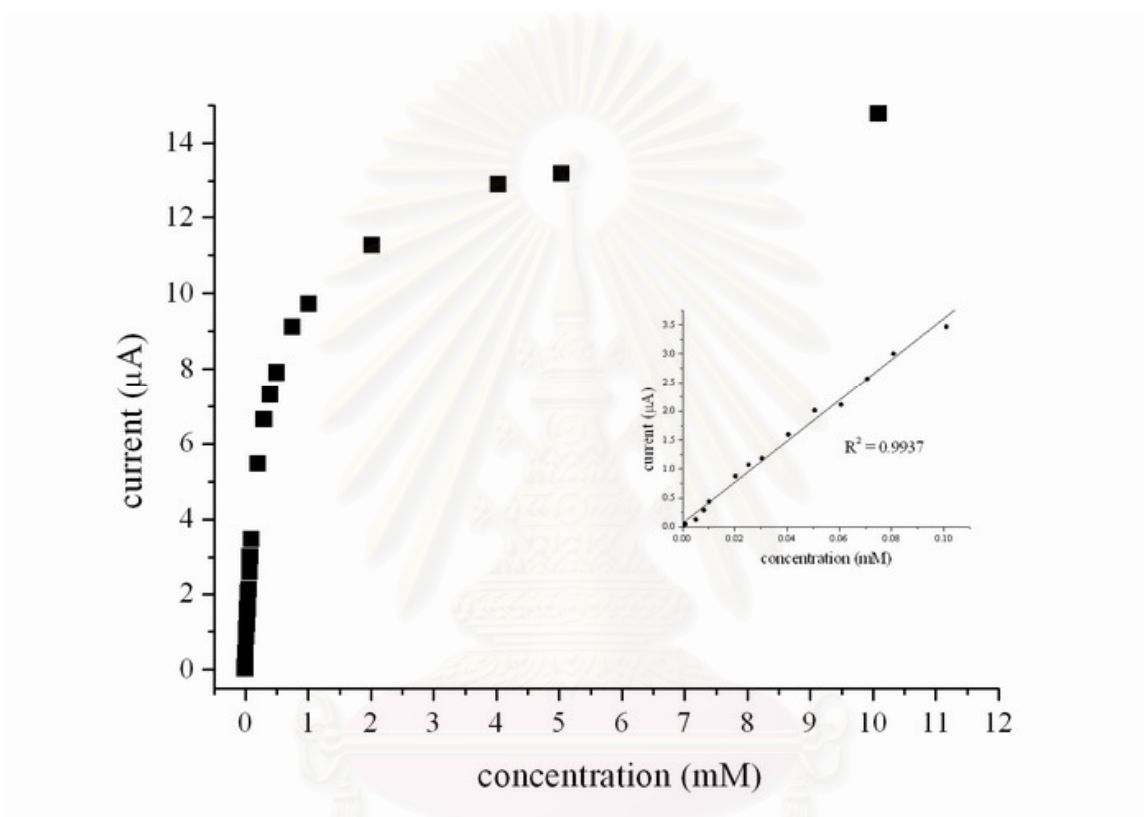


**Figure 3.25** Hydrodynamic voltammetric I-E curve obtained at the BDD electrode for 20  $\mu\text{L}$  injection of 0.05 mM of malachite green and leucomalachite green in 0.1 M phosphate buffer pH 2 . The signals were obtained from the homemade flow cell.

At the chosen operating potential, a series of repetitive 20  $\mu\text{L}$  of each compound were injected. The current signal increased with the increasing of concentration. For the commercial flow cell, BDD electrode provides a linear concentration range of 0.1 – 100  $\mu\text{M}$  and 0.8 – 80  $\mu\text{M}$  for malachite green and leucomalachite green, respectively. In case of the homemade flow cell, the linear concentration range for leucomalachite green was smaller.



**Figure 3.26** Signals of malachite green (above) and leucomalachite green (bottom) at the various concentrations. The data were obtained from commercial flow cell.



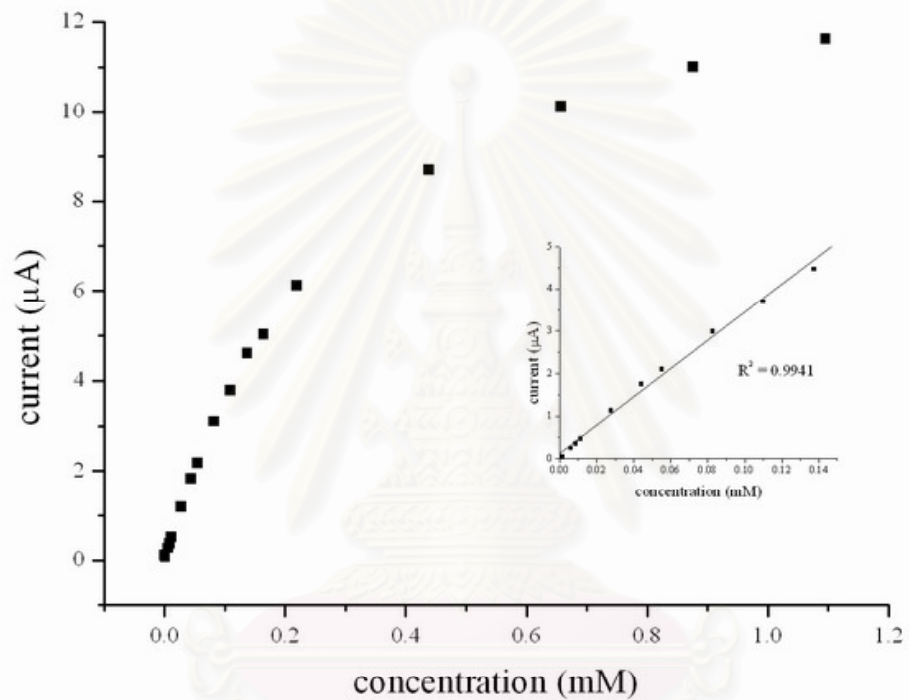


**Figure 3.28** A relationship between the current response and the concentrations of leucomalachite green using a commercial flow cell. A linear range is shown in the inset

สถาบันวิทยบริการ  
จุฬาลงกรณ์มหาวิทยาลัย

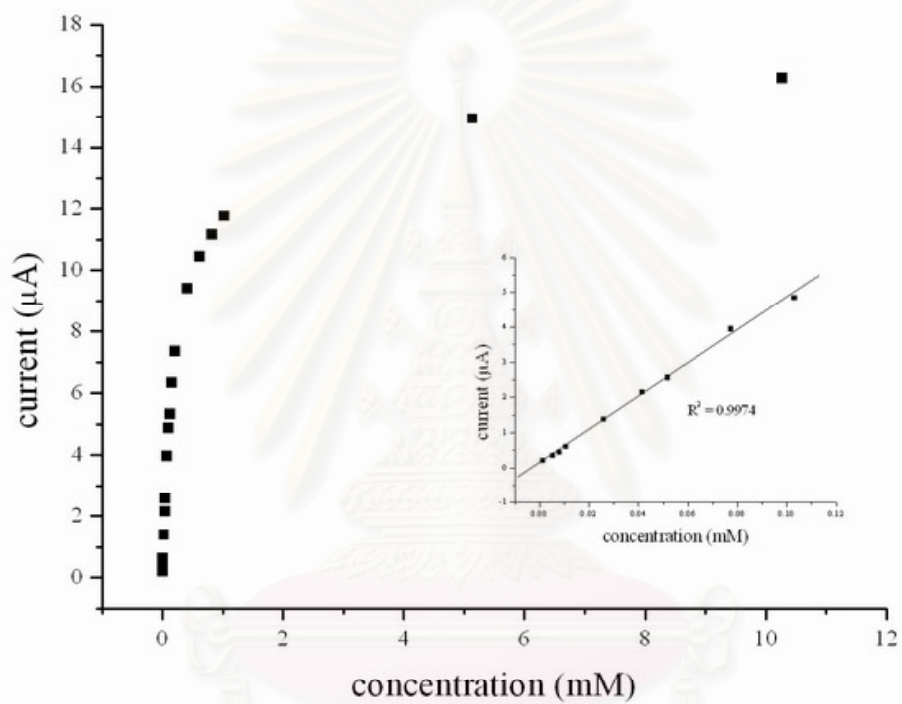


**Figure 3.29** A relationship between the current response and the concentrations of malachite green using a homemade flow cell. A linear range is shown in the inset.

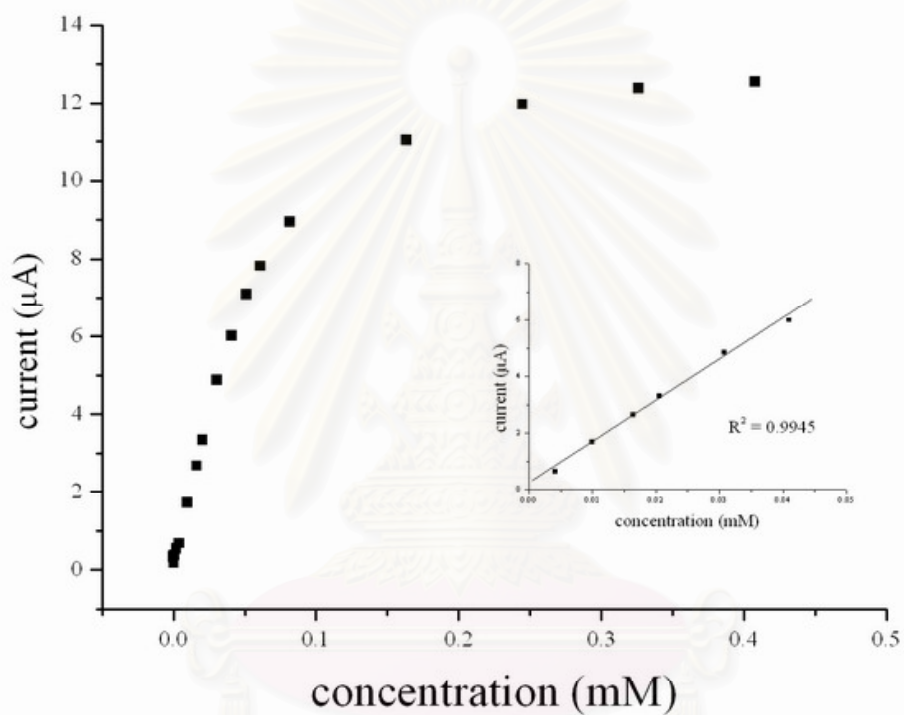


**Figure 3.30** A relationship between the current response and the concentrations of leucomalachite green using a homemade flow cell. A linear range is shown in the inset.

The reproducibility of the response was also investigated. Fig. 3.31 shows the currents response to 0.2 mM malachite green by using the homemade flow cell (flow rate 1 mL/min, operating potential 1.1 V vs. Ag/AgCl). The well-defined signals without peak tailing indicate that the homemade flow cell is working properly. The limit of detection (LOD) of both compounds were obtained at the concentration as low as 50 nM, at S/N > 3, regardless of the flow cell. The results were also summarized in Table 3.2.

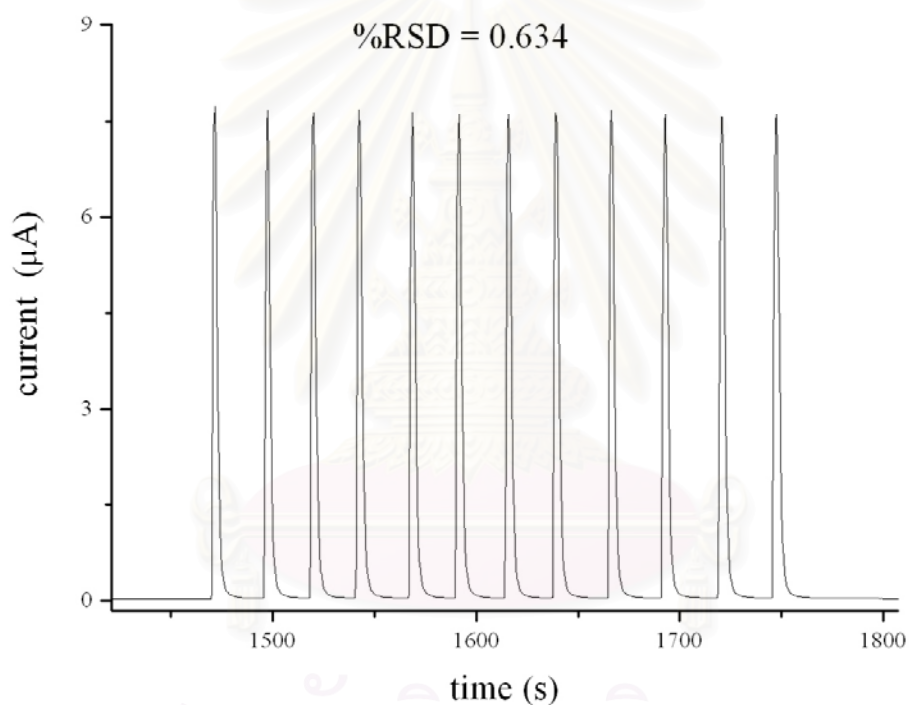


**Figure 3.31** Flow injection signals of 0.2 mM malachite green in 0.1 M phosphate buffer pH 2 at flow rate 1 ml / min. The signals were obtained from the homemade flow cell (at 1.1 V vs. Ag/AgCl).

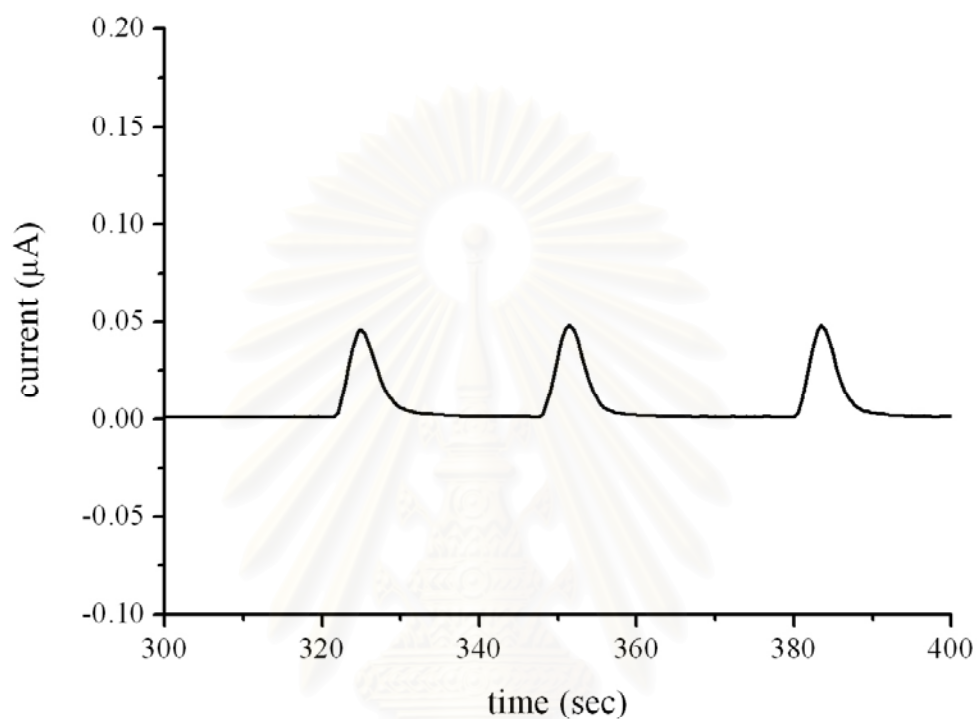


**Figure 3.32** The limit of detection of malachite green (50 nM at  $S/N > 3$ ) in 0.1 M phosphate buffer pH 2 at flow rate 1 ml / min. The signals were obtained from the commercial flow cell (at 8.5 V vs. Ag/AgCl).

สถาบันวิทยบริการ  
จุฬาลงกรณ์มหาวิทยาลัย



**Table 3.2** Comparison of FIA data obtained from both flow cells.

	BAS flow cell		Homemade flow cell	
	MG	LMG	MG	LMG
Optimal Potential (V vs. Ag/AgCl)	0.85	0.85	1.1	1.1
Linear Range (mM)	0.001 – 0.1	0.008 – 0.08	0.001 – 0.1	0.004 – 0.04
%RSD (10 injections)	1.49	0.81	0.63	1.07
LOD (nM)	50	50	50	50

FIA = Flow injection analysis; BAS = Bioanalytical System, Inc; %RSD = % Relative standard deviation

LOD = Limit of detection; MG = malachite green; LMG = leucomalachite green

สถาบันวิทยบริการ  
จุฬาลงกรณ์มหาวิทยาลัย

### 3.8 Amperometric Detection of MG and LMG in HPLC System

#### 3.8.1 Instrument, Reagents and Chemicals

HPLC system consisted of a homemade flow cell (channel electrode), a 20  $\mu$ L stainless steel loop of injection port (Rheodyne 7725), HPLC column (Inersil<sup>®</sup> ODS-3, C<sub>18</sub>, 5  $\mu$ m, 4.6 mm  $\times$  25 cm, GL Sciences Inc., Japan). These parts were equipped with HPLC pump (Model 510, Waters). The mixed solution of acetonitrile and phosphate buffer solution (50% v/v) was used as a mobile phase. The phosphate buffer solution of pH 2 was prepared daily by mixing of 0.01 M H<sub>3</sub>PO<sub>4</sub> + 0.1 M Na<sub>2</sub>HPO<sub>4</sub> (a few drops to adjust the pH). The phosphate buffer was filtered with a 0.45  $\mu$ m Nylon membrane filter.

#### 3.8.2 HPLC Coupled with Boron-Doped Diamond Thin Film Electrode

It is the limitation of as-deposited BDD electrode that cannot be used for the selective determination at both high and low operating potential. To amend this weak point the separation technique such as HPLC has to be employed to separate all species before detection with BDD electrode. HPLC column was added to the flow system (see Fig. 3.33 for the schematic diagram). The mixture standard solution of MG and LMG was injected. The mobile phase was regulated at a flow rate of 1 ml/min. A homemade Teflon flow cell was used, in order to increase the chemical resistance from organic mobile phase (Fig. 3.34). The operating potential was kept constant at 1.1 V (vs. Ag/AgCl). Fig. 3.35 shows the chromatographic signals of mixture solution of standard MG and LMG (5 ppm) by using BDD electrode as an amperometric detector.

Determination of malachite and leucomalachite green in real sample using BDD electrode as an amperometric detector for HPLC was also demonstrated. By using the sample preparation methods from the literature surveys<sup>87</sup>, both compounds can be detected at BDD electrode without the interferences. The mixture standard solution of MG and LMG (5 ppm) was spiked into fish sample prior to the preparation procedure. Then, the extracted liquid obtained from this step was injected. A chromatogram obtained from this sample was shown in Fig. 3.36. The signals of both MG and LMG can be clearly observed. The matrices from real sample were mostly eliminated. These results

indicate that BDD electrode has a potential to be developed as a detector for HPLC system.

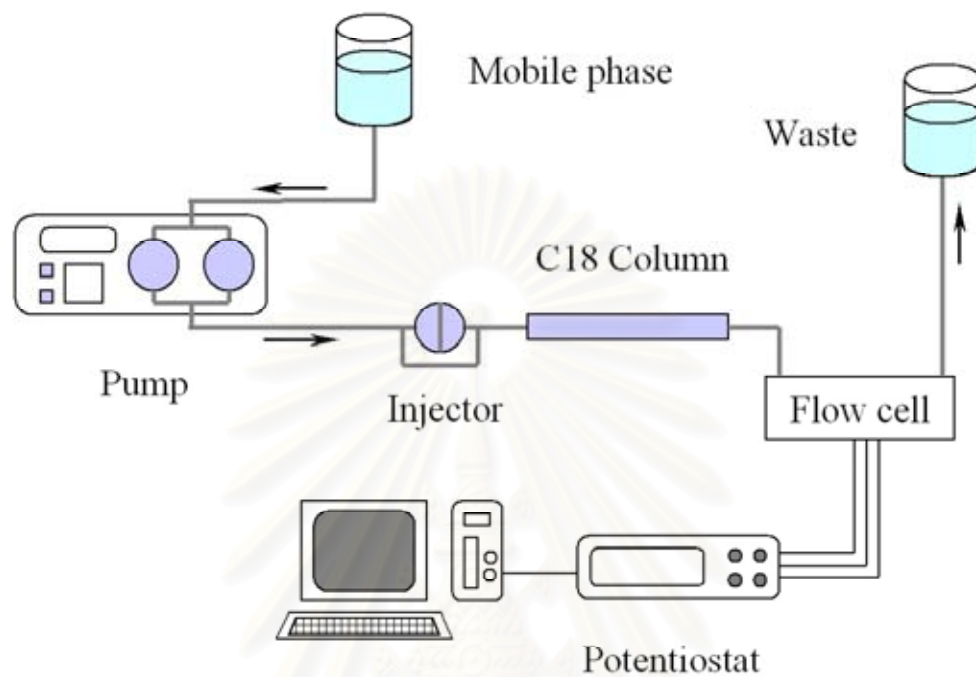


**Figure 3.33** A schematic diagram of HPLC system with amperometric detector.

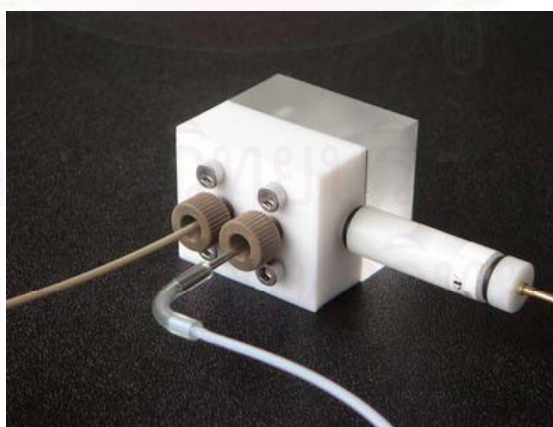


**Figure 3.34** A Teflon version of channel electrode.

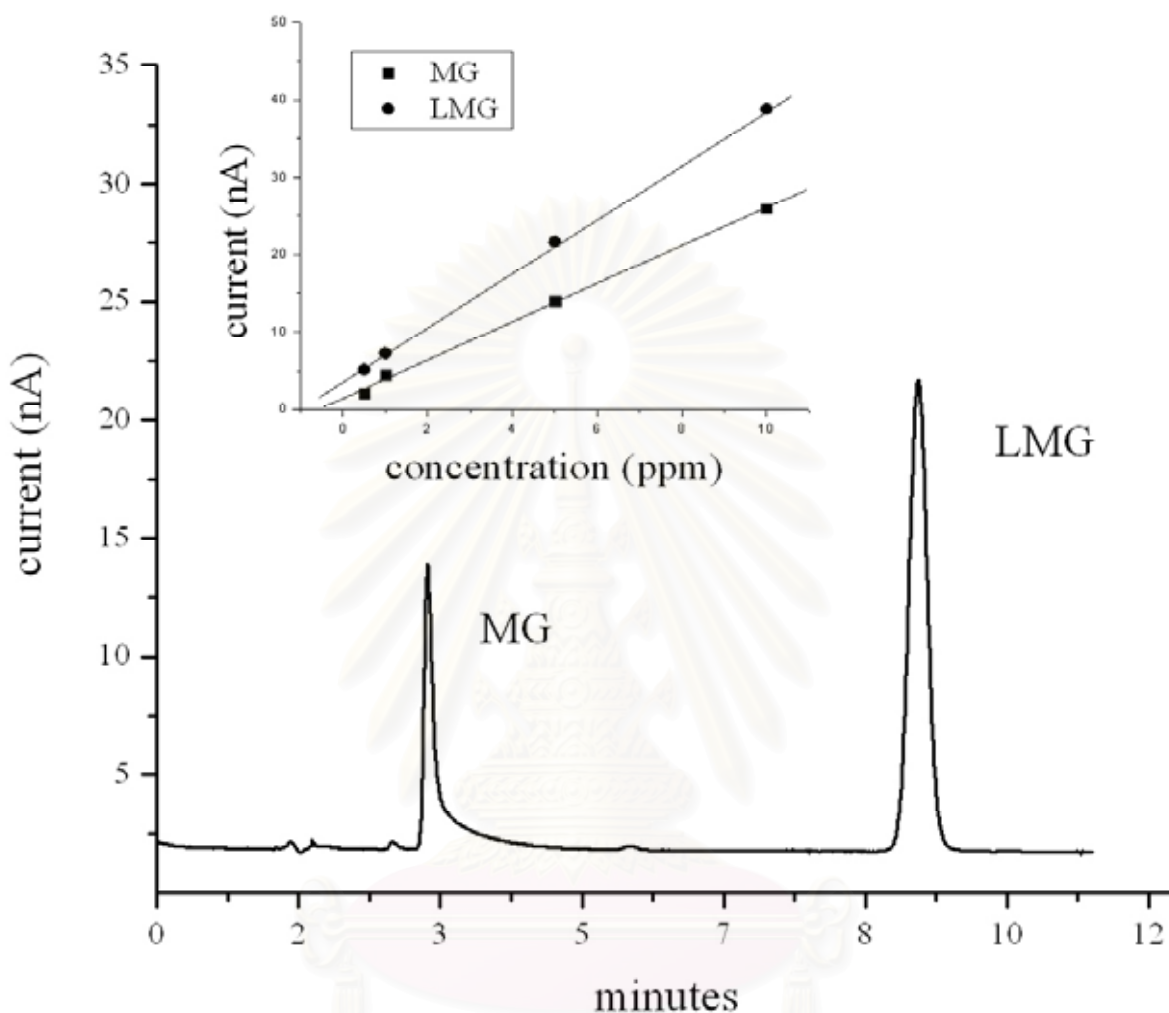


**Figure 3.35** Signals of MG (5.38  $\mu\text{M}$ ) and LMG (15.13  $\mu\text{M}$ ) standard solution obtained from HPLC system (C18 column) using BDD electrode as an amperometric detector. The calibration curve of both compounds also shown in the inset (Linear Range<sub>MG</sub> 50 nM – 10  $\mu\text{M}$ , Linear Range<sub>LMG</sub> 0.15  $\mu\text{M}$  – 30  $\mu\text{M}$ ;  $R^2_{\text{MG}}$  0.998,  $R^2_{\text{LMG}}$  0.999).

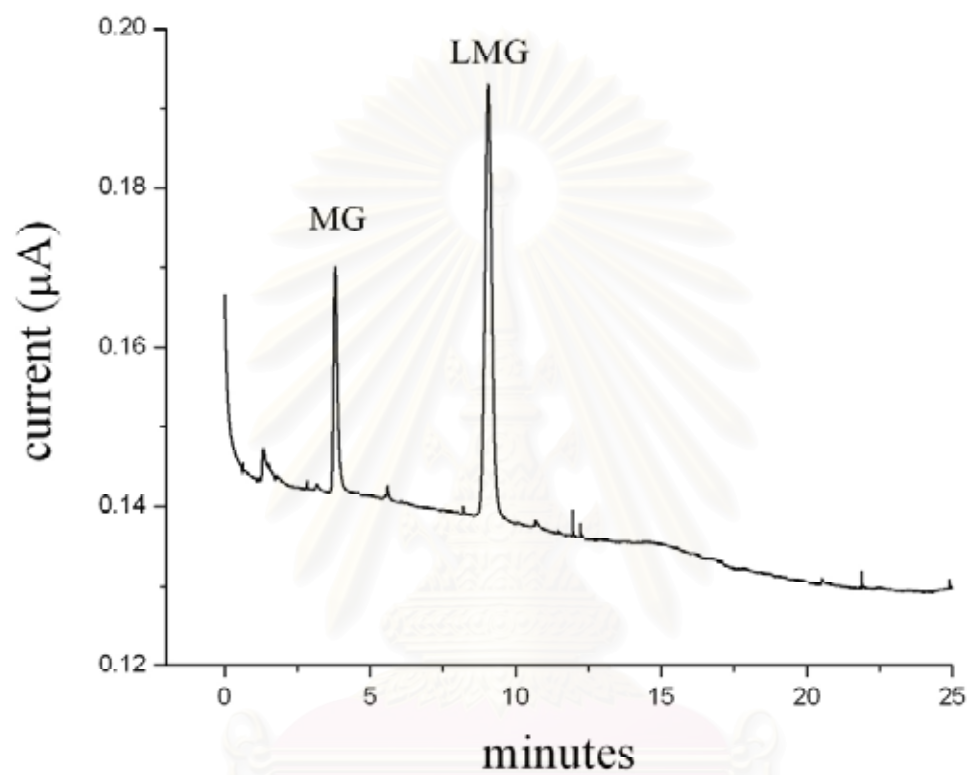


**Figure 3.36** A chromatogram of spiked sample using preparation procedure from the literatures to eliminate the matrices. The signals of both malachite green and leucomalachite green can be clearly observed.

### 3.9 Conclusion

The flow cell was designed and constructed with Plexiglas and Teflon. These materials can be purchased from the local hardware stores (relatively low-cost). The design is simple, easy to operate and maintenance. Hydrodynamic behavior of each configuration was confirmed by mathematical equation. All flow cells work properly and can be applied with the commercial accessories available in the laboratory such as electrodes, sample injection port, HPLC column, peristaltic pump and HPLC pump.

Channel electrode configuration is ideal for the continuous monitoring and can be used as an electrochemical detector in FIA or HPLC system. A lower background current or noise was obtained due to the laminar flow condition over the electrode surface. A higher background current was obtained from wall-jet configuration, because turbulent flow (higher mass-transport) occurred at all time. Hybrid electrode also works well, but need more mathematical approach to explain the hydrodynamics behavior at the electrode surface.

This, to the best of our knowledge, is the first report for the electroanalysis of malachite green and leucomalachite green by using of BDD thin film electrode. This electrode exhibits excellent performance for the oxidative detection of both compounds. Well-defined voltammograms were obtained at BDD electrode, which exhibited high sensitivity, and demonstrated significant advantage over GC electrode. Flow injection analysis with amperometric detection using BDD electrode provides a linear concentration range of 0.1 – 100  $\mu\text{M}$  and 0.8 – 80  $\mu\text{M}$  for MG and LMG, respectively. The detection limits for both compounds are remarkably low (50 nM). The design of the homemade flow cell is simple, but provides reliable results with the relatively low-cost.

## CHAPTER IV

### EC-SPR SENSING OF DECANETHIOL

This chapter describes the oxidative desorption of decanethiol self-assembled monolayer (SAM) from the gold surface using cyclic voltammetry technique. A real-time monitoring of thiol desorption using electrochemical-surface plasmon resonance (SPR) instrument was also demonstrated. Both of electrochemical and optical signal can be measured simultaneously. The Plexiglas channel electrode flow cell was used as an interface to combine both techniques together. The experiments were performed at the School of Chemistry and Optoelectronics Research Centre (ORC), University of Southampton, United Kingdom.

#### 4.1 Oxide Formation on Gold Surface

The generally agreed mechanism for the oxide formation on gold surface is shown in Fig. 4.1. The application of potential in anodic direction (positive direction) gives rise to a reversible electrostatic adsorption of anions on the surface. Further application of potential leads to a chemisorption of anions. These chemisorbed anions undergo partial charge transfer. The species of chemisorbed anions depend on the electrolyte solution. As the coverage of chemisorbed anions on the metal surface increases with increasing anodic potential, the number of water molecule bond to each anion decrease. A further increase of anodic potential leads to the complete discharge of  $\text{OH}^-$  species. A typical cyclic voltammogram of bare gold in 10 mM sulfuric acid was shown in Fig. 4.2. Platinum gauze and a saturated mercury/mercurous sulfate electrode (SMSE) were used as a counter and a reference electrode, respectively.

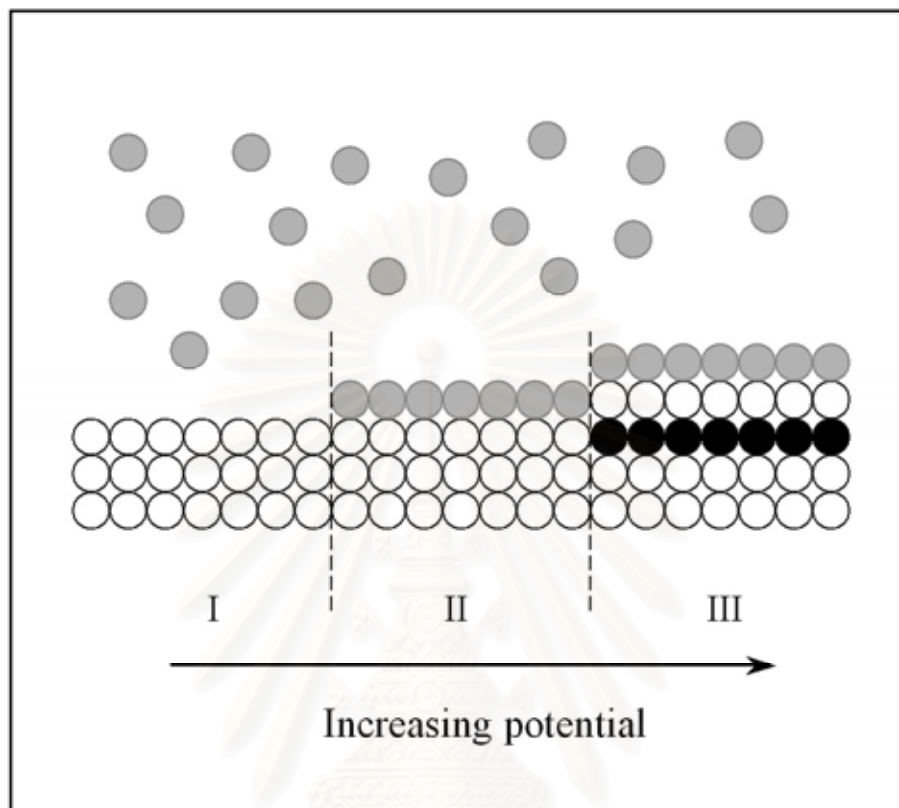


**Figure 4.1** Schematics diagram of the mechanism of oxide formation on gold metal. Region **I** represents the state of gold surface when no potential is applied. Region **II** shows the adsorption of the OH<sup>-</sup> layer onto the gold surface. Region **III** represents the replacement turnover of oxygen layer underneath gold layer and another OH<sup>-</sup> layer on top. (white circle = gold atom, gray circle = OH<sup>-</sup> ion and black circle = oxygen atom)

จุฬาลงกรณ์มหาวิทยาลัย



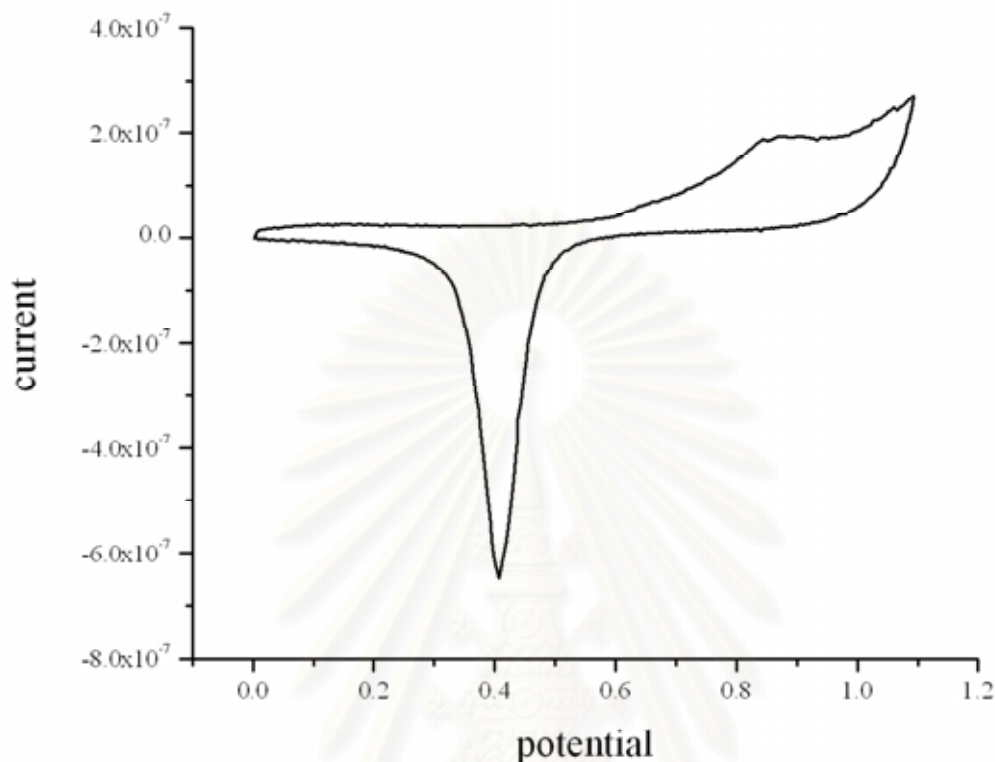


**Figure 4.2** Cyclic voltammogram of bare gold electrode in 1 mM sulfuric acid.

Scan rate = 20 mV/s (vs. SMSE)

#### 4.2 Preparation of Thiol-SAM

A gold disc electrode was pretreated by sequential polishing with 1 and 0.05  $\mu\text{m}$  of alumina/water slurries on felt pads, followed by rinsing with ultra pure water. Then, the gold electrode was electrochemically-cleaned by cycling in 10 mM  $\text{H}_2\text{SO}_4$  until a stable reduction current was obtained. Next, the electrode was rinsed with water, acetone and iso-propanol, respectively. Then, the electrode was dried with nitrogen gas. The dried, cleaned electrode was immersed in ethanoic solution of 1 mM decanethiol to form a self-assembled monolayer of decanethiol. After 12 hours or overnight, the electrode was rinsed with ethanol to remove loosely bound molecules from the surface then immersed in pure ethanol for additional 15 minutes. After that, the electrode was

rinsed again with ethanol and dried with nitrogen gas. The modified electrode was immersed in water at least 30 minutes prior to use.

### 4.3 Contact Angle Measurement

The modified electrode can be roughly investigated by measuring the contact angle of water on the electrode surface (as shown in Fig. 4.3). The gold substrate was hydrophilic with contact angle  $< 45^\circ$  for a pure water droplet, while the alkanethiol SAMs were hydrophobic with contact angles in the range of  $100^\circ\sim 110^\circ$ , which is consistent with the hydrophobic character of methyl end groups in the SAMs. The wettability of surfaces covered with monolayers can be correlated with the quality of the monolayers. Therefore, contact angle measurement is a preliminary tool in the investigation of the alkanethiol films.

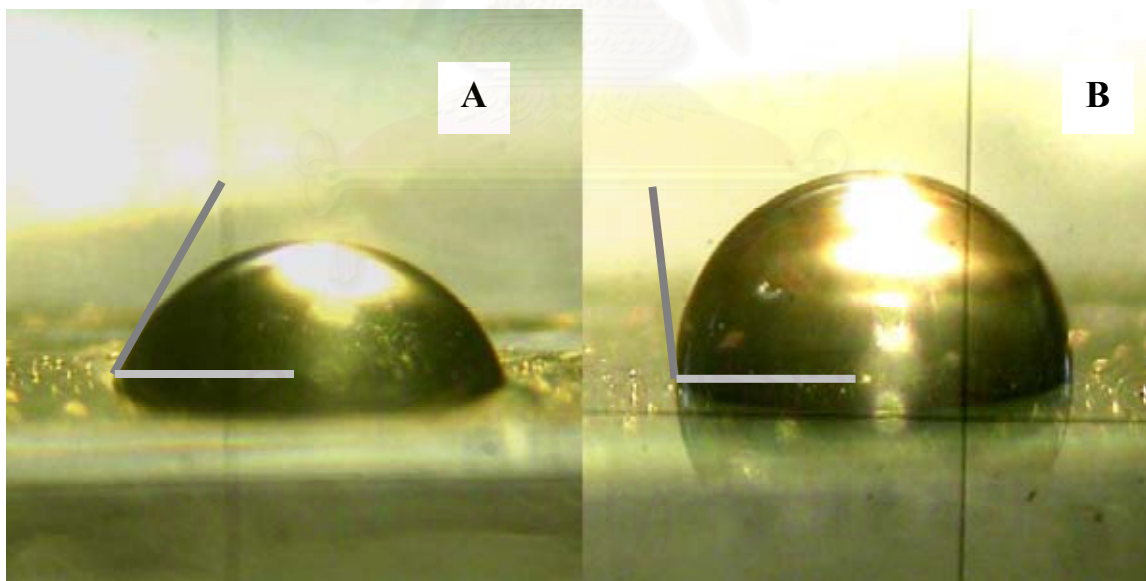


**Figure 4.3** The contact angle measurements of the water droplet on gold surface.

A) bare gold, B) decanethiol-modified electrode

#### 4.4 Oxidative Desorption of Thiol-SAM on Gold Electrode

Fig. 4.4 shows the cyclic voltammetry in 1 mM H<sub>2</sub>SO<sub>4</sub> for 12 cycles at 20 mV/s. Each cycle shows an oxidative process starting from around 0.6 V on the forward scan and a reduction peak around 0.4 V on the reverse scan. The oxidation current belongs to both the oxidative desorption of the thiol and oxidation of the gold surface. The reduction peak belongs to the reduction of the gold surface oxide. In order to obtain better understanding on the desorption process; a comparison between the gold area after each cycle was examined. An effective area of the gold electrode after each cycle was calculated from the charge under the reduction peak associated with the reduction of the gold oxide (as shown in the inset of Fig 4.4). For the first cycle, an oxidation current is barely observed and correspondingly a small reduction current ( $i_p = 0.42 \mu\text{A}$ ). With each cycle the reductive peak currents increase until reaching a reductive peak current of 1.93  $\mu\text{A}$ , similar to the current found for the bare gold surface (1.95  $\mu\text{A}$ ). These results are consistent with the reports in the literature<sup>88, 89</sup>. On the first scan, only small current is measured because the thiol layer passivates the gold surface. However, there are some defects in the thiol layer at the polycrystalline electrode surface so that some of the gold surface is available to take part in the oxidation/reduction reaction. This results in a small oxidation and reduction current. At around 1.0 V oxidative desorption of the thiol film itself takes place. The cycling in acid from 0 to 0.8 V results in no desorption of the thiol film indicating that the desorption only takes place at higher anodic potentials. It is apparent that the electrochemical oxidation of the thiol takes place initially at defects in the thiol layer. The oxidative desorption of some of the thiol results in there being a larger area of gold available to be oxidized on the subsequent cycle so that the oxidation and reduction currents increase until, after 12 cycles, all of the thiol is desorbed from the electrode surface; the voltammetry is then almost identical to the polished bare gold electrode (Fig 4.5). The number of cycles required to fully remove the thiol layer will depend on the sweep rate and the positive limit since the oxidative desorption process is known to be slow. By stopping the scan before all the thiol has been desorbed we are able to control the extent of desorption.

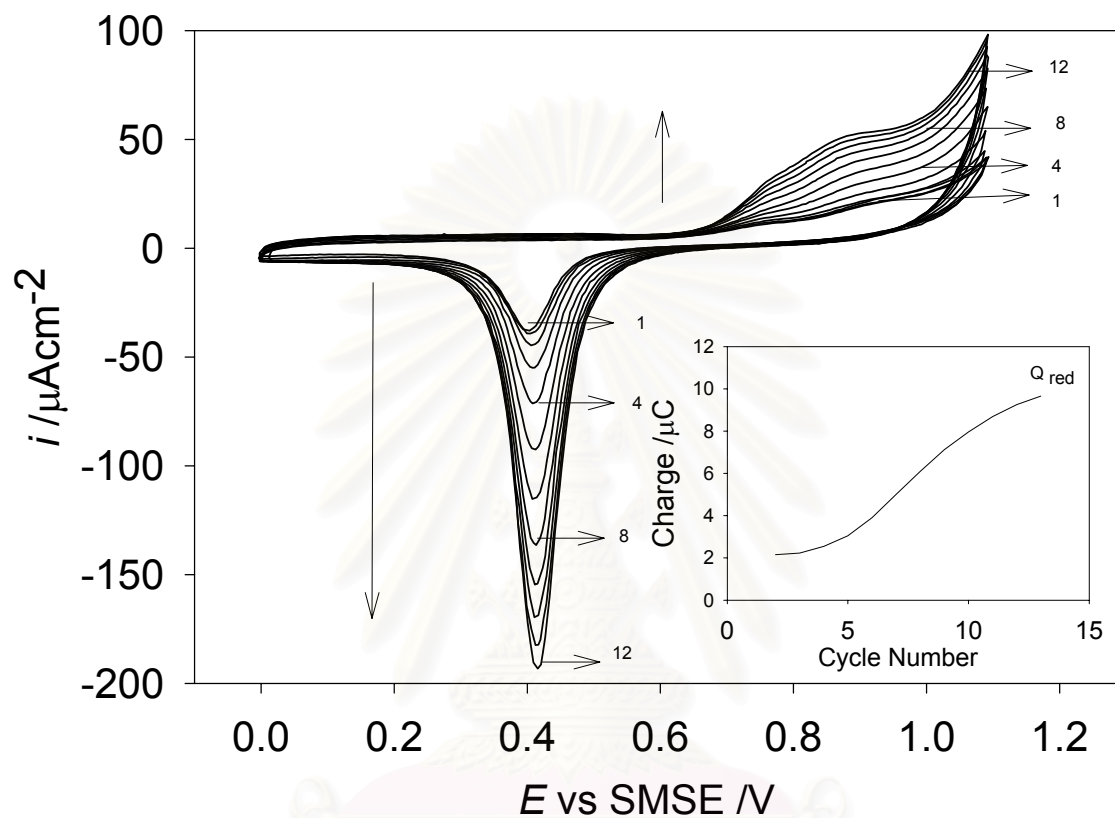


**Figure 4.4** A set of sequential cyclic voltammograms for a decanethiol-modified gold electrode recorded at a scan rate of 20 mV/s in 10 mM H<sub>2</sub>SO<sub>4</sub>. Inset: Charge calculated from area under the reduction peak for sequential cycles.

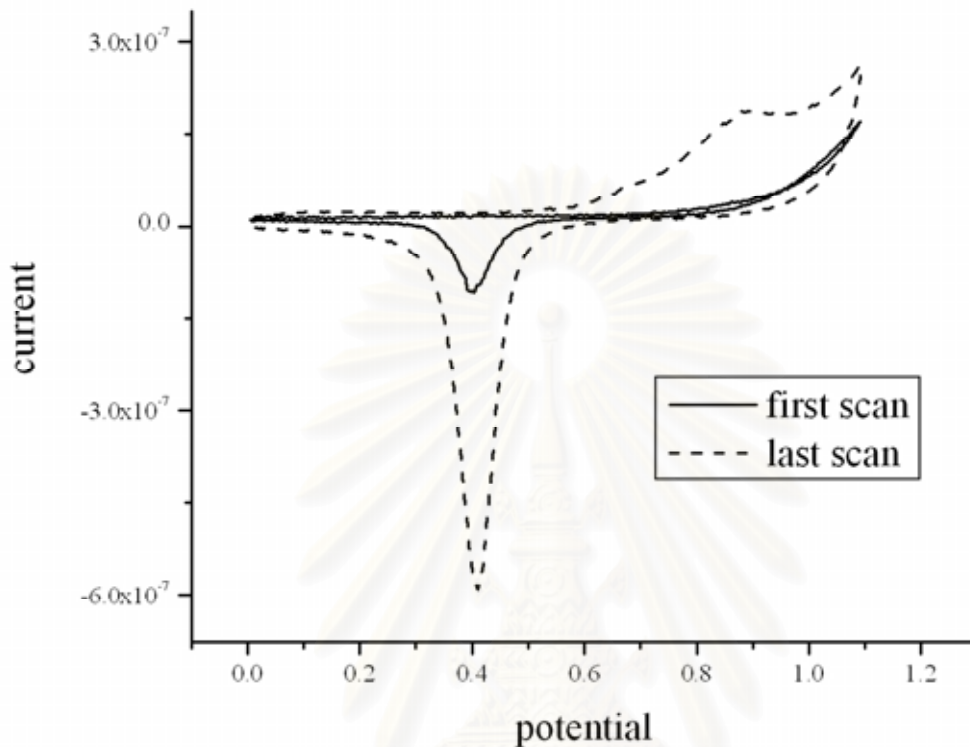


**Figure 4.5** Cyclic voltammograms of decanethiol-modified electrode (solid line) and bare gold electrode (dashed line) recorded at a scan rate of 20 mV/s in 10 mM H<sub>2</sub>SO<sub>4</sub>.

#### 4.5 Fabrication of Waveguide

The integrated optical waveguide structure (Fig. 4.6) was fabricated using photolithographic techniques. A Pyrex wafers (60 mm x 60 mm) were cleaned, first with acetone in an ultrasonic bath at 50 °C for 20 min and then in fuming nitric acid. The wafers were coated with a 200 nm thick film of aluminum and coated with photoresist. The wafer was exposed to UV light through a mask and developed. The aluminum was etched to leave channels 3 μm wide in the Y pattern that was repeated several times over

the wafer. The wafer was immersed in molten  $\text{KNO}_3$  at  $380\text{ }^\circ\text{C}$  for  $7\frac{1}{2}$  hours where the ion exchange of  $\text{K}^+$  to replace  $\text{Na}^+$  took place to form channel waveguides in the exposed areas of the Pyrex. The change in refractive index at  $633\text{ nm}$  due to  $\text{K}^+$  ion exchange in Pyrex is approximately  $8 \times 10^{-3}$ , and single mode waveguides at  $633\text{ nm}$  were formed by this procedure. The end faces of the waveguides were mechanically polished, using Syton (Logitech) to allow efficient coupling of the incident light. The aluminum mask was then removed using Al etch (containing acetic, phosphoric and nitric acids) at  $50\text{ }^\circ\text{C}$ . In order to form the gold electrodes, the glass was first treated with (3-mercaptopropyl) trimethoxysilane (MPS) to enhance the adhesion of the gold to the glass. The sample was refluxed in water, iso-propanol and MPS in the ratio 48:1:1 for 15 min, then rinsed thoroughly with iso-propanol, dried with nitrogen gas and baked at  $110\text{ }^\circ\text{C}$  for 8 min. This procedure was repeated to improve the adhesion properties. A  $55\text{ nm}$  thick gold film was then deposited by thermal evaporation and patterned to form gold sensing areas ( $20\text{ }\mu\text{m}$  wide and of lengths  $1\text{ mm}$  or  $2\text{ mm}$  on several Y-junction devices) using a mask and photoresist as described above. A Teflon layer was used to isolate the waveguides and electrode contact tracks during the electrochemical experiments. Photoresist was spun directly onto the surface and patterned photolithographically. Approximately  $1\text{ }\mu\text{m}$  of Teflon ( $n = 1.31$ ) was deposited using thermal evaporation. The wafer was washed in acetone to remove the remaining photoresist. After washing in iso-propanol, the sample was dried with nitrogen. The gold electrodes were electrochemically cleaned using cyclic voltammetry in sulfuric acid

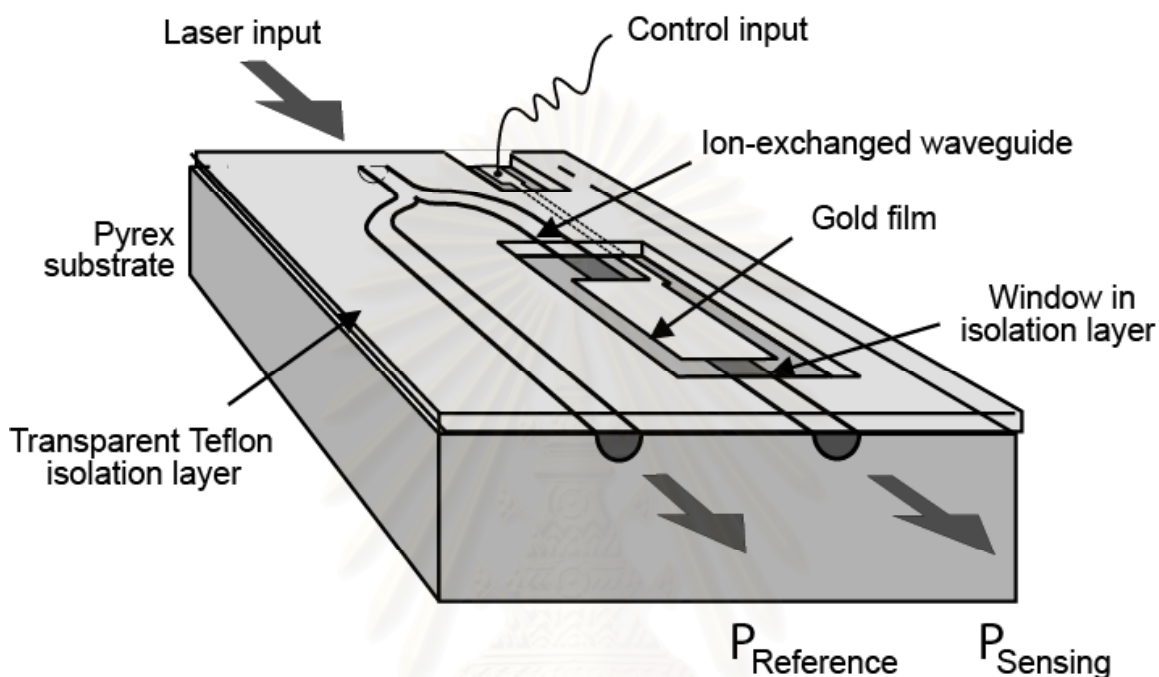


**Figure 4.6** Schematic diagram of the integrated waveguide sensor chip used in EC-SPR instrument.

#### 4.6 EC-SPR System

The electrochemical measurements were carried out in 10 mM sulfuric acid using a Hg/HgSO<sub>4</sub> (mercury mercurous sulphate) reference electrode and gold wire counter electrode. The gold sensing area acts as the working electrode and is connected, via photolithographically defined micro-tracks and an edge connector, to the potentiostat. A drop of sulfuric acid was placed onto the working electrode surface, and the reference and counter electrode were held in the drop and connected to a computer-controlled potentiostat for data collection. The working electrode was ramped from 0 V to 1.1 V and back to 0 V repeatedly using a scan rate of 20 mV s<sup>-1</sup>.

For the SPR measurements, polarized light from a HeNe laser at 633 nm was mechanically chopped at approximately 100 Hz and then coupled into a polarization maintaining fiber for efficient coupling into the waveguides in the TM polarization. The output from the waveguides was focused using a microscope objective lens and onto silicon photodiodes. The signal ( $P_{\text{sig}}$ ) and the reference ( $P_{\text{ref}}$ ) powers were recorded on a PC after noise reduction using lock-in amplifiers. The transmission of the gold-coated section of waveguide, including the transitions from the uncoated waveguide, is given by the ratio of the signal to the reference powers ( $P_{\text{sig}}/P_{\text{ref}}$ ). The schematic diagram of EC-SPR instrument setup is shown in Fig. 4.7.

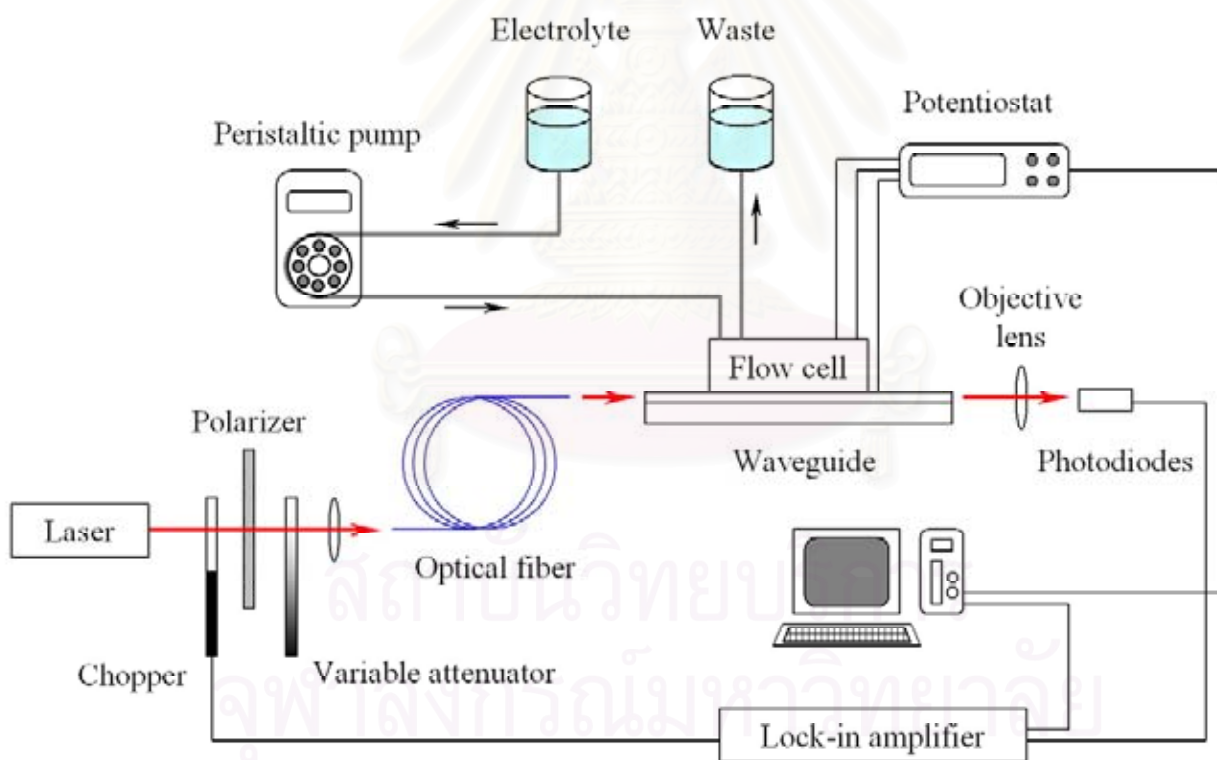


**Figure 4.7** Schematic diagram of EC-SPR instrument.



#### 4.7 EC-SPR Sensing of Decanethiol

Fig. 4.8 shows the current flowing as a result of the oxidation and reduction of a clean 1 mm long gold electrode by cyclic voltammetry in acid (solid line) together with the corresponding waveguide SPR measurements (dotted line). The current peaks associated with the oxidation (starting from 0.7 V) and reduction (0.4 V) of the gold can be clearly observed. The SPR measurements show a sharp drop in transmission on cycling to potentials anodic of 0.8 V, corresponding to the oxidation of gold, and a sharp increase in the transmission when stripping of the oxide occurs at 0.4 V on the reverse scan.

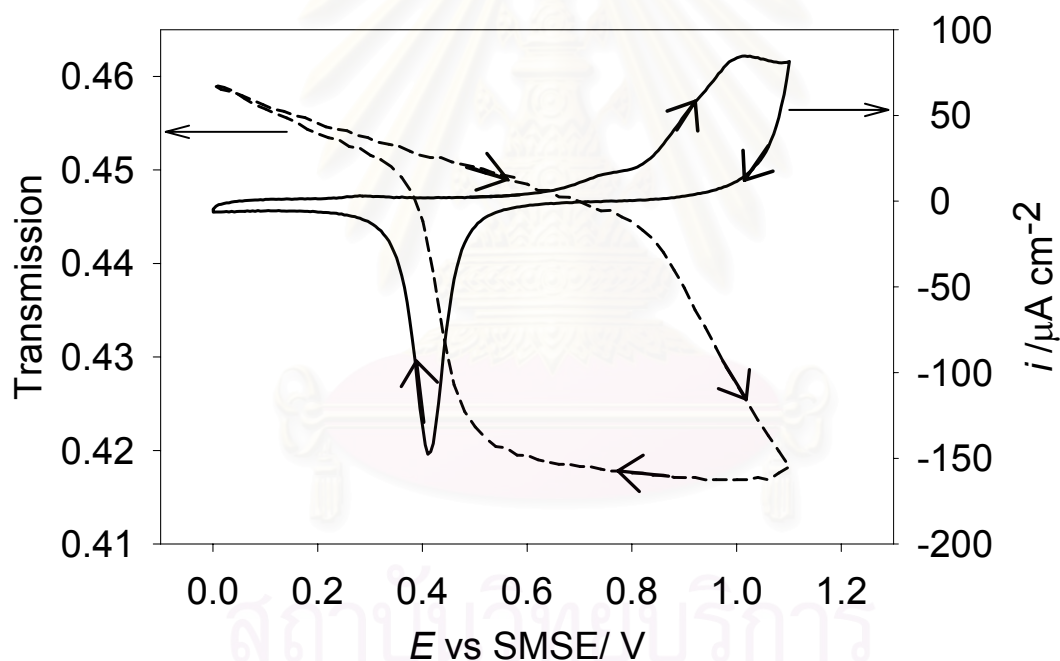


**Figure 4.8** Simultaneous signals of cyclic voltammetry (solid line) and SPR transmission (dashed line) recorded from a bare evaporated gold electrode (1 mm long) in 10 mM  $\text{H}_2\text{SO}_4$  at 20 mV/s.

The cyclic voltammetry was repeated for 10 cycles in order to clean the gold of any surface impurities before deposition of the decanethiol. Fig. 4.9 shows both the electrochemical (solid dark line) and the SPR (dotted line) response to the cyclic voltammetry in acid for evaporated gold electrodes coated with a decanethiol monolayer for a device of length 2 mm (Fig. 4.9a) and 1 mm (Fig. 4.9b). The electrochemical data is very similar to the data shown in Fig. 4.8 for the thiol desorption from a gold disk electrode. For example, in Fig. 4.9a the first electrochemical cycle shows a small oxidation current and correspondingly a very small reduction current at 0.4 V. For subsequent cycles, larger oxidation and reduction currents are observed, until the reproducible cyclic voltammograms are obtained with peak currents of 85 nA, similar to those expected for an untreated gold film. This device provides simultaneous SPR measurements to be made during the electrochemical desorption experiment.

The optical signals are shown by the dotted lines in Figs. 4.9a and 4.9b. In the first cycle the transmission shows only a small drop when compared to the data for the bare gold disc electrode. This result is consistent with the presence of a well-packed thiol layer at the electrode surface, which prevents the close approach of the anions to the electrode surface. At around 0.8 V, the transmission starts to fall. The optical data also show that the transmission at the end of each cycle increases with each subsequent cycle. The increase is largest for the first cycle, where a change of 2% is observed. After ten cycles, the shape and magnitude of both the optical and electrochemical data are similar to those measured for the untreated film. Similar behavior was observed in Fig. 4.9b, with currents approximately two times smaller, as expected for an electrode with a half in the surface area. Only 6 cycles are required to completely remove the thiol layer from the gold surface.

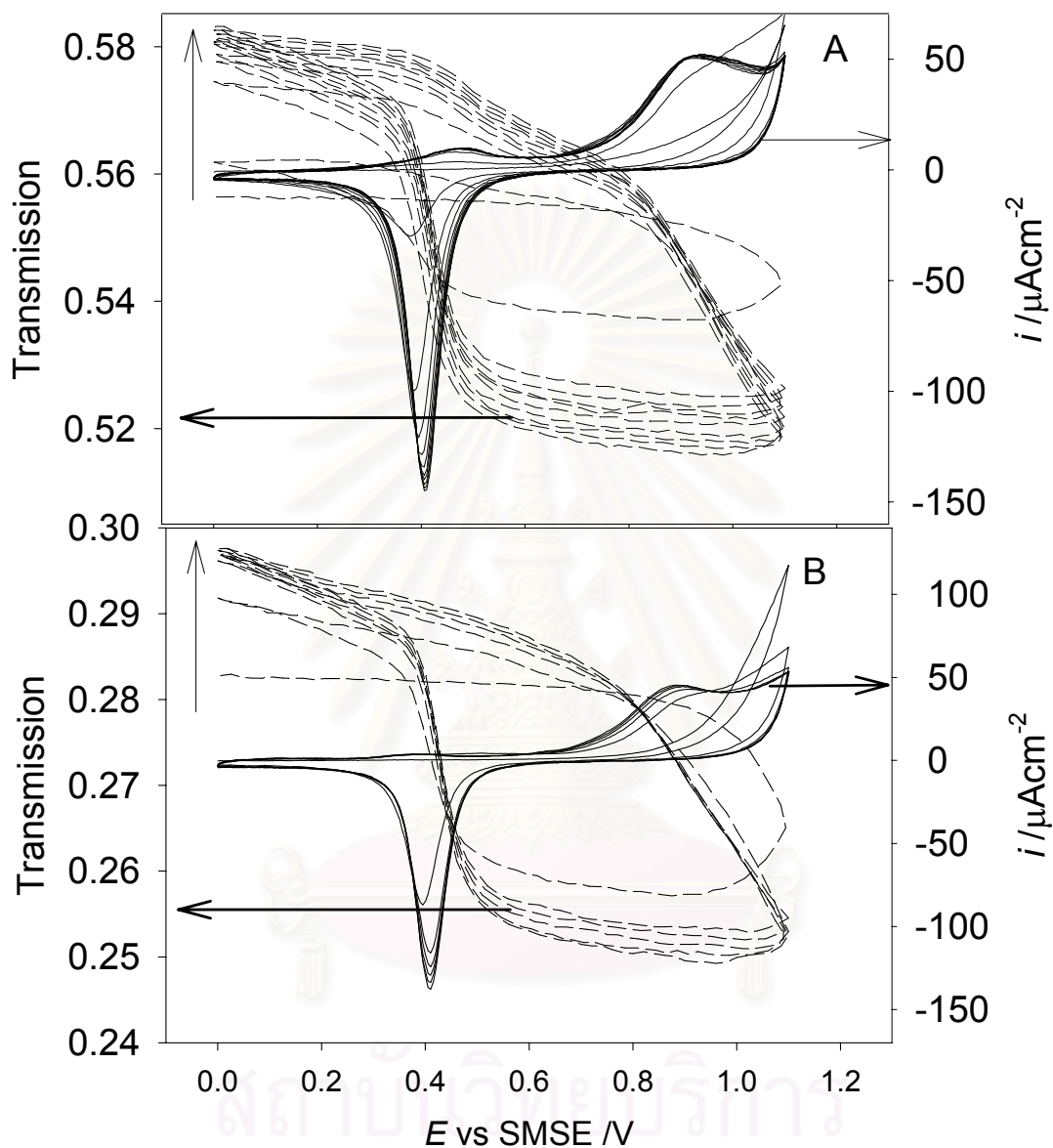


**Figure 4.9** The sequential cyclic voltammograms (solid lines) and simultaneous measurement of the SPR transmission (dashed lines) showing the oxidative desorption of decanethiol from the evaporated gold electrodes recorded at 20 mV/s in 10 mM H<sub>2</sub>SO<sub>4</sub>. The signals were obtained from a 2 mm (A) and a 1 mm long electrode (B).

These results show that cycling in acid causes the thiol to be desorbed from the evaporated gold surface as expected from the measurements on the gold disc electrode. An increase in the optical transmission on removal of the thiol layer together with an increase in the area under the reduction peak was observed. After ten cycles the thiol is completely stripped off and the cyclic voltammetry and SPR responses are almost identical to the responses of the clean gold surface. These results are consistent with the reports in the literature which show that oxidative desorption leads to the complete removal of the thiol from the electrode surface.

In order to understand the reaction in more detail we have calculated the area of gold exposed by the removal of the thiol during the experiment. The surface area of the electrode was calculated by assuming that the charge under the reduction peak corresponds to the desorption of one oxygen atom from each gold surface atom. The integral of the area under the reduction peak over time gives the charge passed during the reaction and, by using the result that  $420 \mu\text{C}$  corresponds to  $1 \text{ cm}^2$ , the area of the gold electrode can be calculated. The area of gold determined in this way for the untreated gold electrode is  $9.4 \times 10^{-4} \text{ cm}^2$  (for the 1 mm long electrode) and  $19.6 \times 10^{-4} \text{ cm}^2$  (for the 2 mm long electrode). This is larger than the actual electrode areas, of  $6 \times 10^{-4} \text{ cm}^2$  and  $12 \times 10^{-4} \text{ cm}^2$  respectively, due to surface roughness of the film produced by the evaporation process. The surface roughness, calculated as the ratio of the measured value to the actual area is  $\sim 1.5$ , similar to that measured for other evaporated gold electrodes. The percentage change in optical transmission measured at the end of each cycle (at 0 V) was plotted against the fractional coverage of thiol, calculated from the oxide stripping charge for each cycle, in Fig. 4.10, for both devices. The solid line is the linear regression for the data, the error bars were calculated assuming a 0.5% error in the current readings. The graph shows that there is a linear relationship between the thiol coverage and the change in optical transmission.

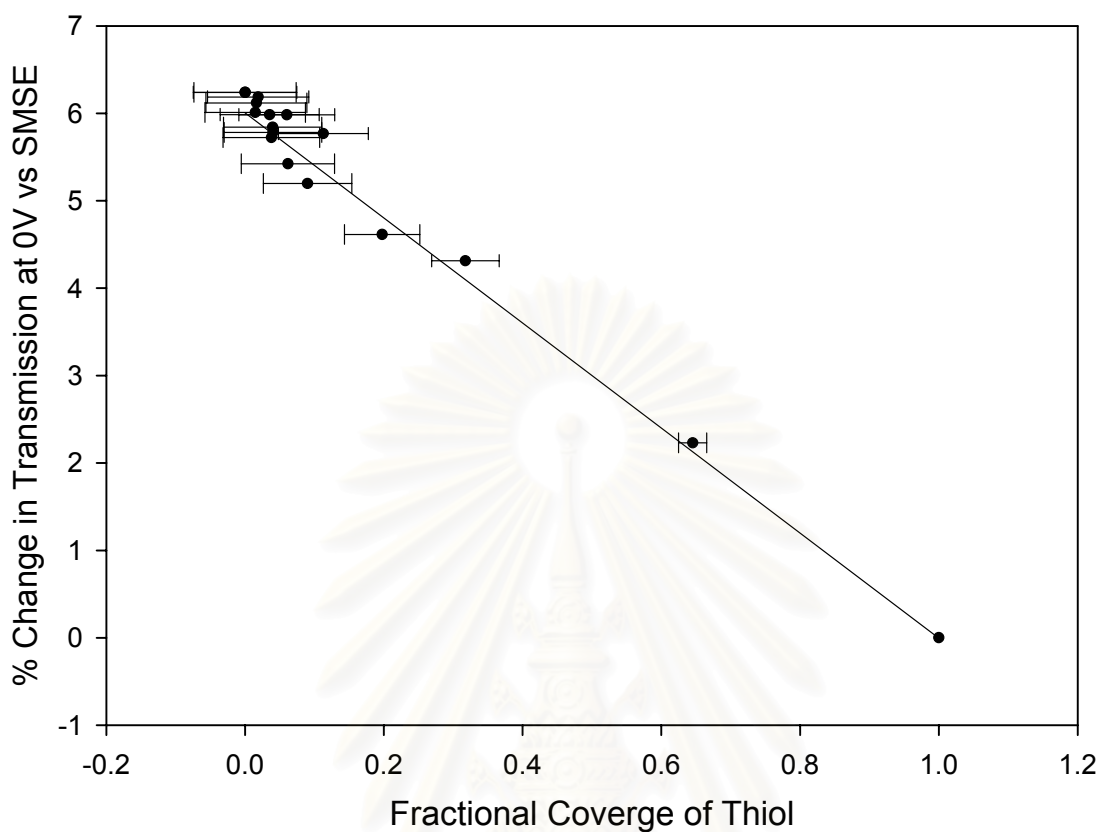


**Figure 4.10** The SPR transmission at 0.0 V plotted against the fractional coverage of the thiol calculated from the charge for the oxide stripping

#### 4.8 Conclusion

A self-assembled thiol layer could be removed from a gold electrode by oxidative desorption through cyclic voltammetry in acid. The removal of the thiol layer can be monitored in real time using both SPR and electrochemical techniques. The desorption process could be examined by comparing the fractional coverage of gold calculated from the area of the reduction peak with the change in SPR transmission. This demonstrates that electrochemical control coupled with sensitive optical measurements provides a basis for further development of this device into a powerful biosensor.

## CHAPTER IV

### CONCLUSION

#### 5.1 Conclusion

The flow cell was designed and constructed with low-cost materials purchased from the local hardware stores. The designs are simple, easy to operate and maintenance. Hydrodynamic behavior of each configuration was examined. All flow cells work properly and can be applied with the commercial accessories available in the laboratory such as electrodes, sample injection port, HPLC column, peristaltic pump or HPLC pump. Hybrid electrode configuration needs more mathematical approach to explain the hydrodynamic behavior at the electrode surface.

Channel flow cell equipped with BDD electrode is used as an amperometric detector in FIA and HPLC system for a determination of malachite green and leucomalachite green. This electrode exhibits excellent performance for the oxidative detection of both compounds. Well-defined voltammograms were obtained at BDD electrode, which exhibited high sensitivity. The results also indicate that BDD electrode has a potential to be used as a detector for other system.

By using a proper design, the flow cell can be used as an interface between electrochemical and optical system. This instrument is called electrochemical-Surface Plasmon Resonance (EC-SPR). A self-assembled thiol layer was removed from a gold electrode by oxidative desorption through cyclic voltammetry in acid. The removal of the thiol layer was observed simultaneously. This demonstrates that electrochemical control coupled with sensitive optical measurements provides a basis for further development of this device into a powerful biosensor.

## 5.2 Suggestions for Future Works

Future works should focus on:

1. Hydrodynamic behavior of hybrid electrode configuration by using a computer simulation.
2. Electrochemical reaction of malachite green and leucomalachite green.
3. Further development of EC-SPR system for biosensor applications



สถาบันวิทยบริการ  
จุฬาลงกรณ์มหาวิทยาลัย

## REFERENCES

- (1) Bard, A. J.; Faulkner, L. R. *Electrochemical Methods Fundamentals and Applications*. USA, John Wiley & Sons, Inc: 1980.
- (2) Pletcher, D.; Greef, R.; Peat, R.; Peter, L. M.; Robinson, J. *Instrumental methods in electrochemistry*. England, Horwood Publishing: 1985.
- (3) Ruzicka, J. *Flow Injection Analysis*. 2 ed.; New York, John Wiley & Sons: 1988.
- (4) Monk, P. M. S. *Fundamentals of Electroanalytical Chemistry*. Chichester, New York, Weinheim, Brisbane, Toronto, Singapore, John Wiley & Sons: 2001.
- (5) Eggins, B. R. *Chemical Sensors and Biosensors*. Chichester, New York, Weinheim, Brisbane, Toronto, Singapore, John Wiley & Sons, Ltd: 2002.
- (6) Cunningham, A. J. *Introduction to Bioanalytical Sensors*. New York, John Wiley & Sons, Inc: 1998.
- (7) Zhongping, Y.; Gonzalez-Cortes, A.; Jourquin, G.; Vire, J.-C.; Kauffmann, J.-M.; Delplancke, J.-L. *Biosensors and Bioelectronics* **1995**, *10*, 789-795.
- (8) Ferretti, S.; Paynter, S.; Russell, D. A.; Sapsford, K. E.; Richardson, D. J. *TrAC Trends in Analytical Chemistry* **2000**, *19*, 530-540.
- (9) Chaki, N. K.; Vijayamohanan, K. *Biosensors and Bioelectronics* **2002**, *17*, 1-12.
- (10) Aizawa, M.; Nishiguchi, K.; Imamura, M.; Kobatake, E.; Haruyama, T.; Ikariyama, Y. *Sensors and Actuators B: Chemical* **1995**, *24*, 1-5.
- (11) Dong, S.; Li, J. *Bioelectrochemistry and Bioenergetics* **1997**, *42*, 7-13.
- (12) Gooding, J. J.; Hibbert, D. B. *TrAC Trends in Analytical Chemistry* **1999**, *18*, 525-533.
- (13) Kasemo, B. *Surface Science* **2002**, *500*, 656-677.
- (14) Busse, S.; Kashammer, J.; Kramer, S.; Mittler, S. *Sensors and Actuators B: Chemical* **1999**, *60*, 148-154.
- (15) Kim, S.-H.; Ock, K.-S.; Kim, J.-H.; Koh, K.-N.; Kang, S.-W. *Dyes and Pigments* **2001**, *48*, 1-6.
- (16) Bartlett, P. N.; Brace, K.; Calvo, E. J.; Etchenique, R. *J. Materials Chem.* **2000**, *10*, 149-156.



- (17) Abanulo, J. C.; Harris, R. D.; Bartlett, P. N.; Wilkinson, J. S. *Applied Optics* **2001**, *40*, 6242-6245.
- (18) Abanulo, J. C.; Harris, R. D.; Sheridan, A. K.; Wilkinson, J. S.; Bartlett, P. N. *Faraday Discuss.* **2002**, *121*, 139-152.
- (19) Badia, A.; Arnold, S.; Scheumann, V.; Zizlsperger, M.; Mack, J.; Jung, G.; Knoll, W. *Sensors and Actuators B: Chemical* **1999**, *54*, 145-165.
- (20) Gooding, J. J.; Erokhin, P.; Hibbert, D. B. *Biosensors and Bioelectronics* **2000**, *15*, 229-239.
- (21) Kodama, C.; Hayashi, T.; Nozoye, H. *Applied Surface Science* **2001**, 264-267.
- (22) Gooding, J. J.; Pugliano, L.; Hibbert, D. B.; Erokhin, P. *Electrochemistry Communications* **2000**, *2*, 217-221.
- (23) Vianello, F.; Cambria, A.; Ragusa, S.; Cambria, M. T.; Zennaro, L.; Rigo, A. *Biosensors and Bioelectronics* **2004**, Inpress.
- (24) Krysinski, P.; Brzostowska-Smolska, M. *Bioelectrochemistry and Bioenergetics* **1998**, *44*, 163-168.
- (25) Nakamura, T.; Aoki, K.; Chen, J. *Electrochemistry Communications* **2002**, *4*, 521-526.
- (26) Tamada, K.; Nagasawa, J.; Nakanishi, F.; Abe, K.; Hara, M.; Knoll, W.; Ishida, T.; Fukushima, H.; Miyashita, S.; Usui, T. *Thin Solid Films* **1998**, *327-329*, 150-155.
- (27) Zerulla, D.; Uhlig, I.; Szargan, R.; Chasse, T. *Surface Science* **1998**, *402-404*, 604-608.
- (28) Diao, P.; Jiang, D.; Cui, X.; Gu, D.; Tong, R.; Zhong, B. *Journal of Electroanalytical Chemistry* **1999**, *464*, 61-67.
- (29) Krysinski, P.; Moncelli, M. R.; Tadini-Buoninsegni, F. *Electrochimica Acta* **2000**, *45*, 1885-1892.
- (30) Xing, Y. F.; O'Shea, S. J.; Li, S. F. Y. *Journal of Electroanalytical Chemistry* **2003**, *542*, 7-11.
- (31) Ulman, A.; Kang, J. F.; Shnidman, Y.; Liao, S.; Jordan, R.; Choi, G.-Y.; Zaccaro, J.; Myerson, A. S.; Rafailovich, M.; Sokolov, J.; Fleischer, C. *Reviews in Molecular Biotechnology* **2000**, *74*, 175-188.

- (32) Batz, V.; Schneeweiss, M. A.; Kramer, D.; Hagenstrom, H.; Kolb, D. M.; Mandler, D. *Journal of Electroanalytical Chemistry* **2000**, *491*, 55-68.
- (33) Madueno, R.; Sevilla, J. M.; Pineda, T.; Roman, A. J.; Blazquez, M. *Journal of Electroanalytical Chemistry* **2001**, *506*, 92-98.
- (34) Raj, C. R.; Ohsaka, T. *Bioelectrochemistry* **2001**, *53*, 251-256.
- (35) Qu, D.; Morin, M. *Journal of Electroanalytical Chemistry* **2001**, *517*, 45-53.
- (36) Ion, A.; Partali, V.; Sliwka, H.; Sliwka, R.; Banica, F. G. *Electrochemistry Communications* **2002**, *4*, 674-678.
- (37) Cordas, C. M.; Viana, A. S.; Leupold, S.; Montforts, F.-P.; Abrantes, L. M. *Electrochemistry Communications* **2003**, *5*, 36-41.
- (38) Yang, Z.; Engquist, I.; Liedberg, B.; Kauffmann, J.-M. *Journal of Electroanalytical Chemistry* **1997**, *430*, 189-195.
- (39) Kretschmann, E.; Raether, H. *Naturforsch* **1968**, 2135-2136.
- (40) Frutos, A. G.; Corn, R. M. *Anal. Chem* **1998**, *70*, 449A-455A.
- (41) Malmqvist, M. *Nature* **1993**, *361*, 186-187.
- (42) Cooper, J. M.; Cass, A. E. G. *Biosensors. A Practical Approach*. Oxford, Oxford University Press: 2003.
- (43) Kötz, R.; Kolb, D. M.; Sass, J. K. *Surf. Sci* **1997**, *69* 359-364.
- (44) Chao, F.; Costa, M.; Tadjeddine, A.; Abeles, F.; Lopez-Rios, T.; Theye, M. L. *J. Electroanal. Chem* **1997**, *83* 65.
- (45) Iwasaki, Y.; Horiuchi, T.; Morita, M.; Niwa, O. *Electroanalysis* **1997**, *9*, 1239-1241.
- (46) Iwasaki, Y.; Horiuchi, T.; Morita, M.; Niwa, O. *Sensors and Actuators B* **1998**, *50*, 145-148.
- (47) Iwasaki, Y.; Horiuchi, T.; Morita, M.; Niwa, O. *Surf. Sci* **1999**, *428*, 195-198.
- (48) Hadjadj, A. *J. Electroanal. Chem.* **1988**, *246*, 43-51.
- (49) Tadjeddine, A.; Kolb, D. M.; Kötz, R. *Surf. Sci* **1980**, *101*, 277-285.
- (50) Itoh, K.; Fujishima, A. *J. Phys. Chem* **1988**, *92* 7043-7045.
- (51) Dunphy, D. R.; Mendes, S. B.; Saavedra, S. S.; Armstrong, N. R. *Anal. Chem.* **1997**, *69*, 3086-3094.

- (52) Lavers, C. R.; Harris, R. D.; Hao, S.; Wilkinson, J. S.; O'Dwyer, K.; Brust, M.; Schiffrin, D. J. *J. Electroanal. Chem.* **1995**, *387*, 11-22.
- (53) Widrig, C. A.; Chung, C.; Porter, M. D. *J. Electroanal. Chem.* **1991**, *310*, 335-359.
- (54) Yang, D. F.; Al-Maznai, H.; Morin, M. *J. Phys. Chem. B* **1997**, *101*, 1158-1166.
- (55) Weissharr, D. E.; Walczak, M. M.; Porter, M. D. *Langmuir* **1993**, *9* 323-329.
- (56) Calvente, J. J.; Kovacova, Z.; Sanchez, M. D.; Andreu, R.; Fawcett, W. R. *Langmuir* **1996**, *12*, 5696-5703.
- (57) Srivastava, S.; Sinha, R.; Roy, D. *Aquatic Toxicology* **2004**, *66*, 319-329.
- (58) Mitrowska, K.; Posyniak, A.; Zmudzki, J. *Journal of Chromatography A* **2005**, *1089*, 187-192.
- (59) Allen, J. L.; Gofus, J. E.; Meinertz, J. R. *Journal of AOAC International* **1994**, *77*, 553-557.
- (60) Mitrowska, K.; Posyniak, A. *BULLETIN OF THE VETERINARY INSTITUTE IN PULAWY* **2004**, *48*, 173-176.
- (61) Bergwerff, A. A.; Scherpenisse, P. *Journal of Chromatography B* **2003**, *788*, 351-359.
- (62) Turnipseed, S. B.; Roybal, J.; Rupp, H. S.; Hurlbut, J. A.; Long, A. R. *Journal of Chromatography B: Biomedical Sciences and Applications* **1995**, *670*, 55-62.
- (63) Turnipseed, S. B.; Roybal, J. E.; Hurlbutt, J. A.; Long, A. R. *Journal of AOAC International* **1995**, *78*, 971-977.
- (64) Matysik, F.-M. *Journal of Chromatography A* **1998**, *802*, 349-354.
- (65) Safarik, I.; Safarikova, M. *Water Research* **2002** *36* 196-200.
- (66) Deviolet, P. F.; Belin, C.; Nougayrede, P.; Marbach, M. *ANALUSIS* **1995** *23*, 110-113.
- (67) Fink, W.; Auch, J. *Deutsche Lebensmittel-Rundschau* **1993**, *89*, 246-251
- (68) Roybal, J. E.; Pfenning, A. P.; Munns, R. K.; Holland, D. C.; Hurlbut, J. A.; Long, A. R. *Journal of AOAC International* **1995**, *78*, 453-457.
- (69) Rushing, L. G.; Hansen, J. E. B. *Journal of Chromatography B: Biomedical Sciences and Applications* **1997**, *700*, 223-231.

- (70) Halme, K.; Lindfors, E.; Peltonen, K. *Food Additives and Contaminants* **2004**, *21*, 641-648.
- (71) Doerge, D. R.; Churchwell, M. I.; Gehring, T. A.; Pu, Y. M.; Plakas, S. M. *Rapid Communications in Mass Spectrometry* **1998**, *12* 1625-1634.
- (72) van de Riet, J. M.; Murphy, C. J.; Pearce, J. N.; Potter, R. A.; Burns, B. G. *Journal of AOAC International* **2005**, *88*, 744-749.
- (73) Valle, L.; Diaz, C.; Zanocco, A. L.; Richter, P. *Journal of Chromatography A* **2005**, *1067*, 101-105.
- (74) Plakas, S. M.; El Said, K. R.; Stehly, G. R.; Roybal, J. E. *Journal of AOAC International* **1995**, *78*, 1388-1394.
- (75) Hajee, C. A. J.; Haagsma, N. *Journal of Chromatography B: Biomedical Sciences and Applications* **1995**, *669*, 219-227.
- (76) Tarbin, J. A.; Barnes, K. A.; Bygrave, J.; Farrington, W. H. H. *ANALYST* **1998**, *123*, 2567-2571.
- (77) Scherpenisse, P.; Bergwerff, A. A. *Analytica Chimica Acta* **2005**, *529*, 173-177.
- (78) Swarbrick, A.; Murby, E. J.; Hume, P. *Journal of Liquid Chromatography & Related Technologies* **1997**, *20*, 2269-2280
- (79) Sagar, K.; Smyth, M. R.; Wilson, J. G.; McLaughlin, K. *Journal of Chromatography A* **1994**, *659*, 329-336.
- (80) Ivandini, T. A.; Sarada, B. V.; Terashima, C.; Rao, T. N.; Tryk, D. A.; Ishiguro, H.; Kubota, Y.; Fujishima, A. *Journal of Chromatography B* **2003**, *791*, 63-72.
- (81) Chailapakul, O.; Popa, E.; Tai, H.; Sarada, B. V.; Tryk, D. A.; Fujishima, A. *Electrochemistry Communications* **2000**, *2*, 422-426.
- (82) Siangproh, W.; Ngamukot, P.; Chailapakul, O. *Sensors and Actuators B: Chemical* **2003**, *91*, 60-66.
- (83) Wangfuengkanagul, N.; Chailapakul, O. *Talanta* **2002**, *58*, 1213-1219.
- (84) Siangproh, W.; Wangfuengkanagul, N.; Chailapakul, O. *Analytica Chimica Acta* **2003**, *499*, 183-189.
- (85) Boonsong, K.; Chuanuwatanakul, S.; Wangfuengkanagul, N.; Chailapakul, O. *Sensors and Actuators B: Chemical* **2005**, *108*, 627-632.

- (86) Banks, C. E.; Simm, A. O.; Bowler, R.; Dawes, K.; Compton, R. G. *Anal. Chem.* **2005**, *77*, 1928-1930.
- (87) Stubbings, G.; Tarbin, J.; Cooper, A.; Sharman, M.; Bigwood, T.; Robb, P. *Analytica Chimica Acta* **2005**, *547*, 262-268.
- (88) Widrig, C. A.; Chung, C.; Porter, M. D. *J. Electroanal. Chem.* **1991**, *310*, 335-359.
- (89) Yang, D. F.; Al-Maznai, H.; Morin, M. *J. Phys. Chem. B* **1997**, *101*, 1158-1166.



สถาบันวิทยบริการ  
จุฬาลงกรณ์มหาวิทยาลัย



**APPENDIX**

สถาบันวิทยบริการ  
จุฬาลงกรณ์มหาวิทยาลัย

# Cost-Effective Flow Cell for the Determination of Malachite Green and Leucomalachite Green at a Boron-Doped Diamond Thin-Film Electrode

Passapol NGAMUKOT,\* Thiraporn CHAROENRAKS,\* Orawon CHAILAPAKUL,\*†  
Shoji MOTOMIZU,\*\* and Suchada CHUANWATANAKUL\*†

\*Sensor Research Unit, Department of Chemistry, Faculty of Science, Chulalongkorn University,  
Phayathai Road, Patumwan, Bangkok 10330, Thailand

\*\*Department of Chemistry, Faculty of Science, Okayama University,  
Tsushima-1-1, Okayama 700-8530, Japan

An electrooxidation and a cost-effective flow-based analysis of malachite green (MG) and leucomalachite green (LMG) were investigated at a boron-doped diamond thin-film (BDD) electrode. Cyclic voltammetry as a function of the pH of the supporting electrolyte solution was studied. Comparison experiments were performed with a glassy carbon electrode. A well-defined cyclic voltammogram, providing the highest peak current, was obtained when using phosphate buffer at pH 2. The potential sweep-rate dependence of MG and LMG oxidation (peak currents for 1 mM MG and LMG linearly proportional to  $v^{1/2}$ , within the range of 0.01 to 0.3 V/s) indicates that the oxidation current is a diffusion-controlled process on the BDD surface. In addition, hydrodynamic voltammetry and amperometric detection using the BDD electrode combined with a flow injection analysis system was also studied. A homemade flow cell was used, and the results were compared with a commercial flow cell. A detection potential of 0.85 V was selected when using a commercial flow cell, at which MG and LMG exhibited the highest signal-to-background ratios. For the homemade flow cell, a detection potential of 1.1 V was chosen because MG and LMG exhibited a steady response. The flow analysis results showed linear concentration ranges of 1 - 100  $\mu\text{M}$  and 4 - 80  $\mu\text{M}$  for MG and LMG, respectively. The detection limit for both compounds was 50 nM.

(Received September 29, 2005; Accepted November 23, 2005)

## Introduction

In a research group having many researchers and students working in the same laboratory, using individual equipment would be the best way to prevent any cross-contamination problems. However, some equipment is very expensive, *e.g.* the flow cells in flow injection, and related technique. Because a commercial flow cell is very expensive, the use of a homemade version would be an alternative choice when a limited budget is available. This paper describes a concept of using a cost-effective flow-based analysis of malachite green and leucomalachite green at a boron-doped diamond thin-film electrode.

Malachite green (MG), a triphenylmethane dye ( $\text{C}_{23}\text{H}_{26}\text{N}_2\text{O}$ ; the chemical structures of MG and LMG are shown in Fig. 1), is used as fungicide, ectoparasiticide and antiseptic in the aquaculture industry. It is extremely effective against protozoal and fungal infections. Moreover, malachite green is also used as a food coloring agent, food additive, a medical disinfectant and anthelmintic as well as a dye in silk, wool, leather, cotton and paper. Presently, many countries are concerned about the residues of MG and its reduced form, leucomalachite green (LMG), because of the toxicity of these dyes. It has been

reported to cause carcinogenesis, mutagenesis, chromosomal fractures, tetragenicity and respiratory toxicity. The use of malachite green has been banned in many countries, and is not approved by the US Food and Drug Administration.<sup>1</sup>

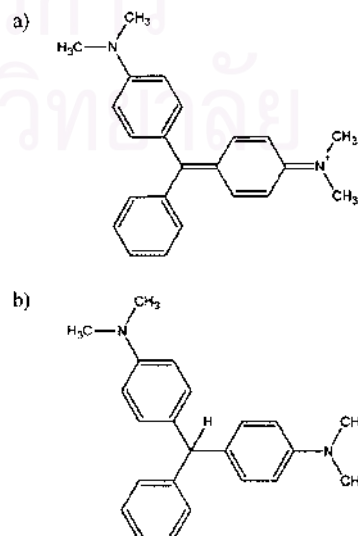


Fig. 1 Chemical structures of (a) MG and (b) LMG.

† To whom correspondence should be addressed.  
E-mail: corawon@chula.ac.th

Therefore; many methods have been developed for the detection of MG and LMG at low levels. Several methods have been described for the determination of MG and LMG in a variety of matrices, including liquid chromatography,<sup>2-6</sup> gas chromatography,<sup>7</sup> capillary electrophoresis,<sup>8</sup> spectrometry,<sup>9</sup> and spectrofluorometry.<sup>10</sup> HPLC is commonly used to detect MG and LMG with different detection techniques, such as visible (VIS),<sup>11,12</sup> fluorescence,<sup>13</sup> mass spectrometry,<sup>14-17</sup> and electrochemical detection. Most of these methods using the postcolumn oxidation of LMG to MG with lead(IV) oxide (PbO<sub>2</sub>),<sup>18-21</sup> or an electrochemical cell<sup>22</sup> are normally required. These techniques need expensive apparatus and reagents, and are also time-consuming. A sensitive, rapid and cheap method for analysis is still needed.

Electrochemical methods are widely used in many applications because they are simple, fast and economical. The electrochemical detection of MG has been reported using a carbon-fiber microelectrode<sup>23</sup> and a Pt electrode as a working electrode and a counter electrode, respectively. However, the sensitivity and reproducibility of electrodes were poor because the electrode surface was contaminated by fouling products and impurities. Boron-doped diamond thin-film electrodes can be used to eliminate these problems. The unique properties of BDD electrodes are more attractive, including a wide electrochemical potential window, a very low background current and long-term stability of the responses.<sup>24,25</sup> BDD electrodes have been successfully used for the detection of various analytes, such as captopril,<sup>26</sup> acetaminophen,<sup>27</sup> tiopronin<sup>28</sup> and lincomycin.<sup>29</sup> No reports described the use of BDD electrodes for the detection of MG and LMG.

In the present work, we used the BDD electrodes to study the electrochemical oxidation of MG and LMG by cyclic voltammetry. In addition, the detection of these analytes was examined by FIA with amperometric detection.

## Experimental

### Reagents and chemicals

All reagents were of analytical grade, and all solutions were prepared by using deionized water. Malachite green oxalate and leucomalachite green were obtained from Sigma Chemical (USA). Sodium dihydrogen orthophosphate (BDH), sodium hydroxide (Merck) and phosphoric acid 85% (Merck) were used to prepare a buffer solution. A phosphate buffer solution with pH ranges from 2.0 to 8.0 were prepared from 0.1 M sodium dihydrogen orthophosphate, and adjusted to the desired pH using phosphoric acid and sodium hydroxide. MG and LMG were prepared by dissolving an appreciate amount of MG and LMG in the buffer solution. The solutions were prepared daily.

In order to characterize the homemade flow cell, concentrated sulfuric acid (BDH) was diluted to prepare a cleaning solution for a gold electrode. K<sub>4</sub>Fe(CN)<sub>6</sub> (Riedel-de Haën) and KCl (Merck) were used as a probe and electrolyte, respectively.

### Electrodes

The BDD electrodes were used as received without any further modifications. A GC electrode was purchased from Bioanalytical System, Inc. (area 0.07 cm<sup>2</sup>). A gold disc electrode ( $\phi$  3 mm) that was used to characterize the homemade flow cell was purchase from Metrohm. Both GC, and gold electrodes were pretreated by sequential polishing with 1 and 0.05  $\mu$ m of alumina/water slurries on felt pads, followed by rinsing with ultrapure water prior to use. In addition, the gold electrode was electrochemically cleaned by cycling in 0.1 M

H<sub>2</sub>SO<sub>4</sub> until a stable reductive current was obtained.

### Cyclic voltammetric investigation

Electrochemical experiments were conducted out in a single-compartment three-electrode glass cell. The BDD electrode was pressed against a smooth ground joint at the bottom of the cell, isolated by an O-ring (area 0.07 cm<sup>2</sup>). Electrical contact was made by placing the backside of the Si substrate onto a brass holder. The GC carbon was used as a working electrode for a comparison. Ag/AgCl with a salt bridge and Pt wire were used as a reference electrode and a counter electrode, respectively. A voltammetric measurement was performed with the three-electrode system using Autolab Potentiostat 100 (Eco-Chemie, The Netherlands).

### Flow injection with amperometric detection

The flow injection system consisted of a thin-layer flow cell (Bioanalytical System, Inc.) and a homemade flow cell, a 20  $\mu$ L stainless-steel loop of injection port (Rheodyne 7725), a peristaltic pump, and electrochemical detection (Autolab potentiostat 100). The carrier solution, 0.1 M sodium dihydrogen orthophosphate, was regulated at a flow rate of 1.0 ml min<sup>-1</sup>. The thin-layer flow cell, through an electrochemical cell, consisted of a silicone rubber gasket as a spacer, a BDD electrode as the working electrode, a Ag/AgCl electrode as the reference electrode and a stainless-steel tube as a counter electrode (also function as an outlet of the flow cell). All experiments were performed at room temperature. In order to reduce the electronic noise, a copper faradaic-cage was used throughout the whole research.

### HPLC chromatography coupled with a boron-doped diamond thin-film electrode

A HPLC column (Inersil<sup>®</sup> ODS-3, C<sub>18</sub>, GL Sciences Inc., Japan) was added to the flow system. A mixture standard solution of MG and LMG (200 ppm) was injected. The mobile phase was prepared by mixing acetonitrile, and 0.1 M phosphate buffer (pH 2); (1:1 ratio) was regulated at a flow rate of 1.0 ml min<sup>-1</sup> using a HPLC pump (Model 510, Waters). The operating potential was kept constant at 1.1 V vs. Ag/AgCl.

## Results and Discussion

### Cyclic voltammetry

Figure 2 shows a typical cyclic voltammogram for 1 mM of MG with a corresponding background current of 0.1 M phosphate buffer (pH 2) at 50 mV/s. A BDD electrode exhibited a well-defined and higher current response than a GC electrode (both the BDD and GC electrodes had the same electrode area). In addition, the background current of the GC electrode was much higher. Malachite green gave a higher current response than leucomalachite green, regardless of the BDD or GC electrodes that were used.

Based on the literature, the electrochemical mechanisms of both compounds have not been investigated. However, it has been reported that MG can be oxidized by the azide radical, which is a well-known one-electron oxidant.<sup>30</sup> This oxidation reaction easily generates the MG radical due to the strong resonance electron-donating effect of the dimethylamino groups. Therefore, we believe that the electrooxidation process would occur *via* the MG/LMG radical at an N atom containing lone-pair electron (the easiest losing electron position).

Two anodic peaks obtained for MG at the GC electrode could have resulted from an electrochemical "ECE" reaction (electron



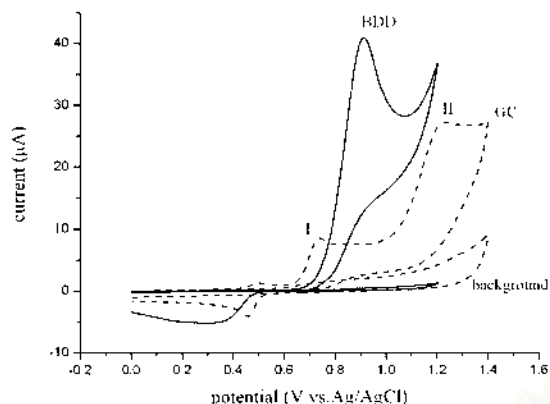


Fig. 2 Cyclic voltammogram of 1 mM malachite green in a buffer (pH 2) at a BDD electrode (solid line) and a glassy carbon electrode (dash line). The scan rate was 50 mV/s.

transfer followed by a chemical reaction, which in turn produces a new electroactive species). In the case of the BDD electrode, the second peak of MG should have been observed if the potential was swept further to the anodic direction. According to the property of the BDD electrode, the potential should be stopped before exceeding 1.2 V to avoid oxide formation on the surface. The slight shift of the oxidation peak on the BDD electrode would be affected by the slower kinetic.

The reduction peak of MG was found at 0.35 V in a reversed scan, and the potential difference between  $E_{ox}$  and  $E_{red}$  was much larger than  $59 \text{ mV}/n$  (in this case  $n = 1$ ), indicating that this electrooxidation was a quasi-reversible process.

For LMG, no reduction peak was observed on the reversed scan, and only one anodic peak was obtained. This evidence made clear that the oxidation of LMG was an irreversible process, and could be an electrochemical "EC" reaction (electron transfer followed by a chemical reaction). The difference in the electrochemical response between MG and LMG can be affected by the structures (Fig. 1) of both compounds. LMG is neutral, whereas MG is positively charge molecule.

#### pH effect

The effect of the pH was investigated from pH 2–8 for malachite green. It was found that the higher was the buffer pH, the smaller was the oxidation peak. It was reported that malachite green has two forms, depending on the pH.<sup>31</sup> The initial strong green color of MG was obtained at a low pH (acidic), while in an alkaline aqueous solution, it was converted to a colorless carbinol form. From this study, MG provided the highest oxidation peak at pH 2 at the BDD electrode, and the lowest response at pH 8. It could be explained that the higher is the pH, the smaller is MG due to the conversion of the MG form to carbinol form.

It also has been found that the pH affects the solubility of both MG and LMG. Because MG has less polarity than water,  $\text{H}^+$  in an acidic solution would protonate on the N atom and increases the polarity of the molecule. Therefore, decreasing the buffer pH would help the compound to dissolve in water. LMG has a solubility problem as well. It couldn't dissolve in a buffer between pH 3 and pH 8. Only in a buffer pH 2, could LMG be dissolved, and provided the oxidation peak. Therefore, a buffer of pH 2 was chosen to prepare both MG and LMG in all experiments.

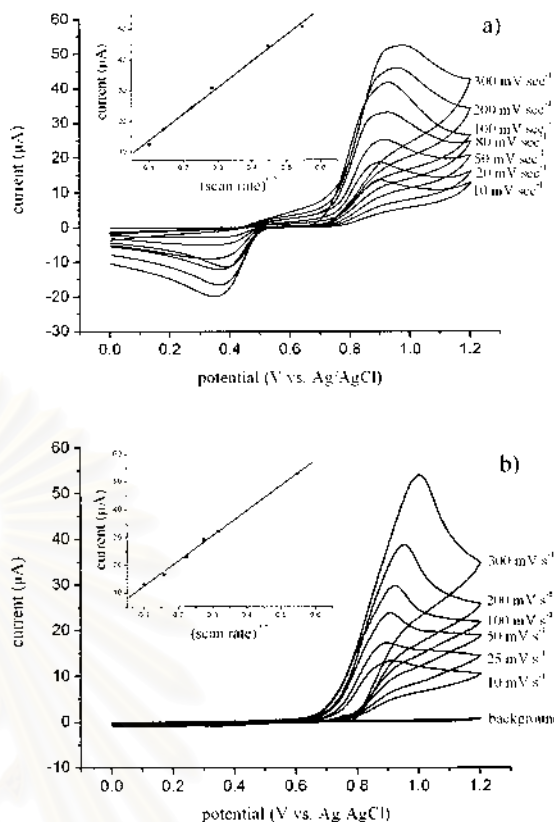


Fig. 3 Cyclic voltammograms of 1 mM malachite green (a) and leucomalachite green (b) in 0.1 phosphate buffer (pH 2) at a BDD electrode with a variation of the scan rates. A plot between the current response and the square root of the scan rate is also shown in the inset.

#### Scan rate dependence study

Figure 3 shows the cyclic voltammetric response of 1 mM malachite and leucomalachite green at the BDD electrode in a 0.1 M phosphate buffer of pH 2 with a variation in the scan rate from 0.01 to 0.3 V/s. A plot of the oxidation current versus the square root of the scan rate,  $v^{1/2}$ , was highly linear ( $r > 0.99$ ) for both compounds, as shown in the inset of the figures. The results indicate that the electrochemical reaction is a diffusion-controlled process.

#### Characterization of the homemade flow cell

A homemade flow cell (as shown in Fig. 4) was constructed from thermoplastic (Plexiglas). This kind of material provides a moderate chemical-resistance, when compared with Teflon or PEEK (polyether-ether-ketone), but is still suitable for an electrochemical system with an aqueous electrolyte or buffer. Because Plexiglas is transparent, any bubble or stain that could be trapped inside the flow cell would be observed quite easily. The thin-layer configuration was chosen to design and construct the flow cell. The BDD electrode was placed upstream in order to avoid any possible contamination of an electrochemical by-product from the counter electrode.

The mass-transport behavior of the homemade flow cell was characterized using a well-known equation,<sup>32</sup>

$$I_{lim} = kc_{\text{analyte}}V_f^y, \quad (1)$$

where  $I_{lim}$  is the limiting current (mA),  $V_f$  is the rate of solution flow (express as a volume per unit of time, normally in  $\text{cm}^3/\text{s}$ )

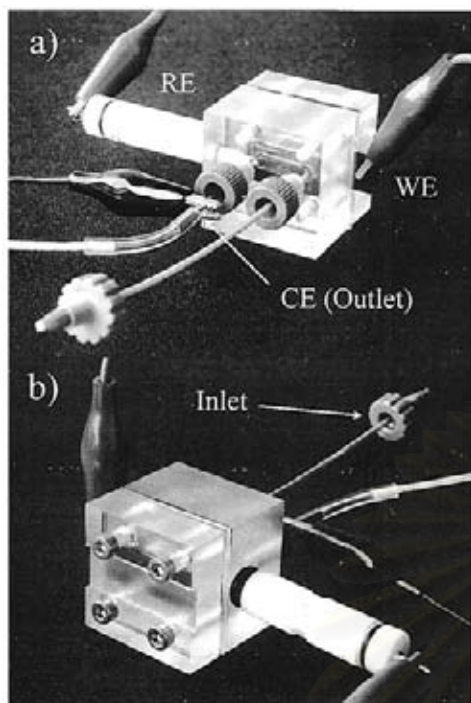


Fig. 4 Homemade flow cell with the BDD electrode as a working electrode (WE), Ag/AgCl as a reference electrode (RE) and a stainless-steel tube as a counter electrode (CE). Front view (a) and rear view (b).

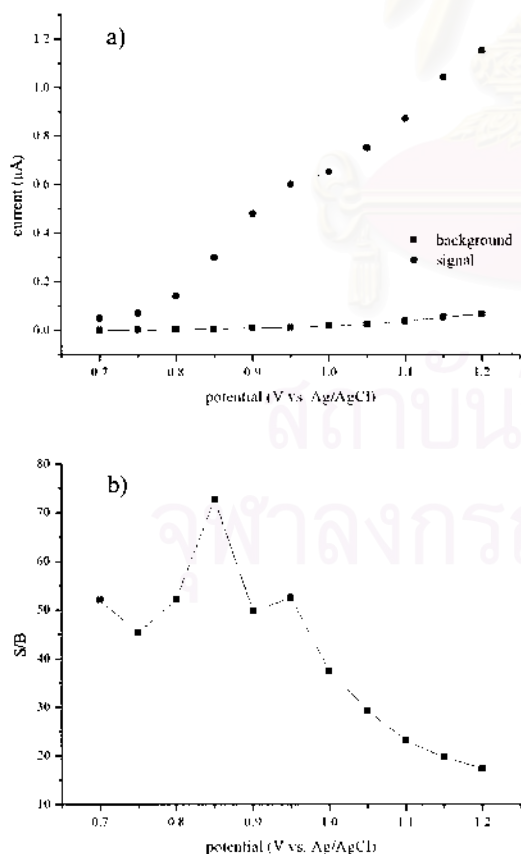


Fig. 5 Hydrodynamic voltammetric  $I-E$  curve obtained at the BDD electrode for 20  $\mu\text{L}$  injection of 0.05 mM of malachite green in 0.1 M phosphate buffer pH 2 (a). Hydrodynamic voltammetric  $S/B$  ratios versus potential curve (b). The signals were obtained from a commercial flow cell.

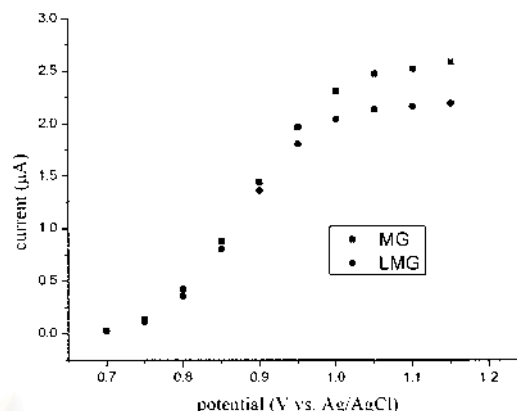


Fig. 6 Hydrodynamic voltammetric  $I-E$  curve obtained at the BDD electrode for 20  $\mu\text{L}$  injection of 0.05 mM of malachite green and leucomalachite green in 0.1 M phosphate buffer pH 2. The signals were obtained from a homemade flow cell.

and  $y$  is an exponent that depends on the cell design. In order to ensure that the solution flow is laminar, a solution of 0.1 M  $\text{K}_4\text{Fe}(\text{CN})_6$  in 0.1 M KCl was pumped into the flow cell continuously and the limiting current was recorded as function of  $V_f$ . A plot of  $\log I_{\text{lim}}$  as "y" against  $\log V_f$  as "x" should be linear with a gradient of 0.33 for a simple flow cell. A peristaltic pump was used with a variation of the flow rate from 0.005 to 0.06  $\text{cm}^3/\text{s}$  (0.3 to 3.6 mL/min). A plot of  $\log I_{\text{lim}}$  and  $\log V_f$  was linear with a gradient of 0.31, which is slightly different from the expected value.

#### Flow injection analysis with amperometric detection

In order to obtain the optimal potential for amperometric detection in flow injection analysis, the hydrodynamic behavior of malachite and leucomalachite green were studied. Figure 5a shows a hydrodynamic voltammetric  $I-E$  curve obtained at the BDD electrode for 20  $\mu\text{L}$  injection of 0.05 mM of malachite green in 0.1 M phosphate buffer (pH 2). Each point represents the average value of a triplicate injection. The background current at each potential is also shown for a comparison. In the case of the commercial flow cell, the  $S/B$  ratio at each point was calculated to obtain the optimum potential. The hydrodynamic voltammetric  $S/B$  ratios versus the potential curve are shown in Fig. 5b with the maximum ratio at 0.85 V. The optimal potential for the amperometric detection of leucomalachite green was also calculated in the same way.

In case of the homemade flow cell, the hydrodynamic voltammogram of both malachite and leucomalachite green exhibited a sigmoidal curve (as shown in Fig. 6). Therefore, the optimal potential was simply chosen from the hydrodynamic voltammogram at the point that gave a steady-state current, which was 1.1 V for both compounds. The results are given in Table 1. The difference in the terms of the hydrodynamic behavior and the optimal potential between both flow cells could be affected by the cell geometry (the position of WE, RE and CE).

At the chosen operating potential, a series of repetitive 20  $\mu\text{L}$  of each compound were injected. The current signal increased along with increasing the concentration. For the commercial flow cell, the BDD electrode provided a linear concentration range of 0.1 - 100  $\mu\text{M}$  and 0.8 - 80  $\mu\text{M}$  for malachite green and leucomalachite green, respectively. In the case of the homemade flow cell, the linear concentration range for leucomalachite green was smaller. The limits of detection

Table 1 Comparison of the FIA data obtained from both flow cells

	BAS flow cell		Homemade flow cell	
	MG	LMG	MG	LMG
Optimal potential (V vs. Ag/AgCl)	0.85	0.85	1.1	1.1
Linear range (mM)	0.001 - 0.1	0.008 - 0.08	0.001 - 0.1	0.004 - 0.04
%RSD (10 injections)	1.49	0.81	0.63	1.07
LOD (nM)	50	50	50	50

FIA, Flow injection analysis; BAS, Bioanalytical System, Inc.; %RSD, % relative standard deviation; LOD, limit of detection; MG, malachite green; LMG, leucomalachite green.

(LOD) of both compounds were obtained at concentrations as low as 50 nM, at  $S/N > 3$ , regardless of the commercial or the homemade flow cell.

The reproducibility of the response was also investigated. Figure 7 shows the current response to 0.2 mM malachite green by using the homemade flow cell (flow rate, 1 mL/min; operating potential, 1.1 V vs. Ag/AgCl). The well-defined signals without any peak tailing indicate that the homemade flow cell was working properly. The results are also summarized in Table 1.

#### HPLC chromatography coupled with a boron-doped diamond thin film electrode

It is the limitation of an as-deposited BDD electrode that can not be used for the selective determination both a high and low operating potential. To amend this weak point, a separation technique, such as HPLC, has to be employed to separate all species before detection using the BDD electrode. Figure 8 shows the chromatographic signals of a mixture solution of the standard MG and LMG (5 ppm) by using the BDD electrode as an amperometric detector.

The determinations of malachite green and leucomalachite green in real samples using the BDD electrode as an amperometric detector for HPLC are now being investigated. A homemade Teflon flow cell was used in order to increase the chemical resistance from the organic mobile phase. By using sample preparation methods from literature surveys, both compounds can be detected at the BDD electrode without any interference.

## Conclusions

This is the first report concerning the electroanalysis of malachite green and leucomalachite green by using BDD thin-film electrode. This electrode has exhibited excellent performance for the oxidative detection of both compounds. Well-defined voltammograms were obtained at the BDD electrode, which exhibited high sensitivity, and demonstrated a significant advantage over the GC electrode. Flow injection analysis with amperometric detection using the BDD electrode provides a linear concentration range of 0.1 - 100  $\mu\text{M}$  and 0.8 - 80  $\mu\text{M}$  for MG and LMG, respectively. The detection limit for both compounds is remarkably low (50 nM). The design of the homemade flow cell is simple, but provides reliable results at a relatively low cost. The results also indicate that the BDD

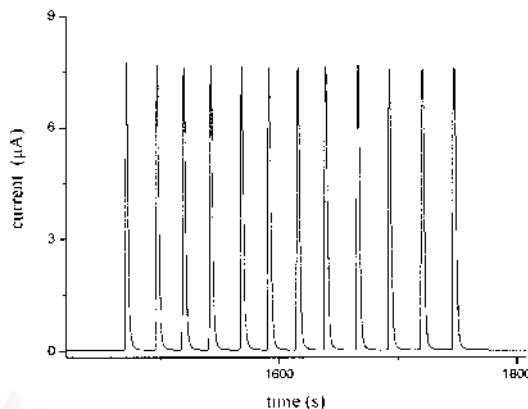


Fig. 7 Flow injection signals of 0.2 mM malachite green in a 0.1 M phosphate buffer (pH 2) at a flow rate of 1 mL min<sup>-1</sup>. The signals were obtained from a homemade flow cell (at 1.1 V vs. Ag/AgCl).

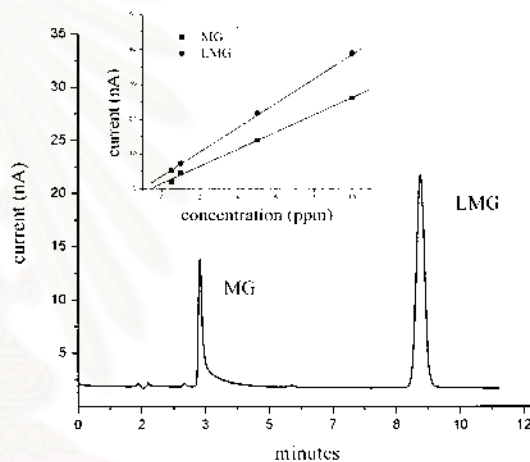


Fig. 8 Signals of MG (5.38  $\mu\text{M}$ ) and LMG (15.13  $\mu\text{M}$ ) standard solutions obtained from the HPLC system (C18 column) using a BDD electrode as an amperometric detector. The calibration curve of both compounds is also shown in the inset (Linear range: MG, 50 nM - 10  $\mu\text{M}$ ; LMG, 0.15  $\mu\text{M}$  - 30  $\mu\text{M}$ .  $R^2$ : MG, 0.998; LMG, 0.999).

electrode has a potential to be used as a detector for other systems. The determinations of malachite green and leucomalachite green using the BDD electrode and a new Teflon flow cell as an amperometric detector for HPLC are now in progress.

## Acknowledgements

Acknowledgment is made to the Thailand Research Fund and the Ratchadaphisek Somphot Grant for financial support.

## References

1. S. Srivastava, R. Sinha, and D. Roy, *Aquat. Toxicol.*, **2004**, *66*, 319.
2. K. Mitrowska, A. Posyniak, and J. Zmudzki, *J. Chromatogr., A*, **2005**, *1089*, 187.
3. J. L. Allen, J. E. Gofus, and J. R. Meinertz, *J. AOAC Int.*, **1994**, *77*, 553.

4. K. Mitrowska and A. Posyniak, *Bull. Vet. Inst. Pulawy*, **2004**, 48, 173.
5. A. A. Bergwerff and P. Scherpenisse, *J. Chromatogr., B*, **2003**, 788, 351.
6. S. B. Turnipseed, J. Roybal, H. S. Rupp, J. A. Hurlbut, and A. R. Long, *J. Chromatogr., B: Biomed. Appl.*, **1995**, 670, 55.
7. S. B. Turnipseed, J. E. Roybal, J. A. Hurlbut, and A. R. Long, *J. AOAC Int.*, **1995**, 78, 971.
8. F.-M. Matysik, *J. Chromatogr., A*, **1998**, 802, 349.
9. I. Safarik and M. Safarikova, *Water Res.*, **2002**, 36, 196.
10. P. F. Deviolet, C. Belin, P. Nougayrede, and M. Marbach, *Analisis*, **1995**, 23, 110.
11. W. Fink and J. Auch, *Dtsch. Lebensm.-Rundsch.*, **1993**, 89, 246.
12. J. E. Roybal, A. P. Pfenning, R. K. Munns, D. C. Holland, J. A. Hurlbut, and A. R. Long, *J. AOAC Int.*, **1995**, 78, 453.
13. L. G. Rushing and J. E. B. Hansen, *J. Chromatogr., B: Biomed. Appl.*, **1997**, 700, 223.
14. K. Halme, E. Lindfors, and K. Peltonen, *Food Addit. Contam.*, **2004**, 21, 641.
15. D. R. Doerge, M. I. Churchwell, T. A. Gehring, Y. M. Pu, and S. M. Plakas, *Rapid Commun. Mass Spectrom.*, **1998**, 12, 1625.
16. J. M. van de Riet, C. J. Murphy, J. N. Pearce, R. A. Potter, and B. G. Burns, *J. AOAC Int.*, **2005**, 88, 744.
17. L. Valle, C. Diaz, A. L. Zanocco, and P. Richter, *J. Chromatogr., A*, **2005**, 1067, 101.
18. S. M. Plakas, K. R. El Said, G. R. Stehly, and J. E. Roybal, *J. AOAC Int.*, **1995**, 78, 1388.
19. C. A. J. Hajee and N. Haagsma, *J. Chromatogr., B: Biomed. Appl.*, **1995**, 669, 219.
20. J. A. Tarbin, K. A. Barnes, J. Bygrave, and W. H. H. Farrington, *Analyst*, **1998**, 123, 2567.
21. P. Scherpenisse and A. A. Bergwerff, *Anal. Chim. Acta*, **2005**, 529, 173.
22. A. Swarbrick, E. J. Murby, and P. Hume, *J. Liq. Chromatogr. Relat. Technol.*, **1997**, 20, 2269.
23. K. Sagar, M. R. Smyth, J. G. Wilson, and K. McLaughlin, *J. Chromatogr., A*, **1994**, 659, 329.
24. T. A. Ivandini, B. V. Sarada, C. Terashima, T. N. Rao, D. A. Tryk, H. Ishiguro, Y. Kubota, and A. Fujishima, *J. Chromatogr., B*, **2003**, 791, 63.
25. O. Chailapakul, E. Popa, H. Tai, B. V. Sarada, D. A. Tryk, and A. Fujishima, *Electrochem. Commun.*, **2000**, 2, 422.
26. W. Siangproh, P. Ngamukot, and O. Chailapakul, *Sens. Actuators, B*, **2003**, 91, 60.
27. N. Wangfuengkanagul and O. Chailapakul, *Talanta*, **2002**, 58, 1213.
28. W. Siangproh, N. Wangfuengkanagul, and O. Chailapakul, *Anal. Chim. Acta*, **2003**, 499, 183.
29. K. Boonsong, S. Chuanuwatanakul, N. Wangfuengkanagul, and O. Chailapakul, *Sens. Actuators, B*, **2005**, 108, 627.
30. A. C. Bhasikuttan, A. V. Sapre, and L. V. Shastri, *J. Photochem. Photobiol., A*, **1995**, 90, 177.
31. <http://www.fishdoc.co.uk/treatments/malachite.htm>.
32. P. M. S. Monk, "Fundamentals of Electroanalytical Chemistry", **2001**, John Wiley and Sons, Chichester, New York, Weinheim, Brisbane, Toronto, Singapore, 212.

## BIOGRAPHY

<b>NAME</b>	Passapol Ngamukot
<b>DATE OF BIRTH</b>	16 October 1975
<b>PLACE OF BIRTH</b>	Bangkok, Thailand
<b>INSTITUTIONS ATTENDED</b>	1994 – 1997, Chulalongkorn University, Bachelor of Science (Chemistry) 1998 – 2000, Chulalongkorn University, Master of science (Chemistry) 2001 – 2005, Chulalongkorn University Ph.D. Candidate in Analytical Chemistry
<b>HOME ADDRESS</b>	21/4 Samsen 28, Samsen, Dusit, BKK, 10300



สถาบันวิทยบริการ  
จุฬาลงกรณ์มหาวิทยาลัย